Description of MIROC6 AGCM

MIROC6 AGCM document writing team[*]

April 13, 2021

[*]**MIROC6 AGCM document writing team** (in alphabetical order)

Authors: Taigo Ando, Taro Higuchi, Haruka Hotta, Tomoki Iwakiri, Takuya Jinno, Kanon Kino, Yuki Takano, Masaki Toda, and Kazuya Yamazaki

Supervisors/Editors: Minoru Chikira, Takanori Kodama, Takuro Michibata, Hiroaki Miura, Tomoko Nitta, Tomoo Ogura, Fuyuki Saito, Miho Sekiguchi, Tatsuo Suzuki, Kentaroh Suzuki, Hiroaki Tatebe, Masahiro Watanabe, Shingo Watanabe, and Kei Yoshimura

Remarks

How to cite

Revision History
March 31, 2021 First version completed.
April 13, 2021 Add Remarks.

Contents

1 Introduction

This document describes about the atmospheric general circulation model (AGCM) of MIROC6 (the sixth version of MIROC or Model for Interdisciplinary Research on Climate; Tatebe et al., 2019), which has been cooperatively developed at the Center for Climate System Research (CCSR; the precursor of a part of the Atmosphere and Ocean Research Institute), the University of Tokyo, the Japan Agency for Marine-Earth Science and Technology (JAMSTEC), and the National Institute for Environmental Studies (NIES). All the descriptions are basically corresponded with the source codes of MIROC6, specifically the version used for CMIP6 DECK experiment, whereas the original document written in Japanese by Dr. Numaguti in 1995 was corresponded with those of CCSR/NIES AGCM5.4.

1.1 Characteristics of MIROC6 AGCM

MIROC6 AGCM are summarized below.

- **System of equations**: Hydrostatic primitive equations
- **Area**: Global 3D
- **Prognostic variables**: Horizontal wind speed, temperature, surface pressure, specific humidity, cloud water
- **Horizontal discretization**: Spectral transformation (Bourke, 1988) method
- **Vertical discretization**: Hybrid $\sigma - p$ coordinate, based on Arakawa and Konor (1996)
- **Resolution for default**: T85 (150 km), 81 levels up to 0.004 hPa
- **Time integration**: Essentially the leap frog scheme, with a time filter (Williams, 2009)
- **Cumulus**: An entrainment plume model with multiple cloud types (Chikira and Sugiyama, 2010)
- **Shallow convection**: A mass-flux-based single-plume model based on Park and Bretherton (2009)
- **Large scale condensation & Cloud microphysics**: A prognostic large scale condensation scheme (Watanabe et al., 2009) and the implementation of a bulk mirco-physical scheme (Wilson and Ballard, 1999)
- **Radiation**: k-distribution scheme (Sekiguchi and Nakajima, 2008) with a hexagonal solid column as ice particle habit and extended mode radius of cloud particles
- **Turbulence**: The Mellor-Yamada-Nakanishi-Niino scheme (Nakanishi 2001; Nakanishi and Niino 2004)'s level 2.5 closure scheme
- **Surface flux**: Bulk coefficients (Louis, 1979; Louis et al., 1982) with convection effects at sea surface (Miller et al., 1992)
- **Gravity wave drag**: An orographic gravity wave parameterization (McFarlane, 1987) with a non-orographic gravity wave parameterization (Hines, 1997; Watanabe et al., 2011)

1.2 Features and Structure of the Model

1.2.1 Basic Features of the Model.

The MIROC6 AGCM is a numerical model for describing the global three-dimensional atmosphere based on physical laws and calculating the time evolution of the system as an initial value problem or a boundary value problem.

The data to be inputted are as follows.

- Initial data for each prognostic variable (horizontal wind speed, temperature, surface pressure, specific humidity, cloud liquid water content, etc.)

- Boundary condition data (surface elevation, surface condition, sea surface temperature, etc.)

- Various parameters of the model (atmospheric components, physical process parameters, etc.)

On the other hand, the output is the following.

- Data for each prognostic parameter and diagnostic parameter, for each time or time average

- Initial data to be used for continuous execution (restart data)

- Progress and various diagnostic messages

The prognostic variable is the data obtained as a time series by integrating the differential equation of time evolution, and the diagnostic variable is the quantity calculated from the prognostic variable, the boundary conditions and the parameters by some method that does not include time integration.

More specifically, the model basically solves the following equations (prognostic equations).

$$\frac{\partial u}{\partial t} = (\mathcal{F}_x)_D + (\mathcal{F}_x)_P . \tag{1.1}$$

$$\frac{\partial v}{\partial t} = (\mathcal{F}_y)_D + (\mathcal{F}_y)_P . \tag{1.2}$$

$$\frac{\partial T}{\partial t} = (Q)_D + (Q)_P . \tag{1.3}$$

$$\frac{\partial p_S}{\partial t} = (M)_D + (M)_P . \tag{1.4}$$

$$\frac{\partial q}{\partial t} = (S)_D + (S)_P . \tag{1.5}$$

$$\frac{\partial T_g}{\partial t} = (Q_g)_D + (Q_g)_P . \tag{1.6}$$

Here, u, v, T, p_S, q, T_g are two-dimensional and three-dimensional prognostic variables such as eastward wind, northward wind, temperature, surface pressure, specific humidity, and surface state amount, respectively, and the right-hand side is a term that causes time variation of each prognostic variable. The terms $\mathcal{F}_x, \mathcal{F}_y, Q, S, Q_g$ are calculated based on the prognostic variables u, v, T, p_S, q, T_g, are divided into two main categories: the terms u and v, such as advection due to the motion of the atmosphere (the terms with index D in the above equation), and the terms such as cloud and radiation (the terms with index P in the above equation). There are two

main types of terms. The former is called the dynamical process, and the latter is called the physical process.

The advection term is the main part of the time-varying term in dynamical processes, and the accurate estimation of the spatial derivative is important in its calculation. The MIROC6 AGCM utilizes the spherical harmonic expansion to calculate the horizontal differential term. On the other hand, it is important for physical processes to be represented in a simple model with parameters (parameterization), such as energy conversions due to the phase change of water, radiative absorption and emission, the effects of small-scale atmospheric motions, and the effects of various processes on the ground surface.

The time integration of the prognostic equation is done by approximating the left-hand side of (1) etc. by the difference. For example,

$$\frac{\partial q}{\partial t} \rightarrow \frac{q^{t+\Delta t} - q^t}{\Delta t} \tag{1.7}$$

By making,

$$q^{t+\Delta t} = q^t + \Delta t \left[(S)_D + (S)_P \right] \tag{1.8}$$

where S is a function of the prognostic variables u, v, T, p_S, q. Although S is a function of the prognostic variables u, v, T, p_S, q, and so on, there are various time difference schemes that can be used in this calculation depending on the time of day the prognostic variables are used to evaluate S. The MIROC6 AGCM uses the Euler method, which uses the value of the t as it is, the leap frog method, which uses the value of the $t + \Delta t/2$, and the implicit method, which uses the (approximate) value of the $t + \Delta t$.

In the MIROC6 AGCM, the time integration of the prognostic variables is done separately for the dynamical and physical processes. The dynamical processes basically use a leap frog,

$$\tilde{q}^{t+\Delta t} = q^{t-\Delta t} + 2\Delta t \, (S)_D^t \tag{1.9}$$

However, some terms are treated as implicit. In the physical process, based on the results of integrating the dynamical terms, the Euler and implicit methods are used together,

$$q^{t+\Delta t} = \tilde{q}^{t+\Delta t} + 2\Delta t \, (S)_P \tag{1.10}$$

in (8). Note that Δt in (8) is replaced by $2\Delta t$.

1.2.2 Model Execution Flow

The flow of the model execution is briefly shown below. The entries in the index are the names of the corresponding subroutine.

1. set the parameters of an experiment, coordinates, etc.

   `SUBROUTINE:[PCONST,ASETCO,SETPAR,SETTSTRT,SETTEND]`

2. read the initial values of the prognostic variables `SUBROUTINE:[RDSTRT]`

3. start the time step `SUBROUTINE:[TIMSTP]`

4. perform time integration by mechanical processes `SUBROUTINE:[DYNMCS]`

5. perform time integration by physical processes `SUBROUTINE:[PHYSCS]`

6. advance the time `MODULE:[TFILT]`

7. Output the data if necessary `MODULE:[HISTOU]`

8. Output the restart data if necessary `SUBROUTINE:[WRRSTR]`

9. Return to 3

1.2.3 Prognostic Variables

The prognostic variables are as follows. The values in parentheses are the coordinate system, and $\lambda, \varphi, \sigma, z$ indicate the longitude, latitude, dimensionless pressure, σ, and vertical depth, respectively. The values in the square brackets are in units of the index.

Element	Symbol	Unit
Eastward wind speed	$u\,(\lambda, \varphi, \sigma)$	[m/s]
Northward wind speed	$v\,(\lambda, \varphi, \sigma)$	[m/s]
Atmospheric temperature	$T\,(\lambda, \varphi, \sigma)$	[K]
Surface pressure	$p_S\,(\lambda, \varphi)$	[hPa]
Specific humidity	$q\,(\lambda, \varphi, \sigma)$	[kg/kg]
Cloud water specific humidity	$l\,(\lambda, \varphi, \sigma)$	[kg/kg]
Cloud ice specific humidity	$q_i\,(\lambda, \varphi, \sigma)$	[kg/kg]
Total water PDF variance	$V\,(\lambda, \varphi, \sigma)$	[ND]
Total water PDF skewness	$S\,(\lambda, \varphi, \sigma)$	[ND]
Variance of liquid potential temperature	$TSQ\,(\lambda, \varphi, \sigma)$	[K^2]
Covariance of liquid potential temperature and total water	$COV\,(\lambda, \varphi, \sigma)$	[K]
Variance of total water	$QSQ\,(\lambda, \varphi, \sigma)$	[ND]
Tracers	-	-

Of these quantities, the quantities for turbulence process, TSQ, COV, QSQ, store only one step at a time, while the quantities for the atmosphere, $u, v, T, p_S, q, l, q_i, V, S$, need to store two steps at a time. This is due to the fact that the leap frog method is used in the time integration of the dynamic process of the quantities related to the atmosphere.

The quantities of the atmosphere, u, v, T, p_S, q, l, are variables managed by the main routine, `Administration of the Atmosphere'[AGCM5\a]`. On the other hand, the quantities relating to the earth's surface and ground, q_i, V, S, TSQ, COV, QSQ, do not appear in the main routine, but are managed by the subroutine `MODULE:[PHYSCS]` of the physical process.

Tracers include mass concentrations of aerosol species,

1.3 Basic Settings

Here we present the basic setup of the model.

1.3.1 Coordinate System

The coordinate system of the atmospheric model consists of longitude λ, latitude φ, and normalized pressure η (definitions are given below), each of which is treated as orthogonal. However, z is used for the vertical coordinate in the ground, which is treated in a land physics component.

Longitude is discretized at equal intervals (SUBROUTINE: [SETLO] in asetc.F).

$$\lambda_i = 2\pi \frac{i-1}{I}, \quad i = 1, \ldots I. \tag{1.11}$$

Latitude grids φ_j are derived from the Gauss-Legendre integral formula (SUBROUTINE: [SETLA] in asetc.F). This is the zero point of the Legendre polynomial of order J with $\mu = \sin\varphi$ as the argument (SUBROUTINE: [GAUSS] in uspst.F). If J is large, we can approximate

$$\varphi_j = \pi \left(\frac{1}{2} - \frac{j-1/2}{J} \right), \quad j = 1, \ldots J. \tag{1.12}$$

Usually, the grid spacing of longitude and latitude is taken to be approximately equal to $J = I/2$, based on the triangular truncation of the spectral method.

Air pressure p is defined at half levels ($p_{k+1/2}, \ k = 1, 2, \ldots K$) using the following formula using constants $A_{k+1/2}, \ B_{k+1/2}$:

$$p_{k+1/2} = A_{k+1/2} + B_{k+1/2}\, p_s, \tag{1.13}$$

where $A_{1/2} = A_{K+1/2} = 0, \ B_{1/2} = 1, \ B_{K+1/2} = 0$ and thus $p_{1/2} = p_s, \ p_{K+1/2} = 0$. Therefore, the normalized pressure $\sigma \equiv p/p_s$ can be written as below:

$$\sigma_{k+1/2} = \frac{A_{k+1/2}}{p_s} + B_{k+1/2}. \tag{1.14}$$

Furthermore, a hybrid normalized pressure η is defined as below:

$$\eta_{k+1/2} = \frac{A_{k+1/2}}{p_0} + B_{k+1/2}, \quad p_0 \equiv 1000 \text{ hPa}. \tag{1.15}$$

Since $A_{k+1/2}, \ B_{k+1/2}, p_0$ are constants, $\eta_{k+1/2}$ is also a constant and we use it as the vertical coordinate of the atmopheric model. However, as described in Chapter 2, basic equations are descretized in such a way that $\eta_{k+1/2}$ does not explicitly appear and $\sigma_{k+1/2}$ is used instead to commonize source codes with the σ-coordinate system used in MIROC 5.

Air pressure p_k at full levels ($p_k, \ k = 1, 2, \ldots K$) is interpolated from half-level pressure as below:

$$p_k = \left\{ \frac{1}{1+\kappa} \left(\frac{p_{k-1/2}^{\kappa+1} - p_{k+1/2}^{\kappa+1}}{p_{k-1/2} - p_{k+1/2}} \right) \right\}^{1/\kappa}. \tag{1.16}$$

Full-level pressure in a 80-level configuration is shown in Fig. 1. While lower layers follow the terrain, upper layers are isobaric, and the two are smoothly connected.

All prognostic variables are defined either on a grid of $(\lambda_i, \varphi_j, \eta_k)$ or $(\lambda_i, \varphi_j, z_l)$. (The underground level, z_l, is described in the section on physical processes.)

In the time direction, the forecast equations are discretized at evenly spaced Δt and time integration is performed. However, Δt may change in cases where the stability of the time integration is insufficient.
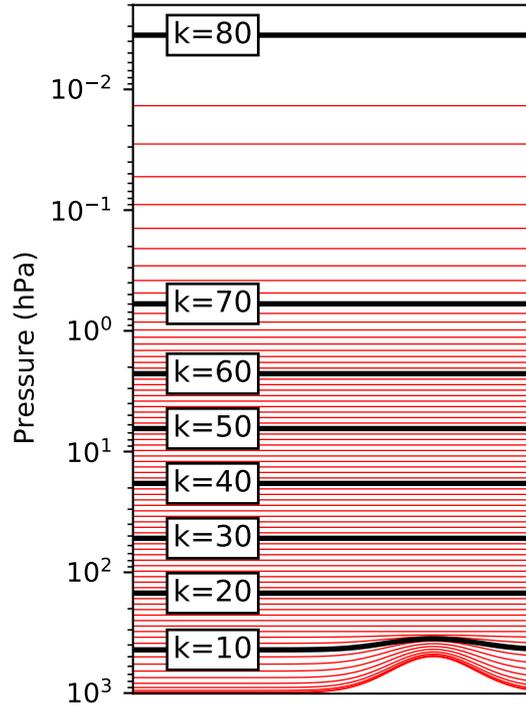
Figure 1: Default arangement of vertical levels for 80-level simulations.

1.3.2 Physical Constants

The basic physical constants are shown below (`SUBROUTINE [PCONST]` in apcon.F).

Element	Symbol	Unit	Value
Earth radius	a	m	6.37×10^6
Gravitational acceleration	g	m s^{-2}	9.8
Atmospheric specific heat at constant pressure	C_p	J kg^{-1} K^{-1}	1004.6
Atmospheric gas constant	R	J kg^{-1} K^{-1}	287.04
Latent heat of water evaporation	L	J kg^{-1}	2.5×10^6
Water vapor specific heat at constant pressure	C_v	J kg^{-1} K^{-1}	1810
Gas constant of water	R_v	J kg^{-1} K^{-1}	461
Density of liquid water	d_{H_2O}	kg m^{-3}	1000
Saturated vapor pressure at 0 °C	$e^*(273K)$	Pa	611
Stefan-Bolzman constant	σ_{SB}	W m^{-2} K^{-4}	5.67×10^{-8}
Kárman constant	k		0.4
Latent heat of ice melting	L_M	J kg^{-1}	3.4×10^5
Freezing point of water	T_M	K	273.15
Constant pressure specific heat of water	C_w	J kg^{-1}	4200
Freezing point of seawater	T_I	K	271.35
Specific heat ratio of ice at constant pressure	$C_I = C_w - L_M/T_M$		2397
Water vapor molecular weight ratio	$\epsilon = R/R_v$		0.622
Coefficient of virtual temperature	$\epsilon_v = \epsilon^{-1} - 1$		0.606

12

Element	Symbol	Unit	Value
Ratio of specific heat to gas constant	$\kappa = R/C_p$		0.286

2 Dynamics

2.1 Basic Equations

2.1.1 Basic Equations

The basic equations are a system of primitive equations at the spherical (λ, φ) and η coordinates, given as follows (Arakawa and Konor 1996).

1. Continuity equation

$$\frac{\partial m}{\partial t} + \nabla_\eta \cdot (m\mathbf{v}_H) + \frac{\partial(m\dot{\eta})}{\partial \eta} = 0 \tag{2.1}$$

2. Hydrostatic equation

$$\frac{\partial \Phi}{\partial \eta} = -\frac{RT_v}{p}m \tag{2.2}$$

3. Equation of motion

$$\frac{\partial \zeta}{\partial t} = \frac{1}{a\cos\varphi}\frac{\partial A_v}{\partial \lambda} - \frac{1}{a\cos\varphi}\frac{\partial}{\partial \varphi}(A_u\cos\varphi) - \mathcal{D}(\zeta) \tag{2.3}$$

$$\frac{\partial D}{\partial t} = \frac{1}{a\cos\varphi}\frac{\partial A_u}{\partial \lambda} + \frac{1}{a\cos\varphi}\frac{\partial}{\partial \varphi}(A_v\cos\varphi) - \nabla_\eta^2(\Phi + R\bar{T}\pi + E) - \mathcal{D}(D) \tag{2.4}$$

4. Thermodynamic equation

$$\begin{aligned}
\frac{\partial T}{\partial t} &= -\frac{1}{a\cos\varphi}\frac{\partial uT'}{\partial \lambda} - \frac{1}{a}\frac{\partial}{\partial \varphi}(vT'\cos\varphi) + T'D \\
&\quad - \dot{\eta}\frac{\partial T}{\partial \eta} + \frac{\kappa T}{\sigma}\left[B\left(\frac{\partial \pi}{\partial t} + \mathbf{v}_H\cdot\nabla_\eta\pi\right) + \frac{m\dot{\eta}}{p_s}\right] + \frac{Q}{C_p} + \frac{Q_{diff}}{C_p} - \mathcal{D}(T)
\end{aligned} \tag{2.5}$$

5. Tracers

For any tracer whose conservative quantity (e.g. mixing ratio) is denoted as q,

$$\begin{aligned}
\frac{\partial q}{\partial t} &= -\frac{1}{a\cos\varphi}\frac{\partial uq}{\partial \lambda} - \frac{1}{a\cos\varphi}\frac{\partial}{\partial \varphi}(vq\cos\varphi) + qD \\
&\quad - \dot{\eta}\frac{\partial q}{\partial \eta} + S_q - \mathcal{D}(q)
\end{aligned} \tag{2.6}$$

Here,

$$m \equiv \left(\frac{\partial p}{\partial \eta}\right)_{p_s}, \tag{2.7}$$

$$\theta \equiv T\,(p/p_0)^{-\kappa}, \tag{2.8}$$

$$\kappa \equiv R/C_p, \tag{2.9}$$

$$\Phi \equiv gz, \tag{2.10}$$

$$\pi \equiv \ln p_S, \tag{2.11}$$

$$\dot{\eta} \equiv \frac{\mathrm{d}\eta}{\mathrm{d}t}, \tag{2.12}$$

$$T_v \equiv T(1 + \epsilon_v q), \tag{2.13}$$

$$T \equiv \bar{T} + T', \tag{2.14}$$

$$\bar{T} \equiv 300\ \mathrm{K}, \tag{2.15}$$

$$\zeta \equiv \frac{1}{a\cos\varphi}\frac{\partial v}{\partial\lambda} - \frac{1}{a\cos\varphi}\frac{\partial}{\partial\varphi}(u\cos\varphi), \tag{2.16}$$

$$D \equiv \frac{1}{a\cos\varphi}\frac{\partial u}{\partial\lambda} + \frac{1}{a\cos\varphi}\frac{\partial}{\partial\varphi}(v\cos\varphi), \tag{2.17}$$

$$A_u \equiv (\zeta + f)v - \dot{\eta}\frac{\partial u}{\partial\eta} - \frac{RT'}{a\cos\varphi}\frac{\partial\pi}{\partial\lambda} + \mathcal{F}_x, \tag{2.18}$$

$$A_v \equiv -(\zeta + f)u - \dot{\eta}\frac{\partial v}{\partial\eta} - \frac{RT'}{a}\frac{\partial\pi}{\partial\varphi} + \mathcal{F}_y, \tag{2.19}$$

$$E \equiv \frac{u^2 + v^2}{2}, \tag{2.20}$$

$$\mathbf{v}_H \cdot \nabla \equiv \frac{u}{a\cos\varphi}\left(\frac{\partial}{\partial\lambda}\right)_\sigma + \frac{v}{a}\left(\frac{\partial}{\partial\varphi}\right)_\sigma, \tag{2.21}$$

$$\nabla_\eta^2 \equiv \frac{1}{a^2\cos^2\varphi}\frac{\partial^2}{\partial\lambda^2} + \frac{1}{a^2\cos\varphi}\frac{\partial}{\partial\varphi}\left[\cos\varphi\frac{\partial}{\partial\varphi}\right]. \tag{2.22}$$

f is the Coriolis parameter. $\mathcal{D}(\zeta), \mathcal{D}(D), \mathcal{D}(T), \mathcal{D}(q)$ are horizontal diffusion terms, $\mathcal{F}_\lambda, \mathcal{F}_\varphi$ are forces due to small-scale kinetic processes (treated as 'physical processes'), Q are forces due to radiation, condensation, small-scale kinetic processes, etc. Heating and temperature change due to 'physical processes', and S_q is a water vapor source term due to 'physical processes' such as condensation and small-scale motion. Q_{diff} is the heat of friction and

$$Q_{\mathrm{diff}} = -\mathbf{v} \cdot \left(\frac{\partial\mathbf{v}}{\partial t}\right)_{\mathrm{diff}}. \tag{2.23}$$

$(\frac{\partial\mathbf{v}}{\partial t})_{\mathrm{diff}}$ is a time-varying term of u, v due to horizontal and vertical diffusion.

2.1.2 Boundary Conditions

Upper and lower boundary conditions for the vertical velocity is:

$$\dot{\eta} = 0 \quad \mathrm{at} \quad \eta = 0,\ 1. \tag{2.24}$$

The prognostic equation for p_s and the diagnostic equation for the vertical velocity can be derived by integrating the continuity equation and applying these boundary conditions.

2.2 Vertical Discretization

Following Arakawa and Konor (1996) except for using the Lorentz grid, the basic equations are discretized vertically by differences. This scheme has the following characteristics.

- Conservation of the total integrated mass.

- Conservation of the total integrated energy.

- Conservation of the globally integrated angular momentum.

- Conservation of the total mass-integrated potential temperature.

- The hydrostatic pressure equation is localized (the altitude of the lower level is independent of the temperature of the upper level).

- For a given temperature distribution, constant in the horizontal direction, the hydrostatic pressure equation becomes precisely accurate and the barometric gradient force becomes zero.

- Isothermal atmosphere stays permanently isothermal.

2.2.1 Model Levels

Model level increases in altitude with the vertical level number k. $k = 1/2$ corresponds with the model bottom ($\eta = 1$), while $k = K + 1/2$ corresponds to the model top ($\eta = 0$). Variables ζ, D, T, q are defined at integer levels ($k = 1, 2, \ldots K$), while the vertical velocity $\dot{\eta}$ is defined at half-integer levels ($k = 1/2, 3/2, \ldots K + 1/2$). Using constants $A_{k+1/2}$ and $B_{k+1/2}$ and variable surface pressure p_s, air pressure at half levels are defined as below:

$$p_{k+1/2} = A_{k+1/2} + B_{k+1/2}\, p_s. \tag{2.25}$$

Thus, the normalized pressure $\sigma \equiv p/p_s$ can be written as below:

$$\sigma_{k+1/2} = \frac{A_{k+1/2}}{p_s} + B_{k+1/2}. \tag{2.26}$$

Using a reference pressure p_0, the hybrid-normalized pressure η is defined as below:

$$\eta_{k+1/2} = \frac{A_{k+1/2}}{p_0} + B_{k+1/2}, \tag{2.27}$$

which is a constant at all levels and is used as the vertical coordinate by default in MIROC 6.0.

Pressure at full levels are interpolated from half-level pressure by the following formula:

$$p_k = \left\{ \frac{1}{1+\kappa} \left(\frac{p_{k-1/2}^{\kappa+1} - p_{k+1/2}^{\kappa+1}}{p_{k-1/2} - p_{k+1/2}} \right) \right\}^{1/\kappa}. \tag{2.28}$$

For later use, let us define the following:

$$\begin{aligned}
\Delta\sigma_k &\equiv \sigma_{k-1/2} - \sigma_{k+1/2}, \\
\Delta B_k &\equiv B_{k-1/2} - B_{k+1/2}.
\end{aligned} \tag{2.29}$$

2.2.2 Vertical Discretization

Basic equations vertically discretized at the η hybrid coordinates are shown below.

1. Continuity equation and diagnosis of the vertical velocity

$$\frac{\partial \pi}{\partial t} = -\sum_{k=1}^{K} \left\{ D_k \Delta \sigma_k + (\mathbf{v}_k \cdot \nabla \pi) \Delta B_k \right\} \tag{2.30}$$

In MIRCO 6.0, the discretization is conducted in a manner similar to the σ coordinate, which can be optionally selected and was the default in previous versions, to commonize source codes. Thus, the vertical velocity is represented as $\dot{\sigma} = m\dot{\eta}/p_s$. Furthermore, vertical advection $\dot{\eta}(\partial/\partial \eta)$ is replaced with an equivalent form $m\dot{\eta}/p_s(\partial/\partial \sigma)$.

$$(\dot{\sigma} =) \frac{(m\dot{\eta})_{k-1/2}}{p_s} = -B_{k-1/2}\frac{\partial \pi}{\partial t} - \sum_{l=k}^{K} \left\{ D_l \Delta \sigma_l + (\mathbf{v}_l \cdot \nabla \pi) \Delta B_l \right\} \tag{2.31}$$

$$\frac{(m\dot{\eta})_{1/2}}{p_s} = \frac{(m\dot{\eta})_{k+1/2}}{p_s} = 0 \tag{2.32}$$

2. Hydrostatic equation

$$\begin{aligned}
\Phi_1 &= \Phi_s + C_p(\sigma_1^{-\kappa} - 1)T_{v,1} \\
&= \Phi_s + C_p\alpha_1 T_{v,1}
\end{aligned} \tag{2.33}$$

$$\begin{aligned}
\Phi_k - \Phi_{k-1} &= C_p\left[\left(\frac{p_{k-1/2}}{p_k}\right)^{\kappa} - 1\right]T_{v,k} + C_p\left[1 - \left(\frac{p_{k-1/2}}{p_{k-1}}\right)^{\kappa}\right]T_{v,k-1} \\
&= C_p\alpha_k T_{v,k} + C_p\beta_{k-1}T_{v,k-1}
\end{aligned} \tag{2.34}$$

Here,

$$\alpha_k \equiv \left(\frac{p_{k-1/2}}{p_k}\right)^{\kappa} - 1, \tag{2.35}$$

$$\beta_k \equiv 1 - \left(\frac{p_{k+1/2}}{p_k}\right)^{\kappa}. \tag{2.36}$$

3. Equations of motion

$$\frac{\partial \zeta_k}{\partial t} = \frac{1}{a\cos\varphi}\frac{\partial (A_v)_k}{\partial \lambda} - \frac{1}{a\cos\varphi}\frac{\partial}{\partial \varphi}(A_u\cos\varphi)_k - \mathcal{D}(\zeta_k) \tag{2.37}$$

$$\frac{\partial D}{\partial t} = \frac{1}{a\cos\varphi}\frac{\partial (A_u)_k}{\partial \lambda} + \frac{1}{a\cos\varphi}\frac{\partial}{\partial \varphi}(A_v\cos\varphi)_k - \nabla_\eta^2(\Phi_k + R\bar{T}\pi + (KE)_k) - \mathcal{D}(D_k) \tag{2.38}$$

$$\begin{aligned}
(A_u)_k = (\zeta_k + f)v_k - &\left[\frac{(m\dot{\eta})_{k-1/2}}{p_s}\frac{u_{k-1} - u_k}{\Delta\sigma_{k-1} + \Delta\sigma_k} + \frac{(m\dot{\eta})_{k+1/2}}{p_s}\frac{u_k - u_{k+1}}{\Delta\sigma_k + \Delta\sigma_{k+1}}\right] \\
&- \frac{1}{a\cos\varphi}\frac{\partial \pi}{\partial \lambda}(C_p T_{v,k}\hat{\kappa} - R\bar{T}) + \mathcal{F}_x
\end{aligned} \tag{2.39}$$

$$\begin{aligned}
(A_v)_k = -(\zeta_k + f)u_k - &\left[\frac{(m\dot{\eta})_{k-1/2}}{p_s}\frac{v_{k-1} - v_k}{\Delta\sigma_{k-1} + \Delta\sigma_k} + \frac{(m\dot{\eta})_{k+1/2}}{p_s}\frac{v_k - v_{k+1}}{\Delta\sigma_k + \Delta\sigma_{k+1}}\right] \\
&- \frac{1}{a}\frac{\partial \pi}{\partial \varphi}(C_p T_{v,k}\hat{\kappa} - R\bar{T}) + \mathcal{F}_y
\end{aligned} \tag{2.40}$$

$$\hat{\kappa}_k = \frac{B_{k-1/2}\alpha_k + B_{k+1/2}\beta_k}{\Delta\sigma_k} \tag{2.41}$$

4. Thermodynamic equation

$$\frac{\partial T_k}{\partial t} = -\frac{1}{a\cos\varphi}\frac{\partial u_k T'_k}{\partial \lambda} - \frac{1}{a\cos\varphi}\frac{\partial}{\partial \varphi}(v_k T'_k \cos\varphi) + H_k + \frac{Q_k}{C_p} + \frac{(Q_{diff})_k}{C_p} - \mathcal{D}(T_k) \qquad (2.42)$$

Here,

$$
\begin{aligned}
H_k \quad \equiv \quad & T'_k D_k - \left[\frac{(m\dot\eta)_{k-1/2}}{p_s}\frac{\hat{T}_{k-1/2} - T_k}{\Delta\sigma_k} + \frac{(m\dot\eta)_{k+1/2}}{p_s}\frac{T_k - \hat{T}_{k+1/2}}{\Delta\sigma_k}\right] \\
& + \left\{\alpha_k\left[B_{k-1/2}\mathbf{v}_k\cdot\nabla\pi - \sum_{l=k}^{K}(D_l\Delta\sigma_l + (\mathbf{v}_l\cdot\nabla\pi)\Delta B_l)\right]\right. \\
& \left. + \beta_k\left[B_{k+1/2}\mathbf{v}_k\cdot\nabla\pi - \sum_{l=k+1}^{K}(D_l\Delta\sigma_l + (\mathbf{v}_l\cdot\nabla\pi)\Delta B_l)\right]\right\}\frac{1}{\Delta\sigma_k}T_{v,k} \\
= \quad & T'_k D_k - \left[\frac{(m\dot\eta)_{k-1/2}}{p_s}\frac{\hat{T}_{k-1/2} - T_k}{\Delta\sigma_l} + \frac{(m\dot\eta)_{k+1/2}}{p_s}\frac{T_k - \hat{T}_{k+1/2}}{\Delta\sigma_l}\right] \\
& + \hat{\kappa}_k(\mathbf{v}_k\cdot\nabla\pi)T_{v,k} \\
& - \alpha_k\sum_{l=k}^{K}(D_l\Delta\sigma_l + (\mathbf{v}_l\cdot\nabla\pi)\Delta B_l)\frac{T_{v,k}}{\Delta\sigma_k} \\
& - \beta_k\sum_{l=k+1}^{K}(D_l\Delta\sigma_l + (\mathbf{v}_l\cdot\nabla\pi)\Delta B_l)\frac{T_{v,k}}{\Delta\sigma_k}, \qquad (2.43)
\end{aligned}
$$

$$\hat{T}_{k-1/2} = a_k T_k + b_{k-1}T_{k-1}, \qquad (2.44)$$

$$a_k = \alpha_k\left[1 - \left(\frac{p_k}{p_{k-1}}\right)^\kappa\right]^{-1}, \qquad (2.45)$$

$$b_k = \beta_k\left[\left(\frac{p_k}{p_{k+1}}\right)^\kappa - 1\right]^{-1}. \qquad (2.46)$$

5. Tracers

$$\frac{\partial q_k}{\partial t} = -\frac{1}{a\cos\varphi}\frac{\partial u_k q_k}{\partial \lambda} - \frac{1}{a\cos\varphi}\frac{\partial}{\partial \varphi}(v_k q_k \cos\varphi) + R_k + S_{q,k} - \mathcal{D}(q_k) \qquad (2.47)$$

$$R_k = q_k D_k - \frac{1}{2}\left[\frac{(m\dot\eta)_{k-1/2}}{p_s}\frac{q_{k-1} - q_k}{\Delta\sigma_k} + \frac{(m\dot\eta)_{k+1/2}}{p_s}\frac{q_k - q_{k+1}}{\Delta\sigma_k}\right] \qquad (2.48)$$

2.2.3 Differences from the σ-Coordinate

In MIROC 6.0, the discretization is conducted in a similar form to the σ coordinate. Thus, differences of discretized equations between the η and σ coordinates are relatively small, which are listed below:

- In the σ coordinate, $A_{k+1/2}$ is equal to zero at all levels.
- While ΔB_k and $\Delta\sigma_k$ are different in the η coordinates, those are equivalent to each other in the σ coordinate.

2.3 Horizontal Discretization

The horizontal discretization is based on the spectral transformation method (Bourke, 1988). The differential terms for longitude and latitude are evaluated by the orthogonal function expansion, while the non-linear terms are calculated on the grid.

2.3.1 Spectral Expansion

As an expansion function, the spherical harmonic functions $Y_n^m(\lambda, \mu)$, which are eigenfunction of Laplacian on a sphere, are used. However, $\mu \equiv \sin\varphi$ is used. Y_n^m satisfies the following equation,

$$\nabla_\sigma^2 Y_n^m(\lambda, \mu) = -\frac{n(n+1)}{a^2} Y_n^m(\lambda, \mu) \tag{2.49}$$

Using the Associated Legendre function P_n^m it is written as follows.

$$Y_n^m(\lambda, \mu) = P_n^m(\mu) e^{im\lambda} \tag{2.50}$$

However, it is $n \geq |m|$.
The expansion by spherical harmonic functions is ,

$$Y_{n\ ij}^m \equiv Y_n^m(\lambda_i, \mu_j) \tag{2.51}$$

When I write ,

$$X_{ij} \equiv X(\lambda_i, \mu_j) = \mathcal{R}] \sum_{m=-N}^{N} \sum_{n=|m|}^{N} X_n^m Y_{n\ ij}^m, \tag{2.52}$$

The inverse of that is ,

$$X_n^m = \frac{1}{4\pi} \int_{-1}^{1} d\mu \int_0^\pi d\lambda X(\lambda, \mu) Y_n^{m*}(\lambda, \mu)$$

$$= \frac{1}{I} \sum_{i=1}^{I} \sum_{j=1}^{J} X_{ij} Y_{n\ ij}^{m*} w_j \tag{2.53}$$

The formula is expressed as To evaluate by replacing the integral with a sum, we use the Gauss trapezoidal formula for the λ integral and the Gauss-Legendre integral formula for the μ integral. μ_j is the Gauss latitude and w_j is the Gaussian weights. Also, λ_i is a grid of evenly spaced Gaussian weights.

Using spectral harmonics transformation, the grid point values of the terms containing the derivatives can be calculated as follows.

$$\left(\frac{\partial X}{\partial \lambda}\right)_{ij} = \mathcal{R}e \sum_{m=-N}^{N} \sum_{n=|m|}^{N} im X_n^m Y_{n\ ij}^m \tag{2.54}$$

$$\left(\cos\varphi\frac{\partial X}{\partial\varphi}\right)_{ij} = \mathcal{R}e \sum_{m=-N}^{N} \sum_{n=|m|}^{N} X_n^m(1-\mu^2)\frac{\partial}{\partial\mu}Y_n^m{}_{ij} \tag{2.55}$$

Furthermore, the grid point values of u, v can be obtained from the spectral components of ζ and D as follows

$$u_{ij} = \frac{1}{\cos\varphi}\mathcal{R}e \sum_{m=-N}^{N} \sum_{\substack{n=|m| \\ n\neq 0}}^{N} \left\{ \frac{a}{n(n+1)}\zeta_n^m(1-\mu^2)\frac{\partial}{\partial\mu}Y_n^m{}_{ij} - \frac{ima}{n(n+1)}D_n^m Y_n^m{}_{ij} \right\} \tag{2.56}$$

$$v_{ij} = \frac{1}{\cos\varphi}\mathcal{R}e \sum_{m=-N}^{N} \sum_{\substack{n=|m| \\ n\neq 0}}^{N} \left\{ -\frac{ima}{n(n+1)}\zeta_n^m Y_n^m{}_{ij} - \frac{a}{n(n+1)}D_n^m(1-\mu^2)\frac{\partial}{\partial\mu}Y_n^m{}_{ij} \right\} \tag{2.57}$$

The derivative appearing in the advection term of the equation is calculated as

$$\begin{aligned}
\left(\frac{1}{a\cos\varphi}\frac{\partial A}{\partial\lambda}\right)_n^m &= \frac{1}{4\pi}\int_{-1}^{1}d\mu\int_{0}^{\pi}d\lambda\frac{1}{a\cos\varphi}\frac{\partial A}{\partial\lambda}Y_n^{m*} \\
&= \frac{1}{4\pi}\int_{-1}^{1}d\mu\int_{0}^{\pi}d\lambda\, imA\cos\varphi\frac{1}{a(1-\mu^2)}Y_n^{m*} \\
&= \frac{1}{I}\sum_{i=1}^{I}\sum_{j=1}^{J}imA_{ij}\cos\varphi_j Y_n^{m*}{}_{ij}\frac{w_j}{a(1-\mu_j^2)}
\end{aligned} \tag{2.58}$$

$$\begin{aligned}
\left(\frac{1}{a\cos\varphi}\frac{\partial}{\partial\varphi}(A\cos\varphi)\right)_n^m &= \frac{1}{4\pi a}\int_{-1}^{1}d\mu\int_{0}^{\pi}d\lambda\frac{\partial}{\partial\mu}(A\cos\varphi)Y_n^{m*} \\
&= -\frac{1}{4\pi a}\int_{-1}^{1}d\mu\int_{0}^{\pi}d\lambda A\cos\varphi\frac{\partial}{\partial\mu}Y_n^{m*} \\
&= -\frac{1}{I}\sum_{i=1}^{I}\sum_{j=1}^{J}A_{ij}\cos\varphi_j(1-\mu_j^2)\frac{\partial}{\partial\mu}Y_n^{m*}{}_{ij}\frac{w_j}{a(1-\mu_j^2)}
\end{aligned} \tag{2.59}$$

Furthermore,

$$\left(\nabla_\sigma^2 X\right)_n^m = -\frac{n(n+1)}{a^2}X_n^m \tag{2.60}$$

to be used for the evaluation of the ∇^2 section.

2.3.2 Horizontal Diffusion Term

The horizontal diffusion term is implemented in the form ∇^{N_D} as follows.

$$\mathcal{D}(\zeta) = K_{MH}\left[(-1)^{N_D/2}\nabla^{N_D} - \left(\frac{2}{a^2}\right)^{N_D/2}\right]\zeta, \tag{2.61}$$

$$\mathcal{D}(D) = K_{MH} \left[(-1)^{N_D/2} \nabla^{N_D} - \left(\frac{2}{a^2} \right)^{N_D/2} \right] D, \qquad (2.62)$$

$$\mathcal{D}(T) = (-1)^{N_D/2} K_{HH} \nabla^{N_D} T, \qquad (2.63)$$

$$\mathcal{D}(q) = (-1)^{N_D/2} K_{EH} \nabla^{N_D} q. \qquad (2.64)$$

This horizontal diffusion term damps high frequency component occuring aliasing for computational stability. In order to represent selective horizontal diffusion on small scales, $4 \sim 16$ is used as N_D. Here, the extra term for vorticity and divergence diffusion indicates that the term of rigid body rotation in $n = 1$ does not decay.

2.3.3 Spectral Representation of Equations

1. A series of equations

$$\frac{\partial \pi_m^m}{\partial t} = - \sum_{k=1}^{K} (D_n^m)_k \Delta \sigma_k$$
$$+ \frac{1}{I} \sum_{i=1}^{I} \sum_{j=1}^{J} Z_{ij} Y_n^{m*}{}_{ij} w_j, \qquad (2.65)$$

where,

$$Z \equiv - \sum_{k=1}^{K} \mathbf{v}_k \cdot \nabla \pi. \qquad (2.66)$$

2. Equation of motion

$$\frac{\partial \zeta_n^m}{\partial t} = \frac{1}{I} \sum_{i=1}^{I} \sum_{j=1}^{J} im(A_v)_{ij} \cos \varphi_j Y_n^{m*}{}_{ij} \frac{w_j}{a(1 - \mu_j^2)}$$
$$+ \frac{1}{I} \sum_{i=1}^{I} \sum_{j=1}^{J} (A_u)_{ij} \cos \varphi_j (1 - \mu_j^2) \frac{\partial}{\partial \mu} Y_n^{m*}{}_{ij} \frac{w_j}{a(1 - \mu_j^2)}$$
$$- (\mathcal{D}_M)_n^m \zeta_n^m, \qquad (2.67)$$

$$\frac{\partial \tilde{D}_n^m}{\partial t} = \frac{1}{I} \sum_{i=1}^{I} \sum_{j=1}^{J} im(A_u)_{ij} \cos\varphi_j Y_n^{m*}{}_{ij} \frac{w_j}{a(1-\mu_j^2)}$$

$$-\frac{1}{I} \sum_{i=1}^{I} \sum_{j=1}^{J} (A_v)_{ij} \cos\varphi_j (1-\mu_j^2) \frac{\partial}{\partial\mu} Y_n^{m*}{}_{ij} \frac{w_j}{a(1-\mu_j^2)}$$

$$-\frac{n(n+1)}{a^2} \frac{1}{I} \sum_{i=1}^{I} \sum_{j=1}^{J} E_{ij} Y_n^{m*}{}_{ij} w_j$$

$$+\frac{n(n+1)}{a^2} (\Phi_n^m + C_p \hat{\kappa}_k \bar{T}_k \pi_n^m) - (\mathcal{D}_M)_n^m D_n^m, \qquad (2.68)$$

where

$$(\mathcal{D}_M)_n^m = K_{MH} \left[\left(\frac{n(n+1)}{a^2}\right)^{N_D/2} - \left(\frac{2}{a^2}\right)^{N_D/2} \right]. \qquad (2.69)$$

3. Thermodynamic equation

$$\frac{\partial T_n^m}{\partial t} = -\frac{1}{I} \sum_{i=1}^{I} \sum_{j=1}^{J} im u_{ij} T'_{ij} \cos\varphi_j Y_n^{m*}{}_{ij} \frac{w_j}{a(1-\mu_j^2)}$$

$$+\frac{1}{I} \sum_{i=1}^{I} \sum_{j=1}^{J} v_{ij} T'_{ij} \cos\varphi_j (1-\mu_j^2) \frac{\partial}{\partial\mu} Y_n^{m*}{}_{ij} \frac{w_j}{a(1-\mu_j^2)}$$

$$+\frac{1}{I} \sum_{i=1}^{I} \sum_{j=1}^{J} \left(H_{ij} + \frac{Q_{ij} + Q_{diff}}{C_p} \right) Y_n^{m*}{}_{ij} w_j$$

$$-(\tilde{\mathcal{D}}_H)_n^m T_n^m, \qquad (2.70)$$

where,

$$(\mathcal{D}_H)_n^m = K_{HH} \left(\frac{n(n+1)}{a^2}\right)^{N_D/2}. \qquad (2.71)$$

4. Water vapor formula

$$\frac{\partial q_n^m}{\partial t} = -\frac{1}{I} \sum_{i=1}^{I} \sum_{j=1}^{J} im u_{ij} q_{ij} \cos\varphi_j Y_n^{m*}{}_{ij} \frac{w_j}{a(1-\mu_j^2)}$$

$$+\frac{1}{I} \sum_{i=1}^{I} \sum_{j=1}^{J} v_{ij} q_{ij} \cos\varphi_j (1-\mu_j^2) \frac{\partial}{\partial\mu} Y_n^{m*}{}_{ij} \frac{w_j}{a(1-\mu_j^2)}$$

$$+\frac{1}{I} \sum_{i=1}^{I} \sum_{j=1}^{J} \left(\hat{R}_{ij} + S_{q,ij} \right) Y_n^{m*}{}_{ij} w_j$$

$$+(\mathcal{D}_H)_n^m q_n^m \qquad (2.72)$$

where

$$(\mathcal{D}_E)_n^m = K_{EH} \left(\frac{n(n+1)}{a^2} \right)^{N_D/2}. \tag{2.73}$$

23

2.4 Time Integration

The time discretization is essentially the leap frog scheme. However, backward or forward differences are used for diffusion terms and physical process terms. A time filter (Williams, 2009), which is a modified version of the Asselin time filter (Asselin 1972), is used to suppress computational modes. A semi-implicit method is applied to the gravitational wave term to make the Δt larger (Bourke, 1988).

2.4.1 Time Integration and Time Filtering with the Leap Frog Method

We use leap frog as the time integration scheme for advection terms and other dynamic terms. A backward difference of $2\Delta t$ is used for the horizontal diffusion term. The p-surface correction of the diffusion term and the frictional heat due to horizontal diffusion are treated by forward differences of $2\Delta t$. The physical process terms $(\mathcal{F}_\lambda, \mathcal{F}_\varphi, Q, S_q)$ use the forward difference of $2\Delta t$ (except for the vertical diffusion term, which uses the forward difference of $\mathcal{F}_\lambda, \mathcal{F}_\varphi, Q, S_q$). However, the calculation of the prognositc veriables of vertical diffusion is treated as a backward difference. Please refer to the chapter on physical processes for details.)

Expressing each prognostic variable as X,

$$\hat{X}^{t+\Delta t} = \bar{X}^{t-\Delta t} + 2\Delta t \dot{X}_{adv}\left(X^t\right) + 2\Delta t \dot{X}_{dif}\left(\hat{X}^{t+\Delta t}\right), \tag{2.74}$$

where $\dot{X}_{adv}$ is the advection term etc., and $\dot{X}_{dif}$ is the horizontal diffusion term.

$\hat{X}^{t+\Delta t}$ is then corrected for diffusion ($\dot{X}_{dis}$ for p-surface correction and the heat of friction) and physical processes ($\dot{X}_{phy}$), yielding $X^{t+\Delta t}$.

$$X^{t+\Delta t} = \hat{X}^{t+\Delta t} + 2\Delta t \dot{X}_{dis}\left(\hat{X}^{t+\Delta t}\right) + 2\Delta t \dot{X}_{phy}\left(\hat{X}^{t+\Delta t}\right) \tag{2.75}$$

To damp numerical modes, a time filter (Williams, 2009) is applied to leap-frog method at every steps. The time filter is given below, where terms with over bars are filtered.

$$\bar{\bar{X}}^t = \bar{X}^t + \nu\alpha[\bar{\bar{X}}^{t-\Delta t} - \bar{X}^t + X^{t+\Delta t}], \tag{2.76}$$

$$\bar{X}^{t+\Delta t} = X^{t+\Delta t} + \nu(1-\alpha)[\bar{\bar{X}}^{t-\Delta t} - 2\bar{X}^t + X^{t+\Delta t}], \tag{2.77}$$

where $\nu = 0.05$ and $\alpha = 0.5$.

2.4.2 Semi-Implicit Time Integration

Basically, the leap frog is used for the dynamic processes, but the trapezoidal implicit scheme is used for some terms. For a vector quantity $\mathbf{q}$, let us write the value at t as $\mathbf{q}$, the value at $t + \Delta t$ as $\mathbf{q}^+$, and the value at $t - \Delta t$ as $\mathbf{q}^-$. Then, in the trapezoidal implicit scheme, the time change term is evaluated for $(\mathbf{q}^+ + \mathbf{q}^-)/2$, instead of $\mathbf{q}$ used in the simple leap forg method. We now divide $\mathbf{q}$ into two time varying terms, one $(\mathcal{A})$ for the leap forg method and the other $(\mathcal{B})$ for the trapezoidal implicit method. We assume that $(\mathcal{A})$ is nonlinear to $\mathbf{q}$, while $(\mathcal{B})$ is linear. In other words,

$$\mathbf{q}^+ = \mathbf{q}^- + 2\Delta t \mathcal{A}(\mathbf{q}) + 2\Delta t B(\mathbf{q}^+ + \mathbf{q}^-)/2, \tag{2.78}$$

where $(\mathcal{B})$ is a square matrix. Defining $\Delta\mathbf{q} \equiv \mathbf{q}^+ - \mathbf{q}$, we get

$$(I - \Delta t B)\Delta\mathbf{q} = 2\Delta t \left(\mathcal{A}(\mathbf{q}) + B\mathbf{q}\right). \tag{2.79}$$

This can be easily solved by matrix operations.

2.4.3 Applying the Semi-Implicit Time Integration

Here, we apply the semi-implicit method and treat terms associated with linear gravity waves as implicit, which allows us to increase the time step Δt.

We divide the basic equation into a linear gravity wave term ($T = \bar{T}_k$) with a static field as the basic field and other terms (with the indices NG). Using a vector representation for the vertical direction ($\mathbf{D} = \{D_k\}$ and $\mathbf{T} = \{T_k\}$),

$$\frac{\partial \pi}{\partial t} = \left(\frac{\partial \pi}{\partial t}\right)_{NG} - \mathbf{C} \cdot \mathbf{D}, \tag{2.80}$$

$$\frac{\partial \mathbf{D}}{\partial t} = \left(\frac{\partial \mathbf{D}}{\partial t}\right)_{NG} - \nabla_\eta^2(\mathbf{\Phi}_S + \underline{W}\mathbf{T} + \mathbf{G}\pi) - \mathcal{D}_M\mathbf{D}, \tag{2.81}$$

$$\frac{\partial \mathbf{T}}{\partial t} = \left(\frac{\partial \mathbf{T}}{\partial t}\right)_{NG} - \underline{h}\mathbf{D} - \mathcal{D}_H\mathbf{T}. \tag{2.82}$$

Here, the non-gravitational wave term is

$$\left(\frac{\partial \pi}{\partial t}\right)^{NG} = -\sum_{k=1}^{K} \mathbf{v}_k \cdot \nabla\pi\Delta B_k, \tag{2.83}$$

$$\frac{(m\dot{\eta})_{k-1/2}^{NG}}{p_s} = -B_{k-1/2}\left(\frac{\partial \pi}{\partial t}\right)^{NG} - \sum_{l=k}^{K} \mathbf{v}_l \cdot \nabla\pi\Delta B_l, \tag{2.84}$$

$$\left(\frac{\partial D}{\partial t}\right)^{NG} = \frac{1}{a\cos\varphi}\frac{\partial(A_u)_k}{\partial\lambda} + \frac{1}{a\cos\varphi}\frac{\partial}{\partial\varphi}(A_v\cos\varphi)_k - \nabla_\eta^2\hat{E}_k - \mathcal{D}(D_k), \tag{2.85}$$

$$\left(\frac{\partial T_k}{\partial t}\right)^{NG} = -\frac{1}{a\cos\varphi}\frac{\partial u_k T_k'}{\partial\lambda} - \frac{1}{a\cos\varphi}\frac{\partial}{\partial\varphi}(v_k T_k'\cos\varphi) + \hat{H}_k - \mathcal{D}(T_k), \tag{2.86}$$

$$\begin{aligned}
\hat{H}_k = {}& T_k'D_k - \left[\frac{(m\dot{\eta})_{k-1/2}}{p_s}\frac{\hat{T}_{k-1/2} - T_k}{\Delta\sigma_k} + \frac{(m\dot{\eta})_{k+1/2}}{p_s}\frac{T_k - \hat{T}_{k+1/2}}{\Delta\sigma_k}\right] \\
& + \hat{\kappa}_k T_{v,k}\mathbf{v}_k \cdot \nabla\pi \\
& - \frac{\alpha_k}{\Delta\sigma_k}T_{v,k}\sum_{l=k}^{K}\mathbf{v}_l \cdot \nabla\pi\Delta B_l - \frac{\beta_k}{\Delta\sigma_k}T_{v,k}\sum_{l=k+1}^{K}\mathbf{v}_l \cdot \nabla\pi\Delta B_l \\
& - \frac{\alpha_k}{\Delta\sigma_k}T_{v,k}'\sum_{l=k}^{K}D_l\Delta\sigma_l - \frac{\beta_k}{\Delta\sigma_k}T_{v,k}'\sum_{l=k+1}^{K}D_l\Delta\sigma_l + \frac{Q_k + (Q_{diff})_k}{C_p},
\end{aligned} \tag{2.87}$$

$$\hat{E}_k = E_k + \sum_{k=1}^{K}W_{kl}(T_{v,l} - T_l), \tag{2.88}$$

where the vector and matrix of the gravitational wave term (underlined) are

$$C_k = \Delta\sigma_k, \tag{2.89}$$

$$W_{kl} = C_p\alpha_l\delta_{k\geq l} + C_p\beta_l\delta_{k-1\geq l}, \tag{2.90}$$

$$G_k = R\bar{T}, \tag{2.91}$$

$$h_{kl} = \frac{\bar{T}}{\Delta\sigma_k}\left[\alpha_k\Delta\sigma_l\delta_{k\geq l} + \beta_k\Delta\sigma_l\delta_{k+1\leq l}\right]. \tag{2.92}$$

Here, $\delta_{k\leq l}$ is 1 if $k \leq l$ is valid and 0 otherwise.

We now use the following expressions for time differences:

$$\delta_t X \equiv \frac{1}{2\Delta t}\left(X^{t+\Delta t} - X^{t-\Delta t}\right), \tag{2.93}$$

$$\overline{X}^t \equiv \frac{1}{2}\left(X^{t+\Delta t} + X^{t-\Delta t}\right)$$

$$= X^{t-\Delta t} + \delta_t X \Delta t. \tag{2.94}$$

Then, applying the semi-implicit method to the system of equations, we get

$$\delta_t \pi = \left(\frac{\partial \pi}{\partial t}\right)_{NG} - \mathbf{C} \cdot \overline{\mathbf{D}}^t, \tag{2.95}$$

$$\delta_t \mathbf{D} = \left(\frac{\partial \mathbf{D}}{\partial t}\right)_{NG} - \nabla_\eta^2(\mathbf{\Phi}_S + \underline{W}\overline{\mathbf{T}}^t + \mathbf{G}\overline{\pi}^t) - \mathcal{D}_M(\mathbf{D}^{t-\Delta t} + 2\Delta t\delta_t \mathbf{D}), \tag{2.96}$$

$$\delta_t \mathbf{T} = \left(\frac{\partial \mathbf{T}}{\partial t}\right)_{NG} - \underline{h}\overline{\mathbf{D}}^t - \mathcal{D}_H(\mathbf{T}^{t-\Delta t} + 2\Delta t\delta_t \mathbf{T}). \tag{2.97}$$

Thus,

$$\left\{(1 + 2\Delta t\mathcal{D}_H)(1 + 2\Delta t\mathcal{D}_M)\underline{I} - (\Delta t)^2(\underline{W}\ \underline{h} + (1 + 2\Delta t\mathcal{D}_M)\mathbf{G}\mathbf{C}^T)\nabla_\eta^2\right\}\overline{\mathbf{D}}^t$$

$$= (1 + 2\Delta t\mathcal{D}_H)(1 + \Delta t\mathcal{D}_M)\mathbf{D}^{t-\Delta t} + \Delta t\left(\frac{\partial \mathbf{D}}{\partial t}\right)_{NG}$$

$$- \Delta t\nabla_\eta^2\left\{(1 + 2\Delta t\mathcal{D}_H)\mathbf{\Phi}_S + \underline{W}\left[(1 + 2\Delta t\mathcal{D}_H)\mathbf{T}^{t-\Delta t} + \Delta t\left(\frac{\partial \mathbf{T}}{\partial t}\right)_{NG}\right]\right\}$$

$$+ (1 + 2\Delta t\mathcal{D}_H)\mathbf{G}\left[\pi^{t-\Delta t} + \Delta t\left(\frac{\partial \pi}{\partial t}\right)_{NG}\right]\right\}. \tag{2.98}$$

Since the spherical harmonic expansion is used, we can rewrite ∇_η^2 as the following:

$$\nabla_\eta^2 = -\frac{n(n+1)}{a^2}, \tag{2.99}$$

which enables us to solve the above equations for $\overline{\mathbf{D}_n^m}^t$. Then, using (2.95), (2.97) and $D^{t+\Delta t} = 2\overline{\mathbf{D}}^t - D^{t-\Delta t}$, we can obtain the value of prognostic variables $\hat{X}^{t+\Delta t}$ at $t + \Delta t$.

2.4.4 Time Scheme Properties and Requiments for Time Steps

Let us consider solving the advection equation with the leap-frog method:

$$\frac{\partial X}{\partial t} = c\frac{\partial X}{\partial x}. \tag{2.100}$$

Assuming $X = X_0 \exp(ikx)$, the descretized form of the above equation becomes:

$$X^{n+1} = X^{n-1} + 2ik\Delta t X^n. \tag{2.101}$$

Assuming X evolves exponentially, we can define λ such that

$$\lambda = X^{n+1}/X^n = X^n/X^{n-1}, \tag{2.102}$$

$$\lambda^2 = 1 + 2ikc\Delta t\lambda . \tag{2.103}$$

Defining $p \equiv kc\Delta t$, the solution becomes:

$$\lambda = -ip \pm \sqrt{1 - p^2}. \tag{2.104}$$

The absolute value of those solutions are

$$|\lambda| = \begin{cases} 1 & |p| \leq 1 \\ p \pm \sqrt{p^2 - 1} & |p| > 1 \end{cases} \tag{2.105}$$

and in the case of $|p| > 1$, we get $|\lambda| > 1$, and the absolute value of the solution increases exponentially with time. This indicates that the computation is unstable.

In the case of $|p| \leq 1$, however, the calculation is neutral since the value of $|\lambda| = 1$. However, there are two solutions to λ, one of which, when set to $\Delta t \to 1$, leads to $\lambda \to 1$, while the other leads to $\lambda \to -1$, which indicates an osscilating solution. This mode is called "computational mode" and is one of the problems of the leap frog method. This mode can be damped by applying a time filter described later.

Given the horizontal grid spacing Δx, the maximum value of k becomes

$$\max k = \frac{\pi}{\Delta x}. \tag{2.106}$$

Then, the condition $|p| = kc\Delta t \leq 1$ requires

$$\Delta t \leq \frac{\Delta x}{\pi c}. \tag{2.107}$$

In case of a spectral model, using the Earth's radius a and the maximum wavenumber N, the requirement becomes

$$\Delta t \leq \frac{a}{Nc}, \tag{2.108}$$

which is a condition for the numerical stability.

To guarantee the stability of the integration, one needs to take the time step Δt smaller than that required by the fastest-propagating mode. If the semi-implicit scheme is not used, the propagation speed of gravity waves, which can be as fast as 300 m/s, sets the criterion for stability. With the gravity waves taken account of by the semi-implicit method, however, the fastest mode usually becomes the maximum easterly wind $U_{\max}$. Therefore,

$$\Delta t \leq \frac{a}{NU_{max}}. \tag{2.109}$$

In practice, this is multiplied by a factor smaller than 1 for further safety.

2.4.5 Handling of the Initiation of Time Integration

When starting from an initial condition that is not calculated by MIROC 6.0 itself, it is not possible to give values of all prognostic variables at two time steps t and $t - \Delta t$ consistently with the model dynamics. However, giving inconsistent values for $t - \Delta t$ results in a large computation mode.

To avoid this, a special procedure is followed at the initiation of time integration. Firstly, assuming $X^{\Delta t/4} = X^0$, a 1/4-step integration is performed to obtain $X^{\Delta t/2}$:

$$X^{\Delta t/2} = X^0 + \Delta t/2 \dot{X}^{\Delta t/4} = X^0 + \Delta t/2 \dot{X}^0. \tag{2.110}$$

Then, a 1/2-step integration is performed to yield $X^{\Delta t}$:

$$X^{\Delta t} = X^0 + \Delta t \dot{X}^{\Delta t/2}. \tag{2.111}$$

Finally, in the normal time step,

$$X^{2\Delta t} = X^0 + 2\Delta t \dot{X}^{\Delta t}. \tag{2.112}$$

From here on, the leap-frog method is executed in the usual manner.

2.5   Tracer Advection Scheme

2.5.1   Introduction of Tracer Advection Scheme

MIROC6 adopts a spectral method based on Spherical harmonic expansion to dynamic core. The spectral method is an excellent method, but it has some drawbacks.

1. Because of Gibbs phenomenon, noisy oscillations are produced when representing a non-smooth field.

2. Associated with Gibbs phenomenon, negative value may occure on grids where they are not supposed to such as, eg., specific humidity.

3. Global conservation of conservative quantity is good enough, but local conservation does not always hold.

4. The property that information is transmitted from upstream to downstream is not always satisfied. In spherical model, information travels instantly to the other side of the world.

Despite of these disadvantages, MIROC has adoptted spectral method as dynamic core. Gibbs phenomenon usually doesn't cause any problems. However, when describing the transport of materials with strong discontinuity, the noisy oscillation and unexpected negative values sometimes appear. For example, water vapor in polar region and the stratosphere often shows discontinuous distribution because there is very small amount of water vapor. Tracers such as aerosols are also distributed locally and often show large discontinuity. These tracers are easy to affected by Gibbs phenomenon. Therefore, in MIROC6, water vapor transport and tracer transport are calculated using a flux form semi-Lagrange (FFSL) scheme (Lin and Rood 1996) instead of using the spectral method.

   Merits of this scheme are described below.

1. Gibbs phenomenon doesn't occur because it's based on gridpoint method. Therefore, non-smooth fields can be represented with better accuracy.

2. Negative values of tracer quantity can be avoided even in unsmooth fields.

3. No new extreme values are created.

4. Information is transmitted from upstream to downstream.

5. Conservation is satisfied locally and globally.

6. Problems which is induced by narrow grid range in polar region can be avoided.

In the next section, the principle of the tracer advection scheme is introduced in detail, and in the following section, we describe the actual implementation of the tracer advection scheme.

2.5.2   Principle of the Tracer Advection Scheme

2.5.2.1   Transport Equation in Flux Form

   The winds and the tracer distributions are staggered in the Arakawa C-grid (Mesinger and Arakawa 1976). As example, three dimension advection equation in (x,y,p) rectangukar coordinate system is given as follows.

$$\frac{\partial q}{\partial t} = -u\frac{\partial q}{\partial x} - v\frac{\partial q}{\partial y} - \omega\frac{\partial q}{\partial p} \tag{2.113}$$

28

Here, q is the amount of tracer (ex. specific humidity for water vapor), u, v is zonal and meridional velocity respectively. By substituting continuity equation to this, we get the advection equation in flux form.

$$\frac{\partial q}{\partial t} = -\frac{\partial}{\partial x}(uq) - \frac{\partial}{\partial y}(vq) - \frac{\partial}{\partial p}(\omega q) = -\frac{\partial}{\partial x}F^x - \frac{\partial}{\partial y}F^y - \frac{\partial}{\partial p}F^p \qquad (2.114)$$

Discretizing by $x = x_i(i = 1, 2, 3...), y = y_j(j = 1, 2, 3...), p = p_k(k = 1, 2, 3...)$, the advection equation is rewritten as

$$\frac{\partial q_{i,j,k}}{\partial t} = \frac{1}{\Delta x_{i,j,k}}(F^x_{i-\frac{1}{2},j,k} - F^x_{i+\frac{1}{2},j,k}) + \frac{1}{\Delta y_{i,j,k}}(F^y_{i,j-\frac{1}{2},k} - F^y_{i,j+\frac{1}{2},k}) + \frac{1}{\Delta p_{i,j,k}}(F^p_{i,j,k-\frac{1}{2}} - F^p_{i,j,k+\frac{1}{2}})$$
$$(2.115)$$

Here, $F^x_{i-\frac{1}{2},j,k}$ is the flux in x direction at boundary between (i, j, k) and $(i - 1, j, k)$, $\Delta x_{i,j,k}$ is x-direction width of grid represented as (i, j, k). This flux formed equation automatically satisfies the conservation law. The accuracy of the scheme depends on how $F^x_{i-\frac{1}{2},j,k}$ is chosen. Next, how $F^x_{i-\frac{1}{2},j,k}$ is determind in MIRIOC6 is explianed in one dimension in x-direction, for simplicity.

2.5.3   The Piecewise Parobolic Method Scheme

In semi-Lagrange scheme, the flux at point $x_{i+\frac{1}{2}}$ at time t is calculated by using q at point $x_{i+\frac{1}{2}} - u\Delta t$ at time $t - \Delta t$. The velocity $u = u(t)$ is used assuming constant locally during this period, and q at time $t - \Delta t$ are used. If CFL condition ($|\frac{u\Delta t}{\Delta x}| < 1$) is satisfied and $u_{i+\frac{1}{2}} > 0$, $x_{i+\frac{1}{2}} - u\Delta t$ is at a point inside grid i.

As the value of q at point $x_{i+\frac{1}{2}} - u\Delta t$, q_i, which is the average value of point i, can be chosen, assuming that q is constant in the grid.

However, the value of q shows large discontinuity at $i + \frac{1}{2}$, which is the boundary between grid i and $i + 1$ in this assumption. This discontinuity strengthens numerical viscosity, and is unwanted for numerical experiments. Therefore, we want to give some kind of distribution to q, which is assumed to be constant in a grid, in order to eliminate the discontinuity and enable us to calculate q at $x_{i+\frac{1}{2}} - u\Delta t$ by interpolation. Given distribution must be satisfied a condition as follows.

$$q_i = \frac{1}{\Delta x_i} \int_{x_{i-\frac{1}{2}}}^{x_{i+\frac{1}{2}}} q(x)dx \qquad (2.116)$$

The old editions of MIROC adoptted van Leer method, in which interpolation function is a linear function, but MIROC6 adopts The Piecewise Parobolic Method (PPM) scheme (Colella and Woodward 1984) , in which interpolation function is a quadrative function (Fig.2). The FFSL scheme which adopts PPM scheme is called FFSL-3 (Lin and Rood 1996).

In PPM scheme, the distribution is determined as follows.

$$q(x) = q_{L,i} + \xi(\Delta q_i + q_{6,i}(1 - \xi))$$
$$\xi = \frac{x - x_{i-\frac{1}{2}}}{\Delta x_i}, x_{i-\frac{1}{2}} \le x \le x_{i+\frac{1}{2}} \qquad (2.117)$$

Here, $q_{L,i}$ is defined as $\lim_{x \to x_{i+\frac{1}{2}}} = q_{L,i}$. $q_{R,i}$ is defined as $\lim_{x \to x_{i+\frac{1}{2}}} = q_{R,i}$ as well. In PPM scheme, q is continuous at boundary $i + \frac{1}{2}$, therefore $q_{L,i+1} = q_{R,i} = q_{i+\frac{1}{2}}$ is hold. In addition,

$$\Delta q_i = q_{R,i} - q_{L,i}, \qquad q_{6,i} = 6(q_i - \frac{1}{2}(q_{L,i}) + q_{R,i}) \qquad (2.118)$$
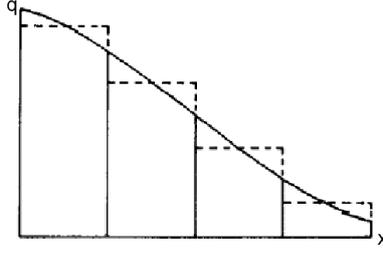
Figure 2: The image of interpolation function in The piecewise parobolic method (PPM) scheme. The interpolation function is in the solid line, the grid mean value is in the dot line.

For calculationg $q_{i+\frac{1}{2}}$ by interpolation, a finite integration of q given as follows is introduced.

$$A(x) = \int^x q(x')dx' \tag{2.119}$$

At boundary of grid,

$$A(x_{i+\frac{1}{2}}) = A_{i+\frac{1}{2}} = \sum_{k \leq i} q_k \Delta x_k \tag{2.120}$$

$q_{i+\frac{1}{2}}$ is calculated by discretization of $q_{i+\frac{1}{2}} = dA/dx|_{x_{i+\frac{1}{2}}}$ by using $(A_{j+k+\frac{1}{2}}, x_{j+k+\frac{1}{2}})$, $k = 0, \pm 1, \pm 2$. Specifically, $q_{i+\frac{1}{2}}$ is calculated as follows.

$$
\begin{aligned}
q_{i+\frac{1}{2}} = & q_i + \Delta x_i \frac{q_{i+1} - q_i}{\Delta x_{i+1} + \Delta x_i} + \frac{1}{\sum_{k=i-1}^{i+2} \Delta x_k} \\
& \times \left[\frac{2\Delta x_i \Delta x_{i+1}}{\Delta x_{i+1} + \Delta x_i} \left(\frac{\Delta x_i + \Delta x_{i-1}}{\Delta x_{i+1} + 2\Delta x_i} - \frac{\Delta x_{i+2} + \Delta x_{i+1}}{2\Delta x_{i+1} + \Delta x_i} \right)(q_{i+1} - q_i) \right. \\
& \left. - \Delta x_i \frac{\Delta x_i + \Delta x_{i-1}}{\Delta x_{i+1} + 2\Delta x_i} \delta q_{i+1} + \Delta x_{i+1} \frac{\Delta x_{i+2} + \Delta x_{i+1}}{2\Delta x_{i+1} + \Delta x_i} \delta q_i \right]
\end{aligned}
\tag{2.121}
$$

In case the grid width is equal in all grids, Eq.(2.121) can be simply rewritten as

$$q_{i+\frac{1}{2}} = \frac{1}{2}(q_{i-1} + qi) - \frac{1}{6}(\delta q_i - \delta q_{i-1}) \tag{2.122}$$

Here, δq_i is given as

$$\delta q_i = \frac{\Delta x_i}{\Delta x_{i-1} + \Delta x_i + \Delta x_{i+1}} \left[\frac{2\Delta x_{i-1} + \Delta x_i}{\Delta x_{i+1} + \Delta x_i}(q_{i+1} - q_i) + \frac{\Delta x_i + 2\Delta x_{i+1}}{\Delta x_{i-1} + \Delta x_i}(q_i - q_{i-1}) \right] \tag{2.123}$$

However, in this case, the interpolation function may have extremes in the grid and may not satisfy monotonicity. In order to avoid such a situation, $q_{i+\frac{1}{2}}$ should be between q_i as q_{i+1}, and δq_i is modified as follows for that.

$$
\begin{aligned}
\delta_m q_i &= \min(|\delta q_i|, 2|q_i - q_{i-1}|, |q_{i+1} - q_i|) &\quad& \text{if} \quad (q_{i+1} - q_i)(q_i - q_{i-1}) > 0, \\
&= 0 &\quad& \text{otherwise}
\end{aligned}
\tag{2.124}
$$

This δq_i is used in Eq.(2.121) to calculate $q_{i+\frac{1}{2}}$.

When $q(x)$ is interpolated as Eq.(2.117), by using Courant number defined as

$$C = \frac{u_{i+\frac{1}{2}} \Delta t}{\Delta x_{i+1}} \tag{2.125}$$

flux $F^x_{i+\frac{1}{2}}$ is wriiten as follows.

$$
F^x_{i+\frac{1}{2}} = \begin{cases}
u_{i+\frac{1}{2}}[q_{R,i} - \frac{C}{2}(\Delta q_i - (1 - \frac{2}{3}C)q_{6,i})] & (u_{i+\frac{1}{2}} \geq 0) \\
u_{i+\frac{1}{2}}[q_{L,i+1} + \frac{C}{2}(\Delta q_{i+1} + (1 - \frac{2}{3}C)q_{6,i+1})] & (u_{i+\frac{1}{2}} \leq 0)
\end{cases}
\tag{2.126}
$$

30

2.5.3.1 Devices for Taking Long Time Steps

The above argument is stable only if $C < 1$ When the grid method is adapted to spherical coordinate, Δx is very small in polar region. Therefore, we have to take very small Δt to satisfy CFL condition. The special treatment when $C > 1$ for taking larger Δt are described below. Although this method is used for any grid widths, in this subsection we assume that Δx does not depend on i for simplicity.

Courant number can be divided into a integral fraction and a decimal fraction.

$$C = I_C + \hat{C}, \quad I_C : \text{an integer fraction}, \quad -0.5 \le \hat{C} \le 0.5 \tag{2.127}$$

When $I_C > 0$

$$F^x_{i-\frac{1}{2}} = F^x_{i-I_C+\frac{1}{2}}{}^{\hat{}} + \sum_{i'=i+1-I_C}^{i} q_{i'} \frac{\Delta x_i}{\Delta t} \tag{2.128}$$

When $I_C < 0$

$$F^x_{i-\frac{1}{2}} = F^x_{i+|I_C|+\frac{1}{2}}{}^{\hat{}} + \sum_{i'=i+1}^{i+|I_C|} q_{i'} \frac{\Delta x_i}{\Delta t} \tag{2.129}$$

Where $F^x_{i-I_C+\frac{1}{2}}{}^{\hat{}}$ is the flux of point $(i - I_C + \frac{1}{2})$ calculated by using $\hat{C}$.

As indicated above, in the case the fluid moves in multiple grids during Δt, we can avoid instability of numerical calculation by evaluating the flux using the quantity $q_{i'}$ corresponding to each grids passed. In actual, these argument is applied only to zonal flux, which can break CFL condition.

2.5.3.2 The Treatment of Cross Terms

In the case velocity of the fluid is not only in the x-direction or y-direction, only adding the flux contributions in the x- and y-directions together underestimate the effect of diagonal advection. To take these cross term into considering, the following procedure is taken. Here, we discuss this in two-dimensional space, not in one-dimensional.

When calculating x-direction flux $F^x_{i+\frac{1}{2},j}$, upstream value of q in y-direction is used as value of q. That is expressed by the following equation.

$$q^y_{i,j} = \frac{1}{2}q(x_i, y_i - v_{i,j}\Delta t) + q_{i,j} \tag{2.130}$$

Here, $q(x_i, y_i - v_{i,j}\Delta t)$ is calculated by linear interpolation of the two nearest grid points. In the same way, when calculating y-direction flux $F^x_{i+\frac{1}{2},j}$,

$$q^x_{i,j} = \frac{1}{2}q(x_i - u_{i,j}\Delta t, y_i) + q_{i,j} \tag{2.131}$$

is used as q.

In the case of three dimensional tracer advection, this procedure is conducted in two dimension.

2.5.4 Actual Tracer Advection Scheme in MIROC6

In this subsection, the procedure implemented in MIROC6 of the tracer advection scheme is described. Although MIROC6 adopts σ-p hybrid coordinate as vertical coordinate, the tracer advection scheme is largely based on σ coordinate because previous version of MIROC adopted σ coordinate. Therefore, firstly the procedure under σ coordinate system is described. After this, the changes in the hybrid coordinate system from the σ coordinate system is described.

2.5.4.1 σ-Coordinate

The transport equation in σ coordinate on the sphere is expressed as

$$
\begin{aligned}
\frac{\partial P^S q}{\partial t} &= -\frac{1}{a\cos\varphi}\frac{\partial}{\partial\lambda}(P^S u q) - \frac{1}{a\cos\varphi}\frac{\partial}{\partial\varphi}(P^S v q \cos\varphi) - \frac{\partial}{\partial\sigma}(P^S\dot\sigma q) \\
&= \frac{1}{a\cos\varphi}\frac{\partial}{\partial\lambda}(F^\lambda) - \frac{1}{a\cos\varphi}\frac{\partial}{\partial\varphi}(F^\varphi) - \frac{\partial}{\partial\sigma}(F^\sigma)
\end{aligned}
\tag{2.132}
$$

P^S is surface pressure, q is quantity of tracers. Continuity equation is given by considering the case of $q = 1$.

$$
\frac{\partial P^S}{\partial t} = -\frac{1}{a\cos\varphi}\frac{\partial}{\partial\lambda}(P^S u) - \frac{1}{a\cos\varphi}\frac{\partial}{\partial\varphi}(P^S v \cos\varphi) - \frac{\partial}{\partial\sigma}(P^S\dot\sigma)
\tag{2.133}
$$

Assuming that grid is equally spaced in zonal direction, the transport equation is discretized as follows.

$$
\frac{\partial P^S_{,i,j,k}q_{i,j,k}}{\partial t} = \frac{1}{\Delta D_{j,k}}[(G^\lambda_{i-\frac{1}{2},j,k}-G^\lambda_{i+\frac{1}{2},j,k})+(G^\varphi_{i,j-\frac{1}{2},k}-G^\varphi_{i,j+\frac{1}{2},k}))+(G^\sigma_{i,j,k-\frac{1}{2}}-G^\sigma_{i,j,k+\frac{1}{2}})]
\tag{2.134}
$$

Here,

$$
G^\lambda_{i-\frac{1}{2},j,k} = F^\lambda_{i-\frac{1}{2},j,k}\Delta y_j\Delta\sigma_k = (P^S u q)_{i-\frac{1}{2},j,k}\Delta y_j\Delta\sigma_k
\tag{2.135}
$$

$$
G^\varphi_{i,j-\frac{1}{2},k} = F^\varphi_{i,j-\frac{1}{2},k}\Delta x_{j-\frac{1}{2}}\Delta\sigma_k = (P^s v q)_{i,j-\frac{1}{2},k}\Delta x_{j-\frac{1}{2}}\Delta\sigma_k
\tag{2.136}
$$

$$
G^\sigma_{i,j,k-\frac{1}{2}} = F^\eta_{i,j,k-\frac{1}{2}}\Delta x_j\Delta y_j = (P^S\dot\sigma q)_{i,j,k-\frac{1}{2}}\Delta x_j\Delta y_j
\tag{2.137}
$$

And

$$
\Delta D_{j,k} = a\cos\varphi_j\Delta\lambda\Delta\varphi_j\Delta\sigma_k, \quad \Delta x_j = a\cos\varphi_j\Delta\lambda, \quad \Delta y_j = a\Delta\varphi_j
\tag{2.138}
$$

This flux form equation ensure the conservation.

For the calculation of the time-averaged mass flux across the cell boundary, the winds and the tracer distributions are staggered in the Arakawa C-grid (Mesinger and Arakawa 1976). The horizontal winds at the cell boundary, $u_{i-\frac{1}{2},j,k}, v_{i-\frac{1}{2},j,k}$, are reconstructed by using the mass convergence field in the spectral model and the discretized continuity eqution:

$$
\frac{\partial P^S_{i,j,k}}{\partial t} = \frac{1}{\Delta D_{j,k}}[(V^\lambda_{i-\frac{1}{2},j,k}-V^\lambda_{i+\frac{1}{2},j,k})+(V^\varphi_{i,j-\frac{1}{2},k}-V^\varphi_{i,j+\frac{1}{2},k}))+(V^\sigma_{i,j,k-\frac{1}{2}}-V^\sigma_{i,j,k+\frac{1}{2}})]
\tag{2.139}
$$

Here, $V^\lambda_{i-\frac{1}{2},j,k}, V^\varphi_{i,j-\frac{1}{2},k}, V^\sigma_{i,j,k-\frac{1}{2}}$ denote zonal, meridional, and vertical mass-weighted wind at the cell boundary, rspectively. That is,

$$
V^\lambda_{i-\frac{1}{2},j,k} = (P^S u)_{i-\frac{1}{2},j,k}\Delta y_j\Delta\sigma_k
\tag{2.140}
$$

$$
V^\varphi_{i,j-\frac{1}{2},k} = (P^S v)_{i,j-\frac{1}{2},k}\Delta x_{j-\frac{1}{2}}\Delta\eta_k
\tag{2.141}
$$

$$
V^\sigma_{i,j,k-\frac{1}{2}} = (P^S\dot\sigma)_{i,j,k-\frac{1}{2}}\Delta x_j\Delta y_j
\tag{2.142}
$$

$\Delta D_{j,k}$ denotes the cell volume, and $\Delta x_j, \Delta y_j$, and $\Delta\sigma_k$ denote zonal, meridional and vertical width of the cell, respectively. That is $\Delta D_{j,k} = a\cos\varphi_j\Delta\lambda\Delta\varphi_j\Delta\sigma$, $\Delta x_j = a\cos\varphi_j\Delta\lambda$ and $\Delta y_j = a\Delta\varphi_j$.

The following are the procedure for the calculation of tracer advection in the staggering-grided horizontal and vertical wind fields:

1. Surface pressure $P^S(t + \Delta t)$ and horizontal wind $\mathbf{v}(\mathbf{t} + \boldsymbol{\Delta}\mathbf{t})$ are predicted in the spectral model.

2. The horizontal component of mass flux divergence at time step t is calculated by using spherical harmonics. The mass fluxes at time step t are reconstructed from the values at $t + \Delta t$ and $t - \Delta t$ because MIROC applies semi-implicit scheme for the time-integration of surface pressure. Zonal and meridional component of mass flux divergence are:

$$C^x = -\frac{1}{a\cos\varphi}\frac{\partial}{\partial\lambda}(P^s u), \quad C^y = -\frac{1}{a\cos\varphi}\frac{\partial}{\partial\lambda}(P^s v \cos\varphi) \tag{2.143}$$

3. By using C_x and C_y, $V^\lambda, V^\varphi, V^\sigma$ are calculated as follows.

$$V^\lambda_{i-\frac{1}{2},j,k} - V^\lambda_{i+\frac{1}{2},j,k} = C^x_{i,j,k}\Delta D_{j,k}, \quad V^\lambda_{i,j-\frac{1}{2},k} - V^\lambda_{i,j+\frac{1}{2},k} = C^y_{i,j,k}\Delta D_{j,k} \tag{2.144}$$

The boundry conditions are $V^\varphi = 0$ at the North Pole and South Pole, $\sigma = 1$ at surface and $V^\sigma = 0$ at $\sigma = 0$. The condition for $V^\lambda = 0$ is:

$$\sum_i V^\lambda_{i-\frac{1}{2},j,k} = \sum_i P^S_{i,j,k} u_{i,j,k}\Delta y_j \Delta\sigma_k \tag{2.145}$$

That means zonal mean of zonal mass transport is equal to that in the spectral model grid. Here, the following equation must be satisfied for boundary condition $V^\varphi = 0$ at the North Pole and the South Pole.

$$\sum_j C^y_{i,j,k}\Delta D_{j,k} = 0 \tag{2.146}$$

However, this is not always satisfied (On the other hand, $\sum_i \sum_j C^y_{i,j,k}\Delta D_{j,k} = 0$ is valid within numerical error.).

In order to satisfy the boundary condition, the following correction is made.

$$C^y_{i,j,k} \leftarrow C^y_{i,j,k} - \delta C, \quad C^y_{i,j,k} \leftarrow C^x_{i,j,k} + \delta C \tag{2.147}$$

Here, $\delta C = \sum_j C^y_{i,j,k}\Delta D_{j,k} / \sum_j \Delta D_{j,k}$. Vertical velocity V^η is obtained by using

$$\frac{\partial P^S_{i,j,k}}{\partial t}\sum_k \Delta D_{j,k} = \sum_k (C^x_{i,j,k} + C^y_{i,j,k}) \tag{2.148}$$

(The contents so far are in [TRACEG] of dtrcr.F. The rest of the content is in [GTRACE] of dtrcr.F.)

4. $G^\lambda, G^\varphi, G^\sigma$ are calculated by PPM scheme from $V^\lambda, V^\varphi, V^\sigma$.

5. $P^s_{i,j,k}q_{i,j,k}$ at time step $t + \Delta t$ is calulated by integration of Eq.(2.134) by leap frog method from $G^\lambda, G^\varphi, G^\sigma$.

6. $q_{t+\Delta t}$ is calculated by dividing $(P^s q)_{t+\Delta t}$ by $P^s_{t+\Delta t}$. There is small quantity of difference between $P^s_{t+\Delta t}$ from Eq. (2.148) and $P^s_{t+\Delta t}$ in the spectral model, because semi-implicit time integration scheme is applied. $P^s_{t+\Delta t}$ from Eq. (2.148) is applied at present for the consistency of mass advection. Mass Conservation is not strictly satisfied because of the discrepancy between the surface pressure in the spectral model and from $P^s_{t+\Delta t}$ Eq. (2.148).

2.5.4.2 σ-p Hybrid Coordinate

The transport equation in η coordinate ($\sigma - p$ hybrid coordinate) on the sphere is:

$$
\begin{aligned}
\frac{\partial mq}{\partial t} &= -\frac{1}{a\cos\varphi}\frac{\partial}{\partial\lambda}(muq) - \frac{1}{a\cos\varphi}\frac{\partial}{\partial\varphi}(mvq\cos\varphi) - \frac{\partial}{\partial\eta}(m\dot\eta q) \\
&= \frac{1}{a\cos\varphi}\frac{\partial}{\partial\lambda}(F^\lambda) - \frac{1}{a\cos\varphi}\frac{\partial}{\partial\varphi}(F^\varphi) - \frac{\partial}{\partial\eta}(F^\eta) \qquad (2.149)
\end{aligned}
$$

Here, m corresponds to the density of the coordinate and is defined as $m = \frac{\partial p}{\partial\eta}$. if you look at Eq. (2.132), you can find that difference of σ coordinate and η coordinate is only that P^S replaces m. The actual tracer advection in η coordinate is mostly the same as σ coordinate.

In the scheme in η coordinate, the following variables are calculated in the same way as the way $G^\lambda, G^\varphi, G^\eta$ is calculated in σ coordinate, except $\Delta\sigma$ replaces with $\Delta\eta$ and $\dot\sigma$ replaces with $\dot\eta$.

$$
G'^\lambda_{i-\frac{1}{2},j,k} = (P^S u q)_{i-\frac{1}{2},j,k}\Delta y_j \Delta\eta_k, \quad G'^\varphi_{i,j-\frac{1}{2},k} = (P^S v q)_{i,j-\frac{1}{2},k}\Delta x_{j-\frac{1}{2}}\Delta\eta_k, \quad G'^\eta_{i,j,k-\frac{1}{2}} = (P^S \dot\eta q)_{i,j,k-\frac{1}{2}}\Delta x_j \Delta y_j
$$
$$(2.150)$$

In the time integration step, multiplying $G\prime$ by m/P^S, $G^\lambda, G^\varphi, G^\eta$ is calculated. After that, mq at time step $t + \Delta t$ is calculated by leap-frog method as well as σ coordinate.

In actual source code, conbining to dividing by m to calculate q at time step $t + \Delta t$, q at point (i, j, k) in time step $t + \Delta t$ is calculated as follows.

$$
\begin{aligned}
q^{t+\Delta t} =& \frac{\Delta A_k + \Delta B_k P^{S,t-\Delta t}_{i,j,k}}{\Delta A_k + \Delta B_k P^{S,t+\Delta t}_{i,j,k}} q^{t-\Delta t}_{i,j,k} + \frac{2\Delta t}{\Delta D} \\
&\times [(G'^{\lambda,t}_{i-\frac{1}{2},j,k} - G'^{\lambda,t}_{i+\frac{1}{2},j,k}) + (G'^{\varphi,t}_{i,j-\frac{1}{2},k} - G'^{\varphi,t}_{i,j+\frac{1}{2},k})) + (G'^{\eta,t}_{i,j,k-\frac{1}{2}} - G'^{\eta,t}_{i,j,k+\frac{1}{2}})] \qquad (2.151) \\
&\times \frac{\Delta A_k + \Delta B_k P^{S,t}_{i,j,k}}{P^{S,t}_{i,j,k}} \frac{1}{\Delta A_k + \Delta B_k P^{S,t+\Delta t}_{i,j,k}}
\end{aligned}
$$

Here, A, B is the coefficients for η coordinate, $\eta_{k+\frac{1}{2}} = A_{k+\frac{1}{2}}/p_0 + B_{k+\frac{1}{2}}$ and $\Delta A_k = A_{k-\frac{1}{2}} - A_{k+\frac{1}{2}}$, $\Delta B_k = B_{k-\frac{1}{2}} - B_{k+\frac{1}{2}}$. And $\Delta A_k + \Delta B_k P^S_{i,j,k} = \Delta p_{i,j,k}$(More details in the section of the vertical discretization).

2.5.4.3 The Mass Fluxes into/out of Polar Caps

The mass fluxes into/out of polar caps are calculated by using the semi–Lagrangian scheme in the polar stereo projection (cf. Fig.3). The horizontal average at the highest latitude band is assumed to be preserved before/after flux calculation for the mass conservation. The sequence of calculation is:

1. Zonal average of $P^S q$ at time step t is calculated at the highest latitude band ($j = j_N, j_S$), and is assumed to equal $P^S q$ at the pole.

2. Horizontal wind at the highest latitude bands is projected into the orthogonal coordinate system centering around the pole, and q at time step $t + \Delta t$ is estimated by using the value at the "departure point".

3. Zonal anerage of $P^S q$ at time step $t + \Delta t$ is fixed to that at t.
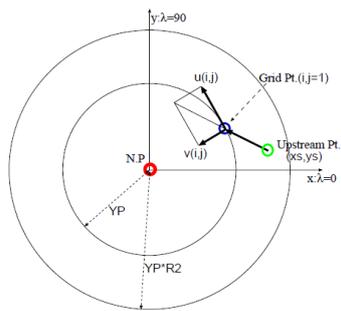
Figure 3: Conceptual figure for the flux on pole-most grids.

2.6 Summary of the Dynamical Core

In this section, we enumerate the calculations performed in the dynamical core, although they overlap with the previous descriptions.

2.6.1 Conversion of Horizontal Wind to Vorticity and Divergence

Obtain grid point values of vorticity and divergence from the grid point values of u_{ij}, v_{ij} for horizontal wind. First, we obtain the vorticity and divergence in spectral space, ζ_n^m, D_n^m,

$$\zeta_n^m = \frac{1}{I}\sum_{i=1}^{I}\sum_{j=1}^{J} \mathrm{i}m v_{ij}\cos\varphi_j Y_n^{m*}{}_{ij}\frac{w_j}{a(1-\mu_j^2)} + \frac{1}{I}\sum_{i=1}^{I}\sum_{j=1}^{J} u_{ij}\cos\varphi_j(1-\mu_j^2)\frac{\partial}{\partial\mu}Y_n^{m*}{}_{ij}\frac{w_j}{a(1-\mu_j^2)} \quad (2.152)$$

$$D_n^m = \frac{1}{I}\sum_{i=1}^{I}\sum_{j=1}^{J} \mathrm{i}m u_{ij}\cos\varphi_j Y_n^{m*}{}_{ij}\frac{w_j}{a(1-\mu_j^2)} - \frac{1}{I}\sum_{i=1}^{I}\sum_{j=1}^{J} v_{ij}\cos\varphi_j(1-\mu_j^2)\frac{\partial}{\partial\mu}Y_n^{m*}{}_{ij}\frac{w_j}{a(1-\mu_j^2)} \quad (2.153)$$

The grid point value is calculated by

$$\zeta_{ij} = \mathcal{R}\mathrm{e}\sum_{m=-N}^{N}\sum_{n=|m|}^{N}\zeta_n^m Y_n^m{}_{ij} , \quad (2.154)$$

and so on.

Corresponding file & subroutines: [G2Wpush, G2Wtrans, G2Wshift, W2Gpush, W2Gtrans, W2Gshift (xdsphe.F)]

2.6.2 Calculating a Virtual Temperature

virtual Temperature T_v is ,

$$T_v = T(1 + \epsilon_v q - l) , \quad (2.155)$$

However, it is $\epsilon_v = R_v/R - 1$ and R_v is the gas constant for water vapor (461 Jkg^{-1}K^{-1}) and R is the gas constant for air (287.04 Jkg^{-1}K^{-1}).

Corresponding file & subroutine: [VIRTMD (dvtmp.F)]

2.6.3 Calculating the Pressure Gradient Term

The pressure gradient term $\nabla\pi = \frac{1}{p_S}\nabla p_S$ is first used to define the π_n^m

$$\pi_n^m = \frac{1}{I}\sum_{i=1}^{I}\sum_{j=1}^{J}(\ln p_S)_{ij}Y_n^{m*}{}_{ij}w_j , \quad (2.156)$$

to a spectral representation and then ,

$$\frac{1}{a\cos\varphi}\left(\frac{\partial\pi}{\partial\lambda}\right)_{ij} = \frac{1}{a\cos\varphi}\mathcal{R}\mathrm{e}\sum_{m=-N}^{N}\sum_{n=|m|}^{N}\mathrm{i}m\tilde{X}_n^m Y_n^m{}_{ij} , \quad (2.157)$$

$$\frac{1}{a}\left(\frac{\partial \pi}{\partial \varphi}\right)_{ij} = \frac{1}{a\cos\varphi}\mathcal{R}e\sum_{m=-N}^{N}\sum_{n=|m|}^{N}\pi_n^m(1-\mu^2)\frac{\partial}{\partial\mu}Y_n^m{}_{ij} \ . \tag{2.158}$$

Corresponding file & subroutine: [PSDOT (dgdyn.F)]

2.6.4 Diagnosis of Vertical Dlow

Pressure change term, and lead DC,

$$\frac{\partial \pi}{\partial t} = -\sum_{k=1}^{K}\{D_k\Delta\sigma_k + (\mathbf{v}_k\cdot\nabla\pi)\Delta B_k\} \tag{2.159}$$

$$\frac{(m\dot{\eta})_{k-1/2}}{p_s} = -B_{k-1/2}\frac{\partial \pi}{\partial t} - \sum_{l=k}^{K}\{D_l\Delta\sigma_l + (\mathbf{v}_l\cdot\nabla\pi)\Delta B_l\} \tag{2.160}$$

and its non-gravity components.

$$\left(\frac{\partial \pi}{\partial t}\right)^{NG} = -\sum_{k=1}^{K}\mathbf{v}_k\cdot\nabla\pi\Delta B_k \tag{2.161}$$

$$\frac{(m\dot{\eta})_{k-1/2}^{NG}}{p_s} = -B_{k-1/2}\left(\frac{\partial \pi}{\partial t}\right)^{NG} - \sum_{l=k}^{K}\mathbf{v}_l\cdot\nabla\pi\Delta B_l \tag{2.162}$$

Corresponding file and subroutine: [PSDOT (dgdyn.F)]

2.6.5 Tendency Terms due to Advection

Momentum advection term:

$$(A_u)_k = \quad (\zeta_k + f)v_k - \left[\frac{(m\dot{\eta})_{k-1/2}}{p_s}\frac{u_{k-1}-u_k}{\Delta\sigma_{k-1}+\Delta\sigma_k} + \frac{(m\dot{\eta})_{k+1/2}}{p_s}\frac{u_k-u_{k+1}}{\Delta\sigma_k+\Delta\sigma_{k+1}}\right]$$
$$- \quad \frac{1}{a\cos\varphi}\frac{\partial \pi}{\partial \lambda}(C_pT_{v,k}\hat{\kappa} - R\bar{T}) + \mathcal{F}_x \tag{2.163}$$

$$(A_v)_k = \quad -(\zeta_k + f)u_k - \left[\frac{(m\dot{\eta})_{k-1/2}}{p_s}\frac{v_{k-1}-v_k}{\Delta\sigma_{k-1}+\Delta\sigma_k} + \frac{(m\dot{\eta})_{k+1/2}}{p_s}\frac{v_k-v_{k+1}}{\Delta\sigma_k+\Delta\sigma_{k+1}}\right]$$
$$- \quad \frac{1}{a}\frac{\partial \pi}{\partial \varphi}(C_pT_{v,k}\hat{\kappa} - R\bar{T}) + \mathcal{F}_y \tag{2.164}$$

Temperature advection term:

$$(uT')_k = u_k(T_k - \bar{T}) \tag{2.165}$$

$$(vT')_k = v_k(T_k - \bar{T}) \tag{2.166}$$

$$H_k = \quad T'_k D_k - \left[\frac{(m\dot{\eta})_{k-1/2}}{p_s} \frac{\hat{T}_{k-1/2} - T_k}{\Delta\sigma_l} + \frac{(m\dot{\eta})_{k+1/2}}{p_s} \frac{T_k - \hat{T}_{k+1/2}}{\Delta\sigma_l} \right]$$
$$+ \quad \hat{\kappa}_k \mathbf{v}_k \cdot \nabla\pi T_{v,k} - \alpha_k \sum_{l=k}^{K} (D_l \Delta\sigma_l + (\mathbf{v}_l \cdot \nabla\pi)\Delta B_l) \frac{T_{v,k}}{\Delta\sigma_k}$$
$$- \quad \beta_k \sum_{l=k+1}^{K} (D_l \Delta\sigma_l + (\mathbf{v}_l \cdot \nabla\pi)\Delta B_l) \frac{T_{v,k}}{\Delta\sigma_k} \tag{2.167}$$

Water vapor advection term:

$$(uq)_k = u_k q_k \tag{2.168}$$

$$(vq)_k = v_k q_k \tag{2.169}$$

$$R_k = q_k D_k - \frac{1}{2} \left[\frac{(m\dot{\eta})_{k-1/2}}{p_s} \frac{q_{k-1} - q_k}{\Delta\sigma_k} + \frac{(m\dot{\eta})_{k+1/2}}{p_s} \frac{q_k - q_{k+1}}{\Delta\sigma_k} \right] \tag{2.170}$$

Corresponding file & subroutine: [GRTADV, GRUADV (dgdyn.F)]

2.6.6 Transformation of Prognostic Variables to Spectral Space

(122) and (123).

Transform $u_{ij}^{t-\Delta t}, v_{ij}^{t-\Delta t}$ to a spectral representation of vorticity and divergence ζ_n^m, D_n^m. Furthermore, transforming the temperature $T^{t-\Delta t}$, specific humidity $q^{t-\Delta t}$, and $\pi = \ln p_S^{t-\Delta t}$ to

$$X_n^m = \frac{1}{I} \sum_{i=1}^{I} \sum_{j=1}^{J} X_{ij} Y_n^{m*}{}_{ij} w_j \,, \tag{2.171}$$

to a spectral representation.
Corresponding file & subroutine: [G2Wpush, G2Wtrans, G2Wshift (xdsphe.F)]

2.6.7 Transformation of Tendency Terms to Spectral Space

Tendency Term of Vorticity

$$\frac{\partial \zeta_n^m}{\partial t} = \quad \frac{1}{I} \sum_{i=1}^{I} \sum_{j=1}^{J} im(A_v)_{ij} \cos\varphi_j Y_n^{m*}{}_{ij} \frac{w_j}{a(1-\mu_j^2)}$$
$$+ \quad \frac{1}{I} \sum_{i=1}^{I} \sum_{j=1}^{J} (A_u)_{ij} \cos\varphi_j (1-\mu_j^2) \frac{\partial}{\partial\mu} Y_n^{m*}{}_{ij} \frac{w_j}{a(1-\mu_j^2)} \tag{2.172}$$

38

The non-gravity wave component of the tendency term of the divergence

$$
\left(\frac{\partial D_n^m}{\partial t}\right)^{NG} = \quad \frac{1}{I}\sum_{i=1}^{I}\sum_{j=1}^{J} im(A_u)_{ij}\cos\varphi_j Y_n^{m*}{}_{ij}\frac{w_j}{a(1-\mu_j^2)}
$$

$$
- \quad \frac{1}{I}\sum_{i=1}^{I}\sum_{j=1}^{J}(A_v)_{ij}\cos\varphi_j(1-\mu_j^2)\frac{\partial}{\partial\mu}Y_n^{m*}{}_{ij}\frac{w_j}{a(1-\mu_j^2)}
$$

$$
- \quad \frac{n(n+1)}{a^2}\frac{1}{I}\sum_{i=1}^{I}\sum_{j=1}^{J}\hat{E}_{ij}Y_n^{m*}{}_{ij}w_j \tag{2.173}
$$

The non-gravity wave component of the tendency term of temperature

$$
\left(\frac{\partial T_n^m}{\partial t}\right)^{NG} = \quad -\frac{1}{I}\sum_{i=1}^{I}\sum_{j=1}^{J} im(uT')_{ij}\cos\varphi_j Y_n^{m*}{}_{ij}\frac{w_j}{a(1-\mu_j^2)}
$$

$$
+ \quad \frac{1}{I}\sum_{i=1}^{I}\sum_{j=1}^{J}(vT')_{ij}\cos\varphi_j(1-\mu_j^2)\frac{\partial}{\partial\mu}Y_n^{m*}{}_{ij}\frac{w_j}{a(1-\mu_j^2)}
$$

$$
+ \quad \frac{1}{I}\sum_{i=1}^{I}\sum_{j=1}^{J}\hat{H}_{ij}Y_n^{m*}{}_{ij}w_j \tag{2.174}
$$

Tendency term of water vapor

$$
\frac{\partial q_n^m}{\partial t} = \quad -\frac{1}{I}\sum_{i=1}^{I}\sum_{j=1}^{J} im(uq)_{ij}\cos\varphi_j Y_n^{m*}{}_{ij}\frac{w_j}{a(1-\mu_j^2)}
$$

$$
+ \quad \frac{1}{I}\sum_{i=1}^{I}\sum_{j=1}^{J}(vq)_{ij}\cos\varphi_j(1-\mu_j^2)\frac{\partial}{\partial\mu}Y_n^{m*}{}_{ij}\frac{w_j}{a(1-\mu_j^2)}
$$

$$
+ \quad \frac{1}{I}\sum_{i=1}^{I}\sum_{j=1}^{J}R_{ij}Y_n^{m*}{}_{ij}w_j \tag{2.175}
$$

Corresponding file & subroutines: [G2Wpush, G2Wtrans, G2Wshift (xdsphe.F)]

2.6.8 Time Integration in Spectral Space

Equations in matrix form

$$
\left\{(1+2\Delta t\mathcal{D}_H)(1+2\Delta t\mathcal{D}_M)\underline{I}-(\Delta t)^2(\underline{W}\ \underline{h}+(1+2\Delta t\mathcal{D}_M)\mathbf{G}\mathbf{C}^T)\nabla_\sigma^2\right\}\overline{\mathbf{D}}^t
$$

$$
= (1+2\Delta t\mathcal{D}_H)(1-\Delta t\mathcal{D}_M)\mathbf{D}^{t-\Delta t}+\Delta t\left(\frac{\partial\mathbf{D}}{\partial t}\right)_{NG}
$$

$$
-\Delta t\nabla_\sigma^2\left\{(1+2\Delta t\mathcal{D}_H)\mathbf{\Phi}_S+\underline{W}\left[(1-2\Delta t\mathcal{D}_H)\mathbf{T}^{t-\Delta t}+\Delta t\left(\frac{\partial\mathbf{T}}{\partial t}\right)_{NG}\right]\right.
$$

$$
\left.+(1+2\Delta t\mathcal{D}_H)\mathbf{G}\left[\pi^{t-\Delta t}+\Delta t\left(\frac{\partial\pi}{\partial t}\right)_{NG}\right]\right\}. \tag{2.176}
$$

Using LU decomposition, $\bar{D}$ is obtained by solving for

$$\frac{\partial \mathbf{T}}{\partial t} = \left(\frac{\partial \mathbf{T}}{\partial t}\right)_{NG} - \underline{h}\mathbf{D} \tag{2.177}$$

$$\frac{\partial \pi}{\partial t} = \left(\frac{\partial \pi}{\partial t}\right)_{NG} - \mathbf{C} \cdot \mathbf{D} \tag{2.178}$$

Calculate the value of the spectrum in $\partial \mathbf{T}/\partial t$, $\partial \pi/\partial t$ and then calculate the value of the spectrum in $t + \Delta t$ using

$$\zeta^{t+\Delta t} = \left(\zeta^{t-\Delta t} + 2\Delta t \frac{\partial \zeta}{\partial t}\right)(1 + 2\Delta t \mathcal{D}_M)^{-1} \tag{2.179}$$

$$D^{t+\Delta t} = 2\bar{D} - D^{t-\Delta t} \tag{2.180}$$

$$T^{t+\Delta t} = \left(T^{t-\Delta t} + 2\Delta t \frac{\partial T}{\partial t}\right)(1 + 2\Delta t \mathcal{D}_H)^{-1} \tag{2.181}$$

$$q^{t+\Delta t} = \left(q^{t-\Delta t} + 2\Delta t \frac{\partial q}{\partial t}\right)(1 + 2\Delta t \mathcal{D}_E)^{-1}$$

$$\pi^{t+\Delta t} = \pi^{t-\Delta t} + 2\Delta t \frac{\partial \pi}{\partial t} \tag{2.182}$$

Corresponding file & subroutine: [TINTGR (dintg.F)]

2.6.9 Transformation of Prognostic Variables to Grid Point Values

Obtain grid values of horizontal wind speed from the spectral values of vorticity and divergence (ζ_n^m, D_n^m) u_{ij}, v_{ij}.

$$u_{ij} = \frac{1}{\cos \varphi_j} \mathcal{R}\mathbf{e} \sum_{m=-N}^{N} \sum_{\substack{n=|m| \\ n \neq 0}}^{N} \left\{ \frac{a}{n(n+1)} \zeta_n^m (1-\mu^2) \frac{\partial}{\partial \mu} Y_n^m{}_{ij} - \frac{ima}{n(n+1)} D_n^m Y_n^m{}_{ij} \right\} \tag{2.183}$$

$$v_{ij} = \frac{1}{\cos \varphi_j} \mathcal{R}\mathbf{e} \sum_{m=-N}^{N} \sum_{\substack{n=|m| \\ n \neq 0}}^{N} \left\{ -\frac{ima}{n(n+1)} \zeta_n^m Y_n^m{}_{ij} - \frac{a}{n(n+1)} \tilde{D}_n^m (1-\mu^2) \frac{\partial}{\partial \mu} Y_n^m{}_{ij} \right\} \tag{2.184}$$

Furthermore,

$$T_{ij} = \mathcal{R}\mathbf{e} \sum_{m=-N}^{N} \sum_{n=|m|}^{N} T_n^m Y_n^m{}_{ij} \,, \tag{2.185}$$

T_{ij}, π_{ij}, q_{ij}, and so on,

$$p_{Sij} = \exp \pi_{ij} \tag{2.186}$$

to calculate.

Corresponding file & subroutines: [W2Gpush, W2Gtrans, W2Gshift (xdsphe.F)]

2.6.10 Diffusion Correction along Pressure Level

The horizontal diffusion is applied on the surface of $\eta-$plane, but it can cause problems in large slopes, such as transporting water vapor uphill and causing false precipitation at the top of a mountain. To mitigate this problem, corrections have been made for T, q, l to make the diffusion closer to that of the p surface, e.g., for T, q, l.

$$
\begin{aligned}
\mathcal{D}_p(T) & = (-1)^{N_D/2} K \nabla_p^{N_D} T \simeq (-1)^{N_D/2} K \nabla_\eta^{N_D} T - \frac{\partial \sigma}{\partial p}(-1)^{N_D/2} K \nabla_\eta^{N_D} p \cdot \frac{\partial T}{\partial \sigma} \\
& = (-1)^{N_D/2} K \nabla_\eta^{N_D} T - (-1)^{N_D/2} K \nabla_\eta^{N_D} \pi \cdot \sigma \frac{\partial T}{\partial \sigma} \\
& = \mathcal{D}(T) - \mathcal{D}(\pi) \sigma \frac{\partial T}{\partial \sigma}
\end{aligned}
\tag{2.187}
$$

So,

$$
T_k \leftarrow T_k - 2\Delta t \sigma_k \frac{T_{k+1} - T_{k-1}}{\sigma_{k+1} - \sigma_{k-1}} \mathcal{D}(\pi)
\tag{2.188}
$$

and so on. In $\mathcal{D}(\pi)$, the spectral value of π is converted to a grid by multiplying the spectral value of π_n^m by the spectral representation of the diffusion coefficient.

Corresponding file & subroutine: [CORDIF (ddifc.F)]

2.6.11 Frictional Heat Associated with Diffusion

Frictional heat from diffusion is ,

$$
Q_{DIF} = -(u_{ij}\mathcal{D}(u)_{ij} + v_{ij}\mathcal{D}(v)_{ij})
\tag{2.189}
$$

It is estimated that Therefore,

$$
T_k \leftarrow T_k - \frac{2\Delta t}{C_p}(u_{ij}\mathcal{D}(u)_{ij} + v_{ij}\mathcal{D}(v)_{ij})
\tag{2.190}
$$

Corresponding file & subroutine: [CORDIF (ddifc.F)]

2.6.12 Horizontal Diffusion and Rayleigh Friction

The coefficients of horizontal diffusion can be expressed spectrally,

$$
\begin{aligned}
\mathcal{D}_{M_n}^m & = K_M \left[\left(\frac{n(n+1)}{a^2} \right)^{N_D/2} - \left(\frac{2}{a^2} \right)^{N_D/2} \right] + K_R \\
\mathcal{D}_{H_n}^m & = K_M \left(\frac{n(n+1)}{a^2} \right)^{N_D/2} \\
\mathcal{D}_{E_n}^m & = K_E \left(\frac{n(n+1)}{a^2} \right)^{N_D/2}
\end{aligned}
\tag{2.191}
$$

K_R is the Rayleigh coefficient of friction. The Rayleigh coefficient of friction is

$$K_R = K_R^0 \left[1 + \tanh \left(\frac{z - z_R}{H_R} \right) \right] \tag{2.192}$$

However, the profile is given in the same way as However,

$$z = -H \ln \sigma \tag{2.193}$$

The results are approximate to those of $K_R^0 = (30day)^{-1}$ and $z_R = -H \ln \sigma_{top}$. The standard values are $K_R^0 = (30day)^{-1}$, $z_R = -H \ln \sigma_{top}$ (σ_{top}: top level of the model), $H = 8000$ m, and $H_R = 7000$ m.

Corresponding file & subroutine [`DSETDF (dsetd.F)`]

2.6.13   Time Filter

To reduce numerical mode associated with leap frog scheme, time filter is applied every time step. MIORC6 used modified Asselin time filter (Williams, 2009), which is updated version of Asselin(1972) used previous version of MIROC. Although Asselin time filter attenuate high frequency physical mode, bringing low accuracy of leap frog scheme, current time filter succeeded in suppressing it.

Modified Asselin filter is expressed as following equation

$$\bar{\bar{X}}^t = \bar{X}^t + \nu\alpha[\bar{\bar{X}}^{t-\Delta t} - 2\bar{X}^t + X^{t+\Delta t}] \tag{2.194}$$

$$\bar{X}^{t+\Delta t} = X^{t+\Delta t} + \nu(1 - \alpha)[\bar{\bar{X}}^{t-\Delta t} - 2\bar{X}^t + X^{t+\Delta t}] \tag{2.195}$$

where bar indicates time filter. The parameters set to $\nu = 0.05$, $\alpha = 0.5$. Assuming $\alpha = 1$, modified Asselin filter is same as Asselin filter.

In the model,

$$\bar{\bar{X}}^{t*} = (1 - \nu\alpha)^{-1}[(1 - 2\nu\alpha)\bar{X}^t + \nu\alpha\bar{\bar{X}}^{t-\Delta t}] \tag{2.196}$$

is firstly calculated at `MODULE: [DADVNC]` where transformation of prognostic variableto grid point values. And then, $X^{t-\Delta t} - 2X^t$ is stored. When the $X^{t+\Delta t}$ is obtained later, time filter conduct at `MODULE [TFILT]`,

$$\bar{\bar{X}}^t = (1 - \nu\alpha)\bar{\bar{X}}^{t*} + \nu\alpha X^{t+\Delta t} \tag{2.197}$$
$$\bar{X}^{t+\Delta t} = X^{t+\Delta t} + \nu(1 - \alpha)[\bar{\bar{X}}^{t-\Delta t} - 2\bar{X}^t + X^{t+\Delta t}] \tag{2.198}$$

Corresponding file & subroutine: [`DADVNC (dadvn.F)`]

2.6.14   Correction for Conservation of Mass

In the spectral method, the global integral of $\pi = \ln p_S$ is preserved with rounding errors removed, but the preservation of the mass, i.e. the global integral of p_S is not guaranteed. Moreover, a wavenumber break in the spectra sometimes results in negative values of the water vapor grid points. For this reason, we perform a correction to preserve the masses of dry air, water vapor, and cloud water, and to remove the regions with negative water vapor content.

Before entering dynamical calculations, [FIXMAS], the global integrals of water vapor and cloud water are calculated for M_q, M_l.

$$M_q^0 = \sum_{ijk} q p_S \Delta\lambda_i w_j \Delta\sigma_k \tag{2.199}$$

$$M_l^0 = \sum_{ijk} l p_S \Delta\lambda_i w_j \Delta\sigma_k \tag{2.200}$$

In the first step of the calculation, the dry mass M_d is calculated and stored.

$$M_d^0 = \sum_{ijk} (1 - q - l) p_S \Delta\lambda_i w_j \Delta\sigma_k \tag{2.201}$$

After exiting dynamical calculation, [MASFIX], the following procedure is followed.

First, negative water vapor is removed by dividing the water vapor from the grid points immediately below the grid points. Suppose that $q_k < 0$ is used,

$$q_k' = 0 \tag{2.202}$$

$$q_{k-1}' = q_{k-1} + \frac{\Delta p_k}{\Delta p_{k-1}} q_k \tag{2.203}$$

However, this should only be done if it is $q_{k-1}' \geq 0$.

Next, set the value to zero for the grid points not removed by the above procedure.

3. calculate the global integral value of M_q and multiply the global water vapor content by a fixed percentage so that it is the same as that of M_q^0.

$$q'' = \frac{M_q^0}{M_q} q' \tag{2.204}$$

4. correct for dry air mass Likewise calculate M_d,

$$p_S'' = \frac{M_d^0}{M_d} p_S \tag{2.205}$$

Corresponding file & subroutine: [FIXMAS, MASFIX (dmfix.F)]

2.7   Computational Flow of Dynamical Core

In this section, calculations of dynamical component based on coding are summarized. `[module name(file name)]`

2.7.1   Overview of Dynamical Core

1. Calculate dynamical term `[DYNTRM(dterm.F)]`

   1.1 Calculate volticity and divergence on wave space and get grid value. `[G2W, W2G(xdsphe.F)]`

   1.2 Diagnose stream function and potential velocity `[DYNTRM(dterm.F)]`

   1.3 Diagnose surface pressure advection, its tendency & vertical flow `[PSDOT(dgdyn.F)]`

   1.4 Calculate factor for hydrostatic eq. & interporation of temprature on Hybrid coord. `[CFACT(dcfct.F)]`

   1.5 Calculate virtual temprature `[VIRTMD(dvtmp.F)]`

   1.6 Calculate temperature advection `[GRTADV(dgdyn.F)]`

   1.7 Calculate momentum advection `[GRUADV(dgdyn.F)]`

   1.8 Spectral transform of tendency terms `[G2W(xdsphe.F)]`

2. Time integration of equation DYNSTP`(dstep.F)`

   2.1 Calculate tracer transport `[TRACEG(dtrcr.F)]`

   2.2 Time integration on wave space `[TINTGR(dintg.F)]`

   2.3 Time integration of tracer terms `[GTRACE(dtrcr.F)]`

   2.4 Time filter `[DADVNC(dadvn.F)]`

   2.5 Get horizontal wind of grid value from wave space `[W2G(xdsphe.F)]`

   2.6 Correction of pressure-level diffusion `[CORDIF(ddifc.F)]`

   2.7 Correction of horizontal friction heating `[CORFRC(ddifc.F)]`

3 Physics

3.1 Overview of Physical Parameterizations

As a physical process, we can consider the following

- Cumulus convection
- Shallow convection
- Large scale condensation
- Cloud microphysics
- Radiation
- Turbulence
- Surface fluxes
- Gravity wave drag

We compute the time-varying terms F_x, F_y, Q, M, S for the prognostic variables from these processes, and perform time integration.

3.1.1 Time Integration of Physical Parameterizations

NOTE: the descriptions in this section are outdated.

In terms of time integration of predictors, we can classify the physical Parameterizations in the following three orders of execution.

1. Cumulus convection, shallow convection, large-scale condensation, and cloud microphysics

2. Radiation, turbulence and surface fluxes

3. Gravitational wave drag

For cumulus convection, shallow convection, large-scale condensation, and cloud microphysics, the values are updated by the usual Euler difference as follows.

$$\hat{T}^{t+\Delta t,(1)} = \hat{T}^{t+\Delta t} + 2\Delta t Q_{CUM}(\hat{T}^{t+\Delta t}) \tag{3.1}$$

$$\hat{T}^{t+\Delta t,(2)} = \hat{T}^{t+\Delta t,(1)} + 2\Delta t Q_{LSC}(\hat{T}^{t+\Delta t,(1)}) \tag{3.2}$$

Note that the large-scale condensation scheme is updated by the cumulus convection scheme. In practice, the routines of cumulus convection and large-scale condensation output the heating rates and so on, and the time integration is performed immediately afterwards by `MODULE:[GDINTG]`.

The calculations of the radiative, vertical diffusion, ground boundary layer and surface processes in the following groups are basically performed with these updated values ($\hat{T}^{t+\Delta t,(1)}$, $\hat{q}^{t+\Delta t,(2)}$, etc.). However, in order to calculate some of the terms as implicit, we calculate the heating rates and so on for all of these terms together, and then perform time integration at the end. In other words, if we write symbolically

$$\hat{T}^{t+\Delta t,(3)} = \hat{T}^{t+\Delta t,(2)} + 2\Delta t Q_{RAD,DIF,SFC}(\hat{T}^{t+\Delta t,(2)}, \hat{T}^{t+\Delta t,(3)}) \tag{3.3}$$

That would be the gravitational wave resistance, mass modulation, and dry convection modulation are the same as those for cumulus convection and large-scale condensation.

$$\hat{T}^{t+\Delta t,(4)} = \hat{T}^{t+\Delta t,(3)} + 2\Delta t Q_{ADJ}(\hat{T}^{t+\Delta t,(3)}) \tag{3.4}$$

3.1.2 Various Physical Quantities

Here are definitions of various physical quantities that can be computed simply from the prognostic variables. Some of them are calculated with `MODULE:[PSETUP]`.

1. Virtual temperature

Virtual Temperature T_v is calculated as follows.

$$T_v = T(1 + \epsilon_v q - l) \tag{3.5}$$

2. Air density

The air density ρ is calculated as follows.

$$\rho = \frac{p}{RT_v} \tag{3.6}$$

3. Altitude

The altitude z is evaluated in the same way as the calculation of the geopotential height in the dynamics.

$$z = \frac{\Phi}{g} \tag{3.7}$$

$$\Phi_1 = \Phi_s + C_p(\sigma_1^{-\kappa} - 1)T_{v,1} \tag{3.8}$$

$$\Phi_k - \Phi_{k-1} = C_p \left[\left(\frac{\sigma_{k-1/2}}{\sigma_k} \right)^\kappa - 1 \right] T_{v,k} + C_p \left[1 - \left(\frac{\sigma_{k-1/2}}{\sigma_{k-1}} \right)^\kappa \right] T_{v,k-1} \tag{3.9}$$

4. Half-level temperature

Half-level temperature is calculated by performing a linear interpolation on $\ln p$, i.e., $\ln \sigma$.

$$T_{k-1/2} = \frac{\ln \sigma_{k-1} - \ln \sigma_{k-1/2}}{\ln \sigma_{k-1} - \ln \sigma_k} T_k + \frac{\ln \sigma_{k-1/2} - \ln \sigma_k}{\ln \sigma_{k-1} - \ln \sigma_k} T_{k-1} \tag{3.10}$$

5. Saturated specific humidity

The saturated specific humidity $q^*(T, p)$ is approximated using the saturated vapor pressure $e^*(T)$,

$$q^*(T, p) = \frac{\epsilon e^*(T)}{p}. \tag{3.11}$$

Here, it is $\epsilon = 0.622$,

$$\frac{1}{e_v^*}\frac{\partial e_v^*}{\partial T} = \frac{L}{R_v T^2} \tag{3.12}$$

Therefore, if the latent heat of evaporation (L) and the gas constant of water vapor (R_v) are held constant,

$$e^*(T) = e^*(T = 273K)\exp\left[\frac{L}{R_v}\left(\frac{1}{273} - \frac{1}{T}\right)\right], \tag{3.13}$$

where $e^*(T = 273[\text{K}]) = 611[\text{hPa}]$.
From eq.3.12,

$$\frac{\partial q^*}{\partial T} = \frac{L}{R_v T^2}q^*(T,p). \tag{3.14}$$

It is noted that if the temperature is lower than the freezing point 273.15[K], the sublimation latent heat $L + L_M$ is used as the latent heat L.

6. Dry static energy and moisture static energy

The dry static energy s is defined by

$$s = C_p T + gz \tag{3.15}$$

The moisture static Energy h is defined by

$$h = C_p T + gz + Lq \tag{3.16}$$

3.2 Cumulus Scheme

3.2.1 Outline of Cumulus Scheme

The Chikira scheme (Chikira and Sugiyama 2010) has been adopted since version 5 of MIROC. It represents updrafts, downdrafts, their detrainment and compensating downward motion over the surrounding area as well as microphysical processes associated with updrafts and downdrafts.

The updraft is based on an entraining plume model, where the mass flux increases upward due to lateral entrainment. The detrainment occurs only at the cloud top which is defined as the neutral buoyancy level of the updraft air parcel. The lateral entrainment rate is formulated in terms of buoyancy and vertical velocity of the air parcel at each level following Gregory (2001). The momentum transport is formulated following Gregory et al. (1997).

The cloud base mass fluxes are determined by the prognostic convective kinetic energy closure proposed by Arakawa and Xu (1990) and Xu (1991, 1993), which was adopted in the prognostic Arakawa–Schubert scheme (Randall and Pan 1993; Pan 1995; Randall et al. 1997; Pan and Randall 1998). The convective kinetic energy increases by buoyancy and decreases by dissipation.

The cloud types are spectrally represented according to the updraft vertical velocity at the cloud base. Larger (smaller) vertical velocities give smaller (larger) entrainment rates which result in higher (lower) cloud tops. The cloud base is diagnosed as the lifting condensation level of the air parcel at the lowest model layer.

The scheme has a simple downdraft model, where a part of the precipitation caused by the updrafts evaporates and forms the cold air which enters into the downdrafts. The detrainment of the downdraft mass fluxes occurs at the neutral buoyancy level and near the surface.

The interaction of the updrafs and downdrafts with the surrounding environment is formulated following Arakawa and Schubert (1974). The areal fractions of the updrafts and downdrafts are assumed to be sufficiently small and the grid-mean prognostic variables are supposed to be the same as those over the environmental area, which are changed by the detrainment of the updrafts and downdrafts, the compensating subsidence and the evaporation and sublimation of the precipitation associated with the updrafts.

The input variables to this scheme are temperature T, specific humidity q, cloud liquid water q_l, cloud ice q_i, zonal wind u, meridional wind v, all tracers including aerosols and greenhouse gases, height z, pressure p, and cloud cover C. The scheme gives the tendencies of T, q_v, q_l, q_i, u, v, C and all the tracers. The vertical profiles of the rainfall and snowfall fluxes, cloud liquid water, cloud ice and cloud fraction associated with the updrafts are also output as diagnostic variables.

The procedure of the calculations is given as follows along with the names of the subroutines.

1. Calculation of cloud base `CUMBAS`.
2. Calculation of in-cloud properties `CUMUP`.
3. Calculation of cloud base mass flux `CUMBMX`.
4. Calculation of cloud mass flux, detrainment, and precipitation `CUMFLX`.
5. Diagnosis of cloud water and cloud cover by cumulus `CUMCLD`.
6. Calculation of tendencies by detrainment `CLDDET`.
7. Calculation of freezing, melting, evaporation, sublimation, and downdraft mass flux `CUMDWN`.
8. Calculation of tendencies by compensating subsidence `CLDSBH`.
9. Calculation of cumulus momentum transport `CUMCMT`.
10. Calculation of tracer updraft `CUMUPR`.
11. Calculation of tracer downdraft `CUMDNR`.
12. Calculation of tracer subsidence `CUMSBR`.
13. Fixing tracer mass `CUMFXR` .

3.2.2 Interaction between Cumulus Ensemble and Large-Scale Environment

Following Arakawa and Schubert (1974), the equations for tendencies of the grid-mean variables are written as

$$\frac{\partial \bar{h}}{\partial t} = M \frac{\partial \bar{h}}{\partial z} + \sum_j D_j \left[h_j(z_{T,j}) - \bar{h} \right],$$ (3.17)

$$\frac{\partial \bar{q}}{\partial t} = M \frac{\partial \bar{q}}{\partial z} + \sum_j D_j \left[q_j(z_{T,j}) - \bar{q} \right],$$ (3.18)

where M, D, h denote total mass flux, detrainment mass flux and moist static energy. q is a substitute for q_v, q_l and q_i and any tracers which are calculated in the same way. z_T is the height of the updraft. The hats indicate in-cloud properties, the overbars grid-mean. The subscripts j are an index for the updraft types.

The total mass flux M and detrainment D are defined as

$$M(z) = \sum_j M_{u,j} + M_d,$$ (3.19)

$$D_j(z) = M_{u,j}(z_{T,j}) \delta(z - z_{T,j})$$ (3.20)

respectively, where M_u and M_d denote mass fluxes of updraft and downdraft respectively. The updraft mass flux is formulated as

$$M_{u,j}(z) = M_{B,j}\, \eta_j(z)$$ (3.21)

where M_B and η are the updraft mass flux at its cloud base and normalized mass flux.

3.2.3 Cloud Base

The cloud base is determined as the lifting condensation level of the air at the lowest model layer. It is defined as the smallest z which satisfies

$$\bar{q}_t(z_1) \geq \bar{q}_v^* + \frac{\gamma}{L_v(1+\gamma)} \left[\bar{h}(z_1) - \bar{h}^*(z) \right],$$ (3.22)

where q_t denotes total water, L_v the latent heat of vaporization, z_1 the height of the lowest model layer at the full level and

$$\gamma \equiv \frac{L_v}{C_p} \left(\frac{\partial \bar{q}^*}{\partial \bar{T}} \right)_{\bar{p}}.$$ (3.23)

C_p denotes the specific heat of dry air at constant pressure and the stars indicate saturation values.

The normalized mass flux below the cloud base is given by $\eta = (z/z_B)^{1/2}$ for all of the updraft types where z_B denotes the cloud base height.

3.2.4 Updraft Velocity and Entrainment Rate

The entrainment rate is defined by

$$\epsilon = \frac{1}{M_u}\frac{\partial M_u}{\partial z} \tag{3.24}$$

and allowed to vary vertically. Based on the formulation of Gregory (2001), the updraft velocity is calculated by

$$\frac{1}{2}\frac{\partial \hat{w}^2}{\partial z} = aB - \epsilon \hat{w}^2 \tag{3.25}$$

where w and B are the vertical velocity and the buoyancy of updraft air parcel respectively. a is a dimensionless constant parameter ranging from 0 to 1 and represents a ratio of buoyancy force used to accelerate the updraft velocity. The hats indicate the values of the updraft. The second term on the right-hand side represents reduction in the upward momentum of the air parcel through the entrainment. Here and hereafter, the equation number corresponds to that in Chikira and Sugiyama (2010).

Then it is assumed that

$$\epsilon \hat{w}^2 \simeq C_\epsilon aB, \tag{3.26}$$

where C_ϵ is a dimensionless constant parameter ranging from 0 to 1. This formulation denotes that a certain fraction of the buoyancy-generated energy is reduced by the entrainment, which is identical to the fraction used to accelerate the entrained air to the updraft velocity. Thus, the entrainment rate is written as

$$\epsilon = C_\epsilon \frac{aB}{\hat{w}^2}. \tag{3.27}$$

Eqs. (3.25) and (3.27) lead to

$$\frac{1}{2}\frac{\partial \hat{w}^2}{\partial z} = a(1 - C_\epsilon)B \tag{3.28}$$

which shows that $\hat{w}$ is continuously accelerated upward when buoyancy is positive. Many CRM and LES results show, however, that updraft velocity is often reduced if the parcel approaches its cloud top. For this reason, adding an additional term, we use

$$\frac{1}{2}\frac{\partial \hat{w}^2}{\partial z} = a(1 - C_\epsilon)B - \frac{1}{z_0}\frac{\hat{w}^2}{2} \tag{3.29}$$

where the last term denotes that the energy of the updraft velocity is relaxed to zero with a height scale z_0. Eq. (3.29) is discretized as

$$\frac{1}{2}\frac{\hat{w}^2_{k+1/2} - \hat{w}^2_{k-1/2}}{\Delta z_k} = a(1 - C_\epsilon)B_k - \frac{1}{z_0}\frac{\hat{w}^2_{k+1/2}}{2} \tag{3.30}$$

where k is an index of full levels and $k + 1/2$ and $k - 1/2$ indicate the upper and lower sides of the half levels. Δz is the depth of the model layer. Note that the equation is solved for $\hat{w}^2$ rather than $\hat{w}$.

The buoyancy of the cloud air parcel is determined by

$$B = \frac{g}{\bar{T}}(\hat{T}_v - \bar{T}_v) \tag{3.31}$$

$$\simeq g \left\{ \frac{\hat{h} - \bar{h}^*}{C_p \bar{T}(1 + \gamma)} + \varepsilon(\hat{q}_v - \bar{q}_v) - [(\hat{q}_l + \hat{q}_i) - (\bar{q}_l + \bar{q}_i)] \right\} \tag{3.32}$$

where g and T_v denote gravity and virtual temperature respectively. $\varepsilon = R_v/R_d - 1$ where R_v and R_d are the gas constants for water vapor and dry air respectively.

$\hat{w}$, B and ϵ are calculated for each of the updraft types separately, but we omit the subscript j for convenience.

3.2.5   Normalized Mass Flux and Updraft Properties

The properties of the updraft are determined by

$$\frac{\partial \eta \hat{h}}{\partial z} = \epsilon \eta \bar{h} + Q_i, \tag{3.33}$$

$$\frac{\partial \eta \hat{q}_t}{\partial z} = \epsilon \eta \bar{q}_t - P \tag{3.34}$$

and

$$\frac{\partial \eta}{\partial z} = \epsilon \eta, \tag{3.35}$$

where Q_i and P denote heating by liquid-ice transition and precipitation respectively. All the other variables such as temperature, specific humidity, and liquid and ice cloud water are computed from these quantities. Tracers are calculated by a method identical to that for $\hat{q}_t$.

Equation (3.35) leads to

$$\frac{\partial \ln \eta}{\partial z} = \epsilon. \tag{3.36}$$

Then, η and ϵ are discretized as

$$\frac{\ln \eta_{k+1/2} - \ln \eta_{k-1/2}}{\Delta z_k} = \epsilon_k. \tag{3.37}$$

Note that this discrete form leads to an exact solution if ϵ is vertically constant. Also, η is finite as far as ϵ is. For ϵ_k, a maximum value of $4 \times 10^{-3} m^{-1}$ is applied.

Equations (3.33) and (3.34) are written as

$$\frac{\partial \eta \hat{h}}{\partial z} = E\bar{h} + Q_i, \tag{3.38}$$

$$\frac{\partial \eta \hat{q}_t}{\partial z} = E\bar{q}_t - P \tag{3.39}$$

respectivuly, where $E = \epsilon \eta$. These equations are discretized as

$$\frac{\eta_{k+1/2}\hat{h}_{k+1/2} - \eta_{k-1/2}\hat{h}_{k-1/2}}{\Delta z_k} = E_k\bar{h}_k + Q_{i,k} \tag{3.40}$$

$$\frac{\eta_{k+1/2}\hat{q}_{t,k+1/2} - \eta_{k-1/2}\hat{q}_{t,k-1/2}}{\Delta z_k} = E_k\bar{q}_{t,k} - P_k \tag{3.41}$$

Considering the relation that $\partial \eta / \partial z = \epsilon \eta$, we descretize E_k as

$$E_k = \frac{\eta_{k+1/2} - \eta_{k-1/2}}{\Delta z_k} \tag{3.42}$$

Note that conservation of mass, energy, and water is guaranteed with Eqs. (3.37)–(3.42). This set of equations leads to exact solutions of $\hat{h}$ under the special case that ϵ and $\bar{h}$ are vertically constant and Q_i is zero. From Eqs. (3.37), (3.40), and (3.42), assuming Q_i is zero,

$$\hat{h}_{k+1/2} = e^{-\epsilon_k \Delta z_k}\hat{h}_{k-1/2} + (1 - e^{-\epsilon_k \Delta z_k})\bar{h}_k, \tag{3.43}$$

which shows that $\hat{h}_{k+1/2}$ is a linear interpolation between $\hat{h}_{k-1/2}$ and $\bar{h}_k$. Thus, the stability of $\hat{h}$ is guaranteed. The same property applies to $\hat{q}_t$ as well, if P is zero.

These calculations are made for each of the updraft types separately, but we omit the subscript j for convenience.

3.2.6 Spectral Representation

Following the spirit of the Arakawa–Schubert scheme, updraft types are spectrally represented. Different values of cloud-base updraft velocities are given from the minimum to the maximum values with a fixed interval. The minimum and maximum values are set to 0.1 and 1.4 ms^{-1}, with an interval of 0.1 ms^{-1} for MIROC6. The minimum and maximum values and the interval can be changed.

Then, the updraft properties are calculated upward with Eqs. (3.27), (3.29), (3.33), (3.34), and (3.35). This upward calculation continues even if the buoyancy is negative as long as the updraft velocity is positive. If the velocity becomes negative at some level, the air parcel detrains at the neutral buoyancy level which is below and closest to the level. That is, the scheme automatically judges whether the rising parcel can penetrate the negative buoyancy layers when there is a positive buoyancy layer above. The effect of the convective inhibition (CIN) near cloud base is also represented by this method. Note, however, that an effect of overshooting above cloud top is not represented for simplicity (i.e., detrainment never occurs above cloud top).

52

3.2.7 Cloud-Base Mass Flux

The cloud-base mass flux is determined with the prognostic convective kinetic energy closure proposed by Arakawa and Xu (1990). That is, the cloud kinetic energy for each of the updraft types is explicitly predicted by

$$\frac{\partial K}{\partial t} = AM_B - \frac{K}{\tau_p},$$ (3.44)

where K and A are the cloud kinetic energy and cloud work function respectively, and τ_p denotes a time scale of dissipation. The cloud work function A is defined as

$$A \equiv \int_{z_B}^{z_T} B\eta \, dz.$$ (3.45)

The cloud kinetic energy is linked with M_B by

$$K = \alpha M_B^2.$$ (3.46)

The cloud-base mass flux is then solved for each of the updraft types.

3.2.8 Microphysics

The method to obtain temperature and specific humidity of in-cloud air from moist static energy is identical to that in Arakawa and Schubert (1974). The ratio of precipitation to the total amount of condensates generated from cloud base to a given height z is formulated as

$$F_p(z) = 1 - e^{-(z-z_B-z_0)/z_p},$$ (3.47)

where z_0 and z_p are tuning parameters.

The ratio of cloud ice to cloud condensate is determined simply by a linear function of temperature,

$$F_i(T) = \begin{cases} 1 & T \leq T_1 \\ (T_2 - T)/(T_2 - T_1) & T_1 < T < T_2 \\ 0 & T \geq T_2 \end{cases}$$ (3.48)

where T_1 and T_2 are set to 258.15 and 273.15 K. The ratio of snowfall to precipitation is also determined by this function.

From the conservation of condensate static energy, $C_p T + gz + L_v q - L_i q_i$ where L_i is the latent heat of fusion, for a cloud parcel, Q_i in Eq. (3.33) is written as

$$Q_i = L_i \left(\frac{\partial \eta \hat{q}_i}{\partial z} - \epsilon \eta \bar{q}_i \right)$$ (3.49)

and discretized as

$$Q_{ik} = L_i \left(\frac{\eta_{k+1/2}\hat{q}_{i,k+1/2} - \eta_{k-1/2}\hat{q}_{i,k-1/2}}{\Delta z_k} - E_k \bar{q}_{i,k} \right)$$ (3.50)

Strictly, the ratio of the cloud ice to the cloud condensate should be recalculated after the modification of temperature by Q_i and the iterations of the calculation are required; however, it is omitted for simplicity.

Melting and freezing of precipitation occurs depending on wet-bulb temperature of large-scale environment and cumulus mass flux.

3.2.9 Evaporation, Sublimation and Downdraft

A part of precipitation is evaporated at each level as

$$E_v = a_e(\bar{q}_w - \bar{q})\left(\frac{P}{V_T}\right), \tag{3.51}$$

where E_v, q_w and V_T are the mass of evaporation per a unit volume and time, wet-bulb saturated specific humidity and terminal velocity of precipitation respectively a_e is a constant. Downdraft mass flux M_d is generated as

$$\frac{\partial M_d}{\partial z} = -b_e\bar{\rho}(\bar{T}_w - \bar{T})P, \tag{3.52}$$

where ρ and T_w are density and wet-bulb temperature, respectively; b_e is a constant. Properties of downdraft air are determined by budget equations and the detrainment occurs at neutral buoyancy level and below cloud base.

If the precipitation is composed of both rain and snow, the rain (snow) is evaporated (sublimated) in the same ratio as the ratio of rain (snow) to the total precipitation when the precipitation evaporates to produce downdrafts.

3.2.10 Cloudiness

Fractional cloudiness of the updrafts C_u used in the radiation scheme is diagnosed by

$$C_u = \frac{C_{\max} - C_{\min}}{\ln M_{\max} - \ln M_{\min}}(\ln \sum_j M_{u,j} - \ln M_{\min}) + C_{\min}, \tag{3.53}$$

where $C_{\max}$, $C_{\min}$, $M_{\max}$, $M_{\min}$ are the maximum and minimum values of the cloudiness and cumulus mass flux respectively.

The grid mean liquid cloud mixing ratio in the updrafts is given by

$$l_c = \frac{\beta C_u}{M} \sum_j \hat{q}_{l,j} M_{u,j}, \tag{3.54}$$

where β is a dimensionless constant. The grid mean ice cloud mixing ratio is determined similarly.

3.2.11 Cumulus Momentum Transport

Following Gregory et al. (1997), the zonal and meridional velocities of the updrafts are calculated as

$$\frac{\partial \eta \hat{u}}{\partial z} = \epsilon \eta \bar{u} + C_m \eta \frac{\partial \bar{u}}{\partial z}, \tag{3.55}$$

where C_m is a constant from 0 to 1 representing the effect of pressure. This equation can be rewitten as

$$\frac{\partial \eta \hat{u}}{\partial z} = (1 - C_m)\epsilon \eta \bar{u} + C_m \frac{\partial \eta \bar{u}}{\partial z}, \tag{3.56}$$

and is discretized as

$$\frac{\eta_{k+1/2}\hat{u}_{k+1/2} - \eta_{k-1/2}\hat{u}_{k-1/2}}{\Delta z_k} = (1 - C_m)E_k\bar{u}_k + C_m \frac{\eta_{k+1/2}\bar{u}_{k+1/2} - \eta_{k-1/2}\bar{u}_{k-1/2}}{\Delta z_k}. \tag{3.57}$$

The horizontal velocities of the downdrafts are calculated similarly. The tendencies of zonal and meridional velocities by the cumulus momentum transport (CMT) are calculated as

$$\left(\frac{\partial u}{\partial t}\right)_{\text{CMT},k} = -g\frac{(\overline{\rho u'w'})_{k+1/2} - (\overline{\rho u'w'})_{k-1/2}}{\Delta p_k}, \tag{3.58}$$

$$\left(\frac{\partial v}{\partial t}\right)_{\text{CMT},k} = -g\frac{(\overline{\rho v'w'})_{k+1/2} - (\overline{\rho v'w'})_{k-1/2}}{\Delta p_k} \tag{3.59}$$

respectively, where $\overline{\rho u'w'}$ and $\overline{\rho v'w'}$ are total zonal and meridional momentum fluxes respectively and $\Delta p_k = p_k - p_{k+1}$.

3.3 Shallow Convection Scheme

3.3.1 Overview of Shallow Convection

Shallow convection is the most frequent type of convective cloud in the tropics and subtropics Its impact on climate through the energy budget due to atmospheric radiation is considered important (Stevens, 2005). Shallow convection is responsible for transporting the boundary layer air to the free atmosphere. It is often not accompanied by precipitation and is characterized by the fact that precipitation-induced downdraft does not reach the surface as in deep convection.

This section briefly describes the vertical structure of the boundary layer favorable for shallow convection. When the ground surface is heated by sunlight or cold air flows in from above, the energy of convective instability is dissipated by turbulence in the bottom of the atmosphere, forming a mixed layer with a nearly uniform vertical distribution of potential temperature and water vapor at a thickness of about 600 m to 800 m from the surface. At the upper end of the mixed layer, there is a transition layer of weakly stable stratification, which is the height at which water vapor in updraft begins to condense (lifting condensation level, LCL). Above LCL, the temperature decreases according to the moist adiabatic lapse rate, and the updraft is observed as clouds. Above the level of free convection (LFC), the cloud continues to grow while mixing with surrounding air. The growth of these convective clouds is limited by the temperature inversion layer at the lower end of the free atmosphere, and the cloud tops are often located about 2 km from the surface.

In the former versions of MIROC, A cumulus parameterization proposed by Chikira and Sugiyama (2010) deals with multiple cloud types including shallow cumulus and deep convective clouds. However, it tends to overestimate low-level cloud amounts. To cope with this bias and improve the performance for reproducing current climate, the shallow convection scheme is introduced from the 6th version of MIROC (Tatebe et al., 2019, Ogura et al., 2017, Ogura, 2015). The source code in concern (pshcn.F) consists of `SUBROUTINE:[PSHCN]` and `SUBROUTINE:[DISTANCE]`. The input values for `SUBROUTINE:[PSHCN]` are temperature, water vapor mixing ratio, and liquid water mixing ratio, ice mixing ratio. It predicts liquid water potential temperature, total water mixing ratio, ice mixing ratio, and horizontal components of wind in response to vertical transport. It also diagnoses cloud fraction and precipitation. `SUBROUTINE:[DISTANCE]`, which is called inside `SUBROUTINE:[PSHCN]`, calculates the degree of buoyancy-induced updraft and mixing with the environment. Since the variables diagnosed in the cumulus scheme (`SUBROUTINE:[CUMLUS]`) are referenced to determine the conditions for shallow convection, `SUBROUTINE:[PSHCN]` is required to be run after `SUBROUTINE:[CUMLUS]`, followed by the diagnosis of cloud fraction. On the other hand, it should be run before the land surface process `SUBROUTINE:[SURFCE]` because precipitation by convection is referenced in the land surface and ocean models.

3.3.2 Basics of Cloud Model

Subgrid clouds are modeled based on the frameworks proposed by Bretherton et al. (2004) and Park and Bretherton (2009). This scheme employs a simple plume model for cloud to calculate vertical transport of conserved variables and precipitation due to updraft. An ensemble of shallow convection in a horizontal grid, which is expressed as a single updraft plume, is supposed to experience horizontal mixing with the environment (entrainment/detrainment). The flux of vertical transport of mass is assumed in the following form:

$$\rho \overline{w'\psi'} \approx M_u(\psi_u - \overline{\psi}), \tag{3.60}$$

where $M_u = \rho_u \sigma_u w_u$ is mass flux of updraft (ρ_u, σ_u, and w_u stand for density in updraft, area fraction of updraft in a grid, and vertical velocity, respectively), ψ_u is a conserved variable

transported by convection (e.g. liquid water potential temperature, total water mixing ratio, horizontal components of momentum) in updraft, $\overline{\psi}$ denotes the average value in the environmental field of the same conserved value. The effects of vertical transport due to shallow convection are represented by determining the vertical profiles of unknown values M_u and ψ_u. Flux of mass and conserved values are diagnosed as

$$\frac{\partial M_u}{\partial z} = E - D \tag{3.61}$$

$$\frac{\partial}{\partial z}(\psi_u M_u) = X_\psi + S_\psi M_u, \tag{3.62}$$

where X_ψ represents horizontal mixing with environmental air, and S_ψ is source term. E and D are rates of entrainment and detrainment, which are described in fractional from

$$E = \epsilon M_u \tag{3.63}$$

$$D = \delta M_u. \tag{3.64}$$

Substituting $\overline{\psi}$ for grid value and assuming the horizontal mixing term as $X_\psi = E\overline{\psi} - D\psi_u$ results in

$$\frac{\partial M_u}{\partial z} = M_u(\epsilon - \delta) \tag{3.65}$$

$$\frac{\partial \psi_u}{\partial z} = \epsilon(\overline{\psi} - \psi_u) + S_\psi. \tag{3.66}$$

In MIROC6, changes in liquid water potential temperature due to precipitation and the effect of subgrid pressure gradient on horizontal momentum are included in S_ψ. Consequently, equations (3.65) and (3.66) results in a closure problem of two parameters δ and ϵ. By determining δ and ϵ by the formulation described in section 3.3.3.4 and solving differential equations along with boundary condition at cloud base, vertical profiles of M_u and ψ_u are calculated.

3.3.3 Computation in PSHCN

The effect of convective updraft is calculated as follows.

- Liquid water potential temperature θ_l and total water q_t are diagnosed from input temperature T, water vapor mixing ratio q_v, liquid water mixing ratio q_l, ice mixing ratio q_i,

- Updraft mass flux at cloud base is diagnosed.

- Height of cloud base is diagnosed.

- Presence of shallow convection is determined.

- Vertical profiles of M_u, θ_l, q_t, horizontal wind components u and v are diagnosed.

- θ_l, q_t, q_i, u, v, liquid water temperature T_l are predicted.

- T, q_v, and q_l are diagnosed according to T_l and q_t.

3.3.3.1 Lower boundary condition: diagnosis of cloud base mass flux

The mass flux at cloud base is formulated as it depends on turbulent kinetic energy (TKE) in boundary layer and convective inhibition (CIN) at the top of boundary layer.

Firstly, the vertical profile of updraft velocity is supposed to fulfill

$$\frac{1}{2}\frac{\partial}{\partial z}w_u^2 = aB_u - b\epsilon w_u^2 \tag{3.67}$$

all over the layers with shallow convection. B_u means updraft buoyancy, a and b are empirical parameters. The first term of the right-hand side of (3.67) is acceleration by buoyancy, and the second term represents drag by entrainment. By assuming no entrainment below LFC and integrating (3.67) from cloud base to LFC, The critical value of upward velocity for updraft plume to reach LFC, w_c, can be determined

$$w_c = \sqrt{2a(CIN)}. \tag{3.68}$$

Updrafts that exceed this critical value penetrates from cloud base.

Computation of CIN is based on Appendix C of Bretherton et al.,

$$CIN = [B_u(p_{base}) + B_u(p_{LCL})]\frac{p_{LCL} - p_{base}}{g(\rho_{LCL} + \rho_{base})} + B_u(p_{LCL})\frac{p_{LFC} - p_{LCL}}{g(\rho_{LFC} + \rho_{LCL})}. \tag{3.69}$$

In the following, subscript *base* represents the value at the top of mixing layer. In MIROC6, for simplicity, $B_u(p_{base})$ is set to zero.

Secondly, to obtain the information of vertical velocity at cloud base, the statistical distribution of w is assumed to follow Gaussian distribution

$$f(w) = \frac{1}{2\pi k_f e_{avg}}\exp\left[-\frac{w^2}{2k_f e_{avg}}\right] \tag{3.70}$$

with variance equal to $k_f e_{avg}$, where e_{avg} is average TKE diagnosed in turbulent and vertical diffusion scheme. k_f is an empirical parameter describing the partitioning of TKE between horizontal and vertical motions at the subcloud layer inversion, whose recommended value based on large eddy simulation is 0.5.

By taking average of vertical velocity above the critical value w_c, cloud base mass flux $M_{u,base}$ is diagnosed as

$$M_{u,base} = \overline{\rho_{base}}\int_{w_c}^{\infty} wf(w)dw = \overline{\rho_{base}}\sqrt{\frac{k_f e_{avg}}{2\pi}}\exp\left[-\frac{w_c^2}{2k_f e_{avg}}\right], \tag{3.71}$$

where $\overline{\rho_{base}}$ is density at LFC. This mass flux is larger for larger boundary layer TKE and smaller for larger CIN.

3.3.3.2 Diagnosing height of cloud base

The cloud base height is set between the top of the boundary layer and the LCL. The larger the CIN is, the lower the cloud base becomes. The top of boundary layer is diagnosed as the level with maximum vertical gradient of relative humidity. Let z_{Hi} be the higher of this level and LCL, and z_{Lo} be the lower, then the cloud base altitude z_{base} is set

$$z_{base} = z_{Hi} - (z_{Hi} - z_{Lo})\frac{CIN - CIN_{Lo}}{CIN_{Hi} - CIN_{Lo}}. \tag{3.72}$$

CIN_{Hi} and CIN_{Lo} are coefficients which satisfy $CIN_{Lo} \leq CIN \leq CIN_{Hi}$ for a typical value of CIN.

3.3.3.3 Determination of the presence of shallow convection

For each horizontal column, whether shallow convection occurs is determined with following criteria.

- If estimated inversion strength (EIS; Wood and Bretherton, 2006) exceeds a certain threshold, the environmental field is judged to be dominated by stratocumulus clouds, and shallow convection is not generated. This criterion is introduced because the vertical resolution of climate models does not sufficiently represent the thin and strong inversion layer over the boundary layer, and underestimates CIN, which leads to an overestimation of shallow convection. EIS is estimated by $EIS = \theta_{700} - \theta_0 - \Gamma_m^{850}(z_{700} - LCL)$ where θ_{700} and θ_0 are potential temperature at 700hPa and surface, Γ_m^{850} is moist adiabatic lapse rate at 850hPa, and z_{700} is height of 700hPa.

- If the intensity of cumulus convection diagnosed by SUBROUTINE:[CUMULUS] exceeds a threshold, the environmental field is supposed to be dominated by deep convection and shallow convection is not generated.

- If the areal fraction of shallow convection is under a threshold, computation of shallow convection is omitted.

3.3.3.4 Diagnosing vertical profile of updraft mass flux

For the grid boxes that contain shallow convection, entrainment and detrainment is calculated using the value of ψ_u at cloud base and $M_{u,base}$. Fractional entrainment and detrainment are computed based on the framework of buoyancy sorting suggested by Kain and Fritsch (1990). In a layer of thickness δz, equal parts $\epsilon_0 M_u \delta z$ of updraft and environmental air are involved in the lateral mixing process that creates a spectrum of mixtures. This yields a total mixing mass flux $2\epsilon_0 M_u \delta z$, with fractional mixing rate $\epsilon_0 = c_0/H$ (c_0 is a certain empirical coefficient and H is the height from surface). In the mixed air, there exists states with probability density such that the air from the environmental field occupies a proportion χ. Here, for simplicity of calculation, it is considered that the state from pure moist air ($\chi = 0$) to pure environmental air ($\chi = 1$) is distributed with uniform probability (Kain-Fritsch scheme assumes Gaussian distribution). Based on the buoyancy force on the mixed air, the entrainment or detrainment is determined. SUBROUTINE:[DISTANCE] is called in SUBROUTINE:[PSHCN]. The output variables in this subroutine are liquid water potential temperature (THETLU) and bool value for entrainment or detrainment (JUDGE).

The occurrence of entrainment is judged as follows. Firstly, if the updraft air is not saturated, entrainment is not assumed to occur. Next, with virtual potential energy in the environmental field ($\overline{\theta_v}$) and updraft (θ_{vu}), buoyancy force on the parcel is defined:

$$B_u = g\frac{\theta_{vu} - \overline{\theta_v}}{\overline{\theta_v}} \tag{3.73}$$

and entrainment occurs when the buoyancy on parcel is positive. Furthermore, even when the buoyancy is negative, entrainment occurs if the parcel can travel longer than a certain eddy mixing distance $l_c = c_1 H$, where $c_1 = 0.1$ is an empirical constant, chosen to optimize the trade-cumulus case. This criterion corresponds to the critical buoyancy value

$$B_c = -\frac{1}{2}\frac{w_u^2}{l_c} \tag{3.74}$$

and otherwise, all the mixed air is detrained. Therefore, Once the critical value of the mixing state χ_c is obtained, which allows the updraft to rise a distance l_c under negative buoyancy,

the air in the environmental field entrained into the cloud and the air in the updraft that is detrained can be determined as follows

$$M_u \epsilon = 2\epsilon_0 M_u \int_0^{\chi_c} \chi q(\chi) d\chi = \epsilon_0 M_u \chi_c^2 \tag{3.75}$$

$$M_u \delta = 2\epsilon_0 M_u \int_{\chi_c}^1 (1-\chi) q(\chi) d\chi = \epsilon_0 M_u (1-\chi_c)^2. \tag{3.76}$$

Thus, letting

$$\epsilon = \epsilon_0 \chi_c^2 \tag{3.77}$$

$$\delta = \epsilon_0 (1-\chi_c)^2, \tag{3.78}$$

equatinons (3.65) and (3.66) are expressed as follows

$$\frac{1}{M_u} \frac{\partial M_u}{\partial z} = \epsilon - \delta = \epsilon_0 (2\chi_c - 1) \tag{3.79}$$

$$\frac{\partial \psi_u}{\partial z} = \epsilon(\overline{\psi} - \psi_u) + S_\psi = \epsilon_0 \chi_c^2 (\overline{\psi} - \psi_u) + S_\psi, \tag{3.80}$$

where χ_c is computed based on virtual potential temperature of mixed air

$$\theta_v(\chi) = \theta_{vu} + \chi \left[\beta(\overline{\theta_l} - \theta_{lu}) - \left(\frac{\beta L}{c_p \Pi} - \theta_u \right) (\overline{q_t} - q_{tu}) \right] \tag{3.81}$$

(Bretherton et al., 2004). β is a thermodynamic parameter which depends on temperature and pressure defined by Randall (1980), θ_{lu} is liquid water potential temperature in updraft, θ_u is updraft potential temperature, $\overline{q_t}$ is total water mixing ratio of environment, q_{tu} is total water mixing ratio of updraft, L is latent heat of vaporization, c_p is specific heat capacity of dry air at constant pressure, and Π is the Exner function.

Consequently, the governing equations (3.67), (3.79), and (3.80) for vertical profiles of w_u, M_u, and ψ_u are obtained. These equations are discretized and integrated upward one layer at a time using the lower boundary condition in section 3.3.3.1 to yield the vertical profile of each variables.

Afterward, from liquid water potential temperature and total water mixing ratio, liquid water mixing ratio q_l and water vapor mixing ratio q_v are diagnosed. The cloud water that exceeds a threshold is disposed as rainwater q_r, and liquid water potential temperature is updated according to the amount of q_r. This corresponds to S_ψ in (3.81).

The formulation of the vertical flux in this scheme is equal to the assumption that the updraft is not large enough to replace all of the air in a grid box in the time step Δt. Therefore, the following limiter is imposed to prevent numerical instability when diagnosing mass flux of the updraft.

$$M_u = min. \left(M_u, \frac{\rho \Delta z}{\Delta t} \right) \tag{3.82}$$

3.4 Large Scale Condensation

The `SUBROUTINE:[PDF2CLD]` and `SUBROUTINE:[CLD2PDF]` are written in `pmlsc.F` file. These are called in `padmn.F`, `pcumc.F`, `pshcn.F`, `pcldphys.F` and `pvdfm.F` files.

3.4.1 Physical Basis for Statistical PDF Scheme

General Circulation Models (GCMs) typically adopt fractional cloud cover (the volume of cloudy air per total air volume in a grid box) assumption to realistically represent clouds because of their coarse horizontal resolution ($O(100km)$). Statistical cloud schemes assume a subgrid-scale probability density function (PDF) of humidity within the grid. Integration of the specific PDFs will give the cloud fraction and the amount of water condensate consistently.

By means of the "fast condensation" assumption, the cloud water amount in a local area in the grid is

$$q_c = (q_t - q_s)\, \delta\, (q_t - q_s) \tag{3.83}$$

where q_s denotes the saturation //mixing ratio and q_c does the cloud water mixing ratio. q_t is sum of water vapor and cloud water mixing ratio. $\delta(x)$ denotes the Heviside function of x.

The majority of statistical cloud schemes use the so-called "s-distribution" following Sommeria and Deardorff (1977). A single variable s, which considers the subgrid-scale perturbations of liquid temperature T_l and total water mixing ratio q_t, is employed. s is defined as

$$s = a_L\, (q_t - \alpha_L T_l) \tag{3.84}$$

where

$$a_L = 1/\left(1 + L\alpha_L/c_p\right),\, \alpha_L = \partial q_s/\,\partial T|_{T=\bar{T}_l}\,. \tag{3.85}$$

For any choice of the PDF of s, denoted as $G(s)$, the grid-mean cloud fraction, C, and cloud water content, q_c, are obtained by integrating $G(s)$ and $(Qc + s)G(s)$,

$$C = \int_{-Q_c}^{\infty} G(s)ds \tag{3.86}$$

$$\bar{q}_c = \int_{-Q_c}^{\infty} (Q_c + s)\, G(s)ds, \tag{3.87}$$

where Qc denotes the grid-scale saturation deficit defined as

$$Q_c \equiv a_L \left\{ \bar{q}_t - q_s\left(\bar{T}_l, \bar{p}\right) \right\}. \tag{3.88}$$

3.4.2 Hybrid Prognostic Cloud scheme

The statistical scheme implemented in MIROC6 is called Hybrid Prognostic Cloud (HPC) scheme (Watanabe et al. 2009). The HPC scheme proposes two types of shape for the PDF $G(s)$, Double-uniform PDF and Skewed-triangular PDF. Here we focus on Skewed-triangular scheme because MIROC6 adoptes the shape. The physical basics of the scheme are in common with Double-uniform PDF.

Example of the basis PDF for HPC: skewed-triangular functions. Copied from Fig.1 in Watanabe et al. 2009.

The scheme predicts variance (V) and skewness (S) of the PDF. V, S, the second moment μ_2, and the third moment μ_3 are defined as follows.

$$\mu_2 \equiv V = \int_{-\infty}^{\infty} s^2 G(s) ds \tag{3.89}$$

$$\mu_3 \equiv \mu_2^{3/2} S = \int_{-\infty}^{\infty} s^3 G(s) ds \tag{3.90}$$

V and S are affected by cumulus convection, cloud microphysics, turbulent mixing, and advection.

The integrals to obtain C and q_c are symbolically expressed as

$$C = I_C \left(\bar{p}, \bar{T}_l, \bar{q}_t, \mathcal{V}, \mathcal{S} \right) \tag{3.91}$$

$$\bar{q}_c = I_q \left(\bar{p}, \bar{T}_l, \bar{q}_t, \mathcal{V}, \mathcal{S} \right) \tag{3.92}$$

where $\bar{p}$ denotes the pressure. The overbars denote the grid-mean quantity.

If the PDF is not too complicated, (1, 2) can be analytically solved for V and S by defining integrand functions $\tilde{I}$ as

$$\mathcal{V} = \tilde{I}_{\mathcal{V}} \left(\bar{p}, \bar{T}_l, \bar{q}_v, \bar{q}_c, C \right) \tag{3.93}$$

$$\mathcal{S} = \tilde{I}_{\mathcal{S}} \left(\bar{p}, \bar{T}_l, \bar{q}_v, \bar{q}_c, C \right) \tag{3.94}$$

The relationship between (1, 2) and (4, 5) is quasireversible. The double-uniform function and skewed-triangular function PDFs are selected for $G(s)$ because of their feasibility in analytically nalderiving $\tilde{I}$.

3.4.3 PDF Change Through Processes

The HPC cloud scheme is composed using prognostic equations for four variables determining I, namely, T_l, q_t, V, and S. The prognostic variables can be T_l, q_t, C, and q_c that determine $\tilde{I}$.

Prognostic equations for the PDF variance and skewness are expressed as

$$\frac{DV}{Dt} = \left. \frac{\Delta \mathcal{V}}{\Delta t} \right|_{\text{conv.}} + \left. \frac{\Delta \mathcal{V}}{\Delta t} \right|_{\text{micro.}} + \left. \frac{\Delta \mathcal{V}}{\Delta t} \right|_{\text{turb.}} + \left. \frac{\Delta \mathcal{V}}{\Delta t} \right|_{\text{others}} - \varepsilon \mathcal{V} \tag{3.95}$$

$$\frac{DS}{Dt} = \left. \frac{\Delta \mathcal{S}}{\Delta t} \right|_{\text{conv.}} + \left. \frac{\Delta \mathcal{S}}{\Delta t} \right|_{\text{micro.}} + \left. \frac{\Delta \mathcal{S}}{\Delta t} \right|_{\text{turb.}} + \left. \frac{\Delta \mathcal{S}}{\Delta t} \right|_{\text{others}} - \varepsilon_{\mathcal{S}} \tag{3.96}$$

where subscripts 'conv.', 'micro.' and 'turb.' indicate cumulus convection, cloud microphysics and turbulent mixing processes respectively, which all affect the PDF shape. The last terms represent dissipation due to subgrid-scale horizontal motions. The specific formulations for each term are described below.

The HPC scheme is referred to as and $G(s)$ is updated every after the process that affects cloud water PDF. $G(s)$ is thus modified several times within a single time step.

3.4.3.1   Cumulus Convection

The total effect of cumulus convection to the PDF moments is written as

$$\left.\frac{\Delta \mathcal{V}}{\Delta t}\right|_{\text{conv.}} = M_c \frac{\partial \mathcal{V}}{\partial z} + \frac{\Delta \tilde{I}_\mathcal{V}}{\Delta t} \tag{3.97}$$

$$\left.\frac{\Delta \mathcal{S}}{\Delta t}\right|_{\text{conv.}} = M_c \frac{\partial \mathcal{S}}{\partial z} + \frac{\Delta \tilde{I}_\mathcal{S}}{\Delta t} \tag{3.98}$$

M_c is the cumulus mass-flux including updraft in the convection tower and downdraft in the environment. The vertical transport of the PDF moments is represented by the first terms on the right side hand of (14, 15).

Cumulus convections modify the grid-mean T_l, q_t, and q_c by upward transportation of grid-mean moist static energy, q_v, and q_c. Detrainment also affects these variables. The detrainment of the cloudy air mass is considered, as in Bushell et al. (2003),

$$\left.\frac{\partial C}{\partial t}\right|_{\text{conv.}} = D(1 - C) \tag{3.99}$$

The second terms on the right hand side of (14, 15) indicates that the changes in the PDF moments is calculated consistent with the changes in the grid-scale temperature, humidity, cloud water, and cloud fraction.

$$\Delta \tilde{I}_\mathcal{X} = \tilde{I}_\mathcal{X}\left(\bar{p}, \bar{T}_l + \Delta \bar{T}_l, \bar{q}_v + \Delta \bar{q}_v, \bar{q}_c + \Delta \bar{q}_c, C + \Delta C\right) - \tilde{I}_\mathcal{X}\left(\bar{p}, \bar{T}_l, \bar{q}_v, \bar{q}_c, C\right) \tag{3.100}$$

$$\tag{3.101}$$

where $\mathcal{X}$ is either $\mathcal{V}$ or $\mathcal{S}$.

3.4.3.2   Cloud Microphysics

The tendency due to microphysical processes can be written in a similar manner to the cumulus convection effect.

$$\left.\frac{\Delta \mathcal{V}}{\Delta t}\right|_{\text{micro.}} = \frac{\Delta \tilde{I}_\mathcal{V}}{\Delta t} \tag{3.102}$$

$$\left.\frac{\Delta \mathcal{S}}{\Delta t}\right|_{\text{micro.}} = \frac{\Delta \tilde{I}_\mathcal{S}}{\Delta t} \tag{3.103}$$

Changes in $\bar{T}_l, \bar{q}_v,$ and $\bar{q}_c$ are derived from microphysical tendency terms including precipitation, evaporation, and melting/freezing.

3.4.3.3 Turbulent Mixing

From the definition of s, the PDF variance $\mathcal{V}$ becomes

$$\mathcal{V} = a_L^2 \left(\overline{q_t'^2} + \alpha_L^2 \Pi \overline{\theta_l'^2} - 2\alpha_L \Pi \overline{q_t' \theta_l'} \right), \tag{3.104}$$

where Π is the Exner function. Assuming the level-2 closure in Nakanishi and Niino (2004), the time evolution of V can be derived as

$$\left. \frac{\Delta \mathcal{V}}{\Delta t} \right|_{\text{turb.}} = 2a_L^2 \left[(\alpha_L \Pi)^2 K_H \left(\frac{\partial \bar{\theta}_l}{\partial z} \right)^2 + K_q \left(\frac{\partial \bar{q}_t}{\partial z} \right)^2 \right.$$
$$\left. -\alpha_L \Pi \left(K_H + K_q \right) \frac{\partial \bar{\theta}_l}{\partial z} \frac{\partial \bar{q}_t}{\partial z} \right] - \frac{2q}{\Lambda_2} \mathcal{V}, \tag{3.105}$$

where K_H and K_q are the mixing coefficients for sensible heat and moisture, respectively. $q^2 = \overline{u'^2 + v'^2 + w'^2}$ denotes the turbulent kinetic energy. The other symbols follow the original notation.

Since the turbulence production does not affect the PDF shape parameter defined by the third moment (cf. Tompkins 2002), the skewness change $\Delta \mathcal{S} / \Delta t|_{\text{turb.}}$ is simply calculated due to the variance change in (28).

3.4.3.4 Subgrid-Scale Horizontal Eddy

In the planetary boundary layer, the subgrid-scale inhomogeneity is dissipated due to the turbulent mixing. In free atmosphere, the grid box will be homogenized mainly due to mesoscale motions, which are expressed by the Newtonian damping as in (Tompkins 2002): $\varepsilon_\mathcal{V} = \frac{\mathcal{V}}{\tau_h}, \varepsilon_\mathcal{S} = \frac{\mathcal{S}}{\tau_h}$, where the relaxation timescale is parameterized by the horizontal wind shear as

$$\tau_h^{-1} = C_s^2 \left\{ \left(\frac{\partial \bar{u}}{\partial x} \right)^2 + \left(\frac{\partial \bar{v}}{\partial y} \right)^2 \right\}^{1/2} \tag{3.106}$$

The coefficient C_s is set to 0.23 following Tompkins (2002).

3.4.3.5 Other Processes

Dynamics, shallow convection, radiation, mass source, and dissipation heating processes change the grid-mean temperature and humidity. Such effects on the shape of PDF are included following (16).

3.4.4 Solving Procedures

The shape of the Skewed-triangular PDF is represented as follows. The widths defined by positions of the left and right edges on the s-coordinate are denoted as a and b, respectively. The position of the top, denoted as q, is constrained by $a + b + q = 0$. By definition, $q \leq b$ and $a \leq q$ must be satisfied. The PDF is then expressed as

$$G(s) = \begin{cases} -\frac{2(s-b)}{(b-q)(b-a)} & \text{for } q < s \leq b \\ \frac{2(s-a)}{(q-a)(b-a)} & \text{for } a < s \leq q \end{cases} \tag{3.107}$$

The pmlsc module includes two main subroutines, PDF2CLD and CLD2PDF. The subroutine PDF2CLD calculates C and $\bar{q}_c$ given $\bar{p}, T_l, \bar{q}_t, \mathcal{V}, \mathcal{S}$. The subroutine CLD2PDF calculates $\mathcal{V}$ and $\mathcal{S}$ given $\bar{p}, T_l, \bar{q}_t, \bar{q}_c, C$. We will derive the concrete calculation processes in this subsection.

3.4.4.1 Caluculation of Cloud Variables from PDF Moments

This is written in `SUBROUTINE:[PDF2CLD]`.

From μ_1, μ_2, μ_3 to a, b, q

The first, second, and third moments of the PDF is calculated as follows.

$$\mu_1 = \int_{q-a}^{q+b} sG(s)ds \quad = q + \frac{b-a}{3} \tag{3.108}$$

$$\mu_2 = \int_{q-a}^{q+b} (s - \mu_1)^2 G(s)ds = \frac{a^2 + ab + b^2}{18} \tag{3.109}$$

$$\mu_3 = \int_{q-a}^{q+b} (s - \mu_1)^3 G(s)ds = \frac{(b-a)\left(2a^2 + 5ab + 2b^2\right)}{270} \tag{3.110}$$

From (7,8,9), we will derive the solution for a, b, q given μ_1, μ_2, μ_3.
We define $\delta \equiv b - a, \beta \equiv ab$. (8,9) are

$$\delta^2 + 3\beta = 18\mu_2 \tag{3.111}$$

$$\delta\left(\beta + 12\mu_2\right) = 90\mu_3 \tag{3.112}$$

Eliminate β or δ from these equations, you will get the equations.

$$\delta^3 - 54\mu_2\delta + 270\mu_3 = 0 \tag{3.113}$$

$$\beta = 6\mu_2 - \frac{1}{3}\delta^2 \tag{3.114}$$

We apply the formula for the solution of a cubic equation to (10) to obtain δ.

$$\delta = 2\sqrt{18\mu_2} \cos\left(\frac{1}{3}\cos^{-1}\left(\frac{-135\mu_3}{\sqrt{(18\mu_2)^3}}\right) + \frac{4}{3}\pi\right) \tag{3.115}$$

β is obtained from (11). We define $\alpha \equiv \sqrt{\delta^2 + 4\beta}$ for simplicity. Finally, a, b, q is calculated as follows.

65

$$a = (\alpha - \delta)/2 \tag{3.116}$$

$$b = (\alpha + \delta)/2 \tag{3.117}$$

$$q = \mu_1 - \delta/3 \tag{3.118}$$

From PDF to C and qc

Once the PDF $G(s)$ is determined by the parameters a, b, q, the cloud fraction C and grid-mean cloud water mixing ratio $\bar{q}_c$ are derived as follows.

$$C = \begin{cases} 0 & \text{if } b < -Q_c \\ \frac{(Q_c+b)^2}{(b-q)(b-a)} & \text{if } q \leq -Q_c \leq b \\ \frac{(Q_c+a)^2}{(q-a)(b-a)} & \text{if } a \leq -Q_c \leq q \\ 1 & \text{if } -Q_c < a \end{cases} \tag{3.119}$$

$$\bar{q}_c = \begin{cases} 0 & \text{if } b < -Q_c \\ \frac{1}{3}C\left(Q_c + b\right) & \text{if } q \leq -Q_c \leq b \\ Q_c - \frac{1}{3}\left(1 - C\right)\left(Q_c + a\right) & \text{if } a \leq -Q_c \leq q \\ Q_c & \text{if } -Q_c < a \end{cases} \tag{3.120}$$

3.4.4.2 Caluculation of PDF moments from cloud variables.

This is written in `SUBROUTINE:[CLD2PDF]`

From $\bar{q}_c, C$ to a, b, q

We can not determine the position of Q_c in the triangle at the beginning of the calculation. Thus we calculate a, b assuming that $a \leq -Q_c \leq q$ at first. If the calculated parameters are physically consistent with the PDF $(a + b \geq 0)$, a, b, q are determined. Otherwise, we regard $q \leq -Q_c \leq b$ and then a, b, q are derived.

1. $a \leq -Q_c \leq q$

From (16), a is derived as follows.

$$a = \frac{3\left(Q_c - q_c\right)}{1 - C} - Q_c \tag{3.121}$$

We eliminate q from (15) using $q = -a - b$. The quadratic equation for b is obtained.

$$b^2 + ab - 2a^2 + \left(Q_c + a\right)^2 / (1 - C) = 0 \tag{3.122}$$

The physically meaningful solution for b is

$$b = \left(-a\sqrt{9a^2 - 4\left(Q_c + a\right)^2 / (1 - C)}\right) / 2 \tag{3.123}$$

66

2. $q \le -Q_c \le b$

From (16), b is

$$b = \frac{3q_c}{C} - Q_c \qquad (3.124)$$

We eliminate q from (15) using $q = -a - b$. The quadratic equation of a is obtained.

$$a^2 + ab - 2b^2 + (Q_c + b)^2 / C = 0 \qquad (3.125)$$

The physically meaningful solution for a is

$$a = \left(-b - \sqrt{9b^2 - 4(Q_c + b)^2 / C} \right) / 2 \qquad (3.126)$$

Adjustment of Cloud Fraction

When there is no physically meaningful solution for (18), C is adjusted so that a reasonable solution is obtained. The critical conditions for the existence of real solutions for (18) are as follows.

$$\begin{array}{ll} 9a^2 - 4(Q_c + a)^2 / (1 - C) = 0 & (a \le -Q_c \le q) \\ 9b^2 - 4(Q_c + b)^2 / C = 0 & (q \le -Q_c \le b) \end{array} \qquad (3.127)$$

Eliminate a and b uging (17), we get the relationship between C and q_c,

$$\begin{array}{ll} 9\left(\frac{3(Q_c - q_c)}{1 - C} - Q_c \right)^2 = \frac{4}{1 - C} \left(\frac{3(Q_c - q_c)}{1 - C} \right)^2 & (a \le -Q_c \le q) \\ 9\left(\frac{3q_c}{C} - Q_c \right)^2 = \frac{4}{C} \left(\frac{3q_c}{C} \right)^2 & (q \le -Q_c \le b) \end{array} \qquad (3.128)$$

We take the square root of the both sides of the equations and define $\gamma_1 \equiv \sqrt{1 - C}$ and $\gamma_2 \equiv \sqrt{C}$. The cubic equations for γ is obtained.

$$\begin{array}{ll} \gamma_1^3 - 3\left(1 - \frac{q_c}{Q_c} \right) \gamma_1 \pm 2\left(1 - \frac{q_c}{Q_c} \right) = 0 & (a \le -Q_c \le q) \\ \gamma_2^3 - 3\frac{q_c}{Q_c}\gamma_2 \pm 2\frac{q_c}{Q_c} = 0 & (q \le -Q_c \le b) \end{array} \qquad (3.129)$$

We define $R_1 = 1 - \frac{q_c}{Q_c}, R_2 = \frac{q_c}{Q_c}$.

$$\gamma^2 = \begin{cases} -4R \sinh^2 \left(\frac{1}{3} \sinh^{-1} \left(\frac{1}{\sqrt{-R}} \right) \right) & (R < 0) \\ 4R \cos^2 \left(\frac{1}{3} \cos^{-1} \left(\frac{1}{\sqrt{R}} \right) + \frac{4}{3}\pi \right) & (R > 1) \end{cases} \qquad (3.130)$$

Note that, $\gamma = \gamma_1, R = R_1 (a \le -Q_c \le q)$ or $\gamma = \gamma_2, R = R_2 (q \le -Q_c \le b)$.

The actual calculation procedure is as follows. If the solution for (18) is not a real number, C is adjusted using (26). Then we solve (18) again.

67

From a, b, q **to** μ_2, μ_3

By definition, the PDF moments are expressed in terms of a and b.

$$\mu_2 = \frac{a^2 + ab + b^2}{6} \tag{3.131}$$

$$\mu_3 = \frac{-(a+b)ab}{10} \tag{3.132}$$

3.4.4.3 Treatment of Cloud Ice and in-Cloud Water Vapor

Because the original HPC scheme by Watanabe et al. (2009) does not consider the cloud ice, it is modified when coupled with the Wilson and Ballard (1999) ice microphysics. Since the statistical PDF scheme employs a 'fast condensation' assumption that is no more valid for ice, the ice mixing ratio is assumed to be conserved in the large scale condensation process.

Here we assume that - the water vapor mixing ratio within the cloudy area in a grid is constant - cloud ice preferentially exists in areas with large total water content

Based on these assumptions, the cloud fraction and each condensate mixing ratios are diagnosed. The notations for the mixing ratios (q_l, q_i, q_v, q_{vi}) of liquid water (subscript l), ice (subscript i), vapor (subscript v), in-cloud vapor (subscript vi) are employed.

At first the total condensate mixing ratio $q_c = q_l + q_i$ is diagnosed from q_t and T_l assuming that ice does not exist in the grid. The saturation mixing ratio is set for liquid (q_{satl}).

Mixed-phase cloud is generated when the condensate amount is more than the ice content ($q_c > q_i$), whereas the cloud fraction and vapor amount are adjusted in the case of a pure ice cloud when the condensate amount is less than the ice content ($q_c < q_i$). Specifically, q_c, C and q_{vi} are calculated as follows.

1. $q_c > q_i$

Liquid-phase clouds and ice clouds coexist.

$$q_l = q_c - q_i \tag{3.133}$$

$$q_{vi} = q_{\mathrm{satl}} \tag{3.134}$$

2. $q_c < q_i$

Only ice clouds exist ($q_l = 0$). In this case, C and q_{vi} are rediagnosed. We eliminate Q_c in (15,16) assuming that $q_c = q_i$. Equations for C are given as

$$C^3 = \frac{9q_i^2}{(b-q)(b-q)} \ (q \le -Q_c \le b) \tag{3.135}$$

$$C^3 + 3C^2 = 4 - \frac{9\left(q_i + a\right)^2}{(q-a)(b-a)} \ (a \le -Q_c < q) \tag{3.136}$$

From these equations, C is obtained as follows.

$$C = \begin{cases} \sqrt[3]{\frac{9q_i^2}{(b-q)(b-a)}} & \left(0 \le q_i \le \frac{(b-q)^2}{3(b-a)}\right) \\ 2\cos\left(\frac{1}{3}\cos^{-1}\left(1 - \frac{9(q_i+a)^2}{2(q-a)(b-a)}\right)\right) - 1 & \left(\frac{(b-q)^2}{3(b-a)} < q_i \le -a\right) \\ 1 & (-a < q_i) \end{cases} \tag{3.137}$$

,where

$$Q_c = \frac{3q_i}{C} - b = \sqrt[3]{3q_i(b-q)(b-a)} - b. \tag{3.138}$$

Given Q_c, $q_{vi} = q_t - Q_c$ is calculated as follows.

$$q_{vi} = \begin{cases} q_t - \frac{3q_i}{C} + b & \left(0 \le q_i \le \frac{(b-q)^2}{3(b-a)}\right) \\ q_t - \frac{3(q_i+a)}{2+C} + a & \left(\frac{(b-q)^2}{3(b-a)} < q_i \le -a\right) \\ q_t - q_i & (-a < q_i) \end{cases} \tag{3.139}$$

3.5 Cloud Microphysics

The `SUBROUTINE:[CLDPHYS]` is written in the `pcldphys.F` file.

3.5.1 Overview of Cloud Microphysics

Cloud microphysics control the conversion from water condensate to precipitate. The condensate parameterization closely links to the lifetime of and radiative properties of the clouds.

The stratiform (non-convective) cloud microphysics in MIROC6 (Tatebe et al. 2019) are basically the same as those used in MIROC5 (Watanabe et al. 2010). MIROC5 implemented a physically based bulk microphysical scheme. The previous version of the scheme in MIROC3.2 diagnoses the fraction of liquid-phase condensate to total condensate simply as a function of the local temperature. In contrast, the explicit treatment of ice cloud processes allows flexible representation of the cloud liquid/ice partitioning in MIROC5 and MIROC6 (Watanabe et al. 2010; Cesana et al. 2015).

The MIROC6 cloud microphysics scheme uses four quantities to describe water in the atmosphere: vapour; liquid-phase cloud droplets; raindrops; and frozen water. Only one quantity, which we will refer to as 'ice', is used to describe all frozen water in large-scale clouds, including aggregated snow, pristine ice crystals and rimed particles. Physically based transfer terms link the four water quantities. The scheme treats two prognostic condansate variables: ice water mixing ratio q_i and cloud water mixing ratio q_c. Water vapor mixing ratio q_v affects the rate of microphysical processes and q_v itself is also modified via microphysical processes. Ice number concentration N_i is diagnosed as a function of q_i and air temperature T in K. Cloud number concentration N_c is predicted by the online aerosol module implemented. Rain water mixing ratio q_r is treated as a diagnostic variable: q_r falls out to the surface within the time step. Cloud fraction is predicted as described in the section 'pmlsc: Large Scale Condensation'.

The cold rain parameterization following Wilson and Ballard (1999) predicts q_i using physically based tendency terms, which represent homogeneous nucleation, heterogeneous nucleation, deposition/sublimation between vapor and ice, riming (cloud liquid water collection by falling ice), and ice melting. The warm rain processes produce rain as the sum of autoconversion and accretion processes. Specific formulations of each process are described in the following "Microphysical Processes" subsection.

The scheme utilizes a "dry" mixing ratio (kg kg^{-1}) to define the amount of water condensate. For example, q_c is the mass of cloud water per mass of dry air in the layer. The dry air density ρ kg m^{-3} is calculated as $\rho = P/(R_{air}T)$, where P is the pressure in Pa, and the gas constant of air $R_{air} = 287.04$ J kg^{-1} K^{-1}. A condensate mass is obtained by multiplying the mixing ratio by the air density. (e.g., the mass of ice $m_i = \rho q_i$). A number concentraion is in units m^{-3}.

Hereafter, unless stated otherwise, the cloud variables $q_c, q_i, N_c,$ and N_i represent grid-averaged values; prime variables represent mean in-cloud quantities (e.g., such that $q_c = Cq_c'$, where C is cloud fraction). Note that $q_v' \neq q_v$. q_v' for ice clouds is determined as described in pmlsc section. The sub-grid scale variability of water content within the cloudy area is not considered at present.

3.5.2 Microphysical Processes

The time evolution of q_i by microphysical processes is written in symbolic form as follows.

$$\left(\frac{\partial q_i}{\partial t}\right)_{\text{micro}} = \left(\frac{\partial q_i}{\partial t}\right)_{\text{esnw}} + \left(\frac{\partial q_i}{\partial t}\right)_{\text{fallin}} + \left(\frac{\partial q_i}{\partial t}\right)_{\text{fallout}} + \left(\frac{\partial q_i}{\partial t}\right)_{\text{hom}}$$
$$+ \left(\frac{\partial q_i}{\partial t}\right)_{\text{het}} + \left(\frac{\partial q_i}{\partial t}\right)_{\text{dep}} + \left(\frac{\partial q_i}{\partial t}\right)_{\text{rim}} + \left(\frac{\partial q_i}{\partial t}\right)_{\text{mlt}} \tag{3.140}$$

, where t is time. The terms of the right hand side denote evaporation of snow (sunscript esnw), ice fall in from above layers (subscript fallin), ice fall out to below layers (subscript fallout), homogeneous nucleation (subscript hom), heterogeneous nucleation (subscript het), deposition/sublimation (subscript dep), riming (subscript rim), and melting (subscript mlt). Similarly, the time evolution of q_c by microphysical processes is

$$\left(\frac{\partial q_c}{\partial t}\right)_{\text{micro}} = \left(\frac{\partial q_c}{\partial t}\right)_{\text{hom}} + \left(\frac{\partial q_c}{\partial t}\right)_{\text{het}} + \left(\frac{\partial q_c}{\partial t}\right)_{\text{rim}} + \left(\frac{\partial q_c}{\partial t}\right)_{\text{evap}} + \left(\frac{\partial q_c}{\partial t}\right)_{\text{auto}} + \left(\frac{\partial q_c}{\partial t}\right)_{\text{accr}} \tag{3.141}$$

, where the terms on the right hand side are homogeneous nucleation, heterogeneous nucleation, riming, evaporation (subscript evap), autoconversion (subscript auto), and accretion (subscript accr). The formulations of these processes are detailed in the following subsections.

The conversion terms of all processes are calculated at every layer downward from the top layer (k=kmax) to the bottom layer of the column (k=1). k is the vertical level increasing with height, i.e., k+1 is the next vertical level above k.

The changes in the temperature of a layer is treated consistent with the phase-change of water.

$$\left(\frac{\partial T}{\partial t}\right)_{\text{phase change}} = \left(\frac{\partial T}{\partial t}\right)_{\text{vapor}\leftrightarrow\text{liquid}} + \left(\frac{\partial T}{\partial t}\right)_{\text{vapor}\leftrightarrow\text{solid}} + \left(\frac{\partial T}{\partial t}\right)_{\text{liquid}\leftrightarrow\text{solid}} \tag{3.142}$$

with

$$\left(\frac{\partial T}{\partial t}\right)_{\text{vapor}\leftrightarrow\text{liquid}} = \frac{L_v}{c_p}\left(\left(\frac{\partial q_c}{\partial t}\right)_{\text{evap}} + \left(\frac{\partial q_r}{\partial t}\right)_{\text{erain}}\right) \tag{3.143}$$

$$\left(\frac{\partial T}{\partial t}\right)_{\text{vapor}\leftrightarrow\text{solid}} = \frac{L_s}{c_p}\left(\left(\frac{\partial q_i}{\partial t}\right)_{\text{esnw}} + \left(\frac{\partial q_i}{\partial t}\right)_{\text{dep}}\right) \tag{3.144}$$

$$\left(\frac{\partial T}{\partial t}\right)_{\text{liquid}\leftrightarrow\text{solid}} = \frac{L_f}{c_p}\left(\left(\frac{\partial q_i}{\partial t}\right)_{\text{hom}} + \left(\frac{\partial q_i}{\partial t}\right)_{\text{het}} + \left(\frac{\partial q_i}{\partial t}\right)_{\text{rim}} + \left(\frac{\partial q_i}{\partial t}\right)_{\text{mlt}}\right), \tag{3.145}$$

where L_v, L_s, and L_f is the latent heat of vaporization, sublimation, and fusion, respectively. C_p is the specific heat of moist air at constant pressure.

3.5.2.1   Ice Properties

The formulation of the ice conversion terms requires parametrization of the mass, fall speed and particle size distributions of ice. These are described first and then subsequently used to derive the conversion terms.

The ice particle size distribution is parametrized as

$$N_i(D) = N_{i0} \exp(-0.1222(T - T_0)) \exp(-\Lambda_i D), \qquad (3.146)$$

where D is the equivolume diameter of the particle in m, $N_{i0} = 2.0 \times 10^6$ m^{-4}, T is the temperature in K, and $T_0 = 273.15$ K. Λ_i represents the slope of the exponential distribution. The temperature function $\exp(-0.1222(T - T_0))$ represents the fact that ice particles tend to be smaller at lower temperatures, and is an implicit way of parametrizing aggregation.

The mass of an ice particle is parametrized as a function of D

$$m_i(D) = aD^b \qquad (3.147)$$

where $a = 0.069$ kg m^{-2} and $b = 2.0$.

The fall-speed of an ice particle at an air density of $\rho_0 = 1$ kg m^{-3} is

$$v_i(D, \rho_0) = cD^d \qquad (3.148)$$

where $c = 25.2 m^{0.473}$ s^{-1} and $d = 0.527$.

At low air densities a particle will fall faster than at high air densities. Considering such ventilation effect, the fall-speed of a particle at arbitrary air density ρ is

$$v_i(D, \rho) = (\rho_0/\rho)^{0.4} v_i(D, \rho_0) \qquad (3.149)$$

The combination of the size distribution, mass and velocity relationships yields a fall-speed and ice water content relationship.

For a given ice content and temperature, Λ_i can be calculated by integrating (A.2) across the particle size distribution (A.1). This gives the result that, for a given temperature, Λ_i is proportional to the inverse cube root of the ice water content.

$$\Lambda_i = \left(\frac{2aN_{i0} \exp(-0.1222(T - T_0))}{m_i} \right)^{\frac{1}{3}} \qquad (3.150)$$

3.5.2.2 Evaporation of Rain and Snow

The evaporation rate of rain $\left(\frac{\partial q_r}{\partial t} \right)_{\text{erain}}$ is expressed as

$$\left(\frac{\partial q_r}{\partial t} \right)_{\text{erain}} = \frac{1}{\rho \Delta z} k_E (q^w - q_v) \frac{F_r}{V_{Tr}} \qquad (3.151)$$

, where F_r denotes the net accumulation of rain water at the layer in kg m^{-2} s^{-1}, V_{Tr} the terminal velocity, and k_E the evaporation factor ($V_{Tr} = 5$ m s^{-1} and $k_E = 0.5$). q^w correcponds to the saturation water vapor mixing ratio at the wet-bulb temperature. The evaporation occurs only when $q^w - q_v > 0$.

Similary to this, the evaporation rate of falling ice $\left(\frac{\partial q_i}{\partial t} \right)_{\text{esnw}}$ is expressed as

$$\left(\frac{\partial q_i}{\partial t} \right)_{\text{esnw}} = k_E (q^w - q_v) \frac{F_i}{V_{Tr}} \qquad (3.152)$$

where F_i denotes sedimentation of cloud ice from above layers. V_{Ts} is set to 5 m s^{-1}.

3.5.2.3　Ice Fall

The total ice flux from the layer 'k' is

$$F_i|_k = \int_0^\infty N_i(D)m_i(D)v_i(D)dD. \tag{3.153}$$

The fraction of ice flux from level the 'k' to the below level 'kk' ($1 <= $ kk $ < $ k) iceweight$|_{k,kk}$, is given as

$$\frac{\int_0^{f(\text{zm(k)}-\text{zm(kk)})} N_i(D)m_i(D)v_i(D)dD - \int_0^{f(\text{zm(k)}-\text{zm(kk+1)})} N_i(D)m_i(D)v_i(D)dD}{\int_0^\infty N_i(D)m_i(D)v_i(D)dD}, \tag{3.154}$$

where zm(k) is the middle of the height of the layer k, and f(dz) is the ice size which falls the distance dz in a single time step.

The net ice fall out from the layer is

$$\left(\frac{\partial q_i}{\partial t}\right)_{\text{fallout}} = -\frac{\Delta t}{\rho \Delta z} F_i \tag{3.155}$$

.

The net ice fall in to the layer 'k' is

$$\left(\frac{\partial q_i}{\partial t}\right)_{\text{fallin}} = \frac{\Delta t}{\rho \Delta z} \sum_{l=k+1}^{l=kmax} F_i|_{k=l} \times \text{iceweight}|_{l,k} \tag{3.156}$$

3.5.2.4　Homogeneous Nucleation

This term simply converts all liquid cloud water to ice if the temperature is less than a given threshold of 233.15 K.

$$\left(\frac{\partial q_i}{\partial t}\right)_{\text{hom}} = -\left(\frac{\partial q_c}{\partial t}\right)_{\text{hom}} = \frac{q_c}{\Delta t} \tag{3.157}$$

3.5.2.5　Heterogeneous Nucleation

A Spectral Radiation-Transport Model for Aerosol Species (SPRINTARS; Takemura et al. 2000, 2002, 2005, 2009) coupled with MIROC6 explicitly predicts the masses and number concentrations for aerosol species. Heterogeneous freezing of cloud droplets takes place through contact and immersion freezing on ice cucleating particles (INPs), which are parameterized according to Lohmann and Diehl (2006) and Diehl et al. (2006). Soil dust and black carbon are assumed to act as INPs. Ratios of activated INPs to the total number concentration of soil dust and black carbon for the contact freezing and the immersion/condensation freezing are based on Fig. 1 in Lohmann and Diehl (2006). Using the number of INPs (N_{nuc}) predicted in SPRINTARS, the rate of heterogeneous freezing is diagnosed as follows.

$$\left(\frac{\partial q_i}{\partial t}\right)_{\text{het}} = -\left(\frac{\partial q_c}{\partial t}\right)_{\text{het}} = \max\{N_{nuc}W_{nuc0}, \frac{q_c}{\Delta t}\} \tag{3.158}$$

The weight of nucleated drop, W_{nuc0}, is set to 1.0×10^{-12}.

3.5.2.6 Deposition/Sublimation

A single ice particle grows or disappears by water vapor diffusion according to the following equation:

$$\frac{\partial m_i(D)}{\partial t} = \left\{4\pi C\left(S_i - 1\right)F\right\} / \left[\left\{L_s/(R_v T) - 1\right\}L_s/\left(k_a T\right) + R_v T/\left(X P_{\text{sati}}\right)\right] \qquad (3.159)$$

where $\frac{\partial m_i(D)}{\partial t}$ is the rate of change of the particle mass; $(S_i - 1)$ is the supersaturation of the atmosphere with respect to ice; R_v is the gas constant for water vapour; k_a is the thermal conductivity of air at temperature T, X is the diffusivity of water vapour; P_{sati} is the saturated vapour pressure over ice; L_s is the latent heat of sublimation of ice; C is a capacitance term and F is a ventilation coefficient. C is assumed to appropriate to spheres, so is equal to $D/2$. F is given by Pruppacher and Klett (1997) as $F = 0.65 + 0.44 Sc^{1/3} Re^{1/2}$, where Sc is the Schmidt number, equal to 0.6, and Re is the Reynolds number, $v(D)\rho D/\mu$, where μ is the dynamic viscosity of air.

Integrating ice size distribution, $\left(\frac{\partial q_i}{\partial t}\right)_{\text{dep}}$ is obtained as

$$\left(\frac{\partial q_i}{\partial t}\right)_{\text{dep}} = \frac{1}{\rho}\int \frac{\partial m_i(D)}{\partial t} N(D)dD \qquad (3.160)$$

The ice grows or disappears depending on the sign of $(S_i - 1)$.

1. $(S_i - 1) > 0$

The ice grows (deposition). If q_c exists in the same grid, q_c is evaporated as fast as the deposition process (Wegener–Bergeron–Findeisen process).

$$\left(\frac{\partial q_c}{\partial t}\right)_{\text{evap}} = -\left(\frac{\partial q_i}{\partial t}\right)_{\text{dep}} \qquad (3.161)$$

The basis of this theory is the fact that the saturation vapor pressure of water vapor with respect to ice is less than that with respect to liquid water at the same temperature. Thus, within a mixture of these particles, the ice would gain mass by vapor deposition at the expense of the liquid drops that would lose mass by evaporation.

2. $(S_i - 1) < 0$

The ice disappears (sublimation).

3.5.2.7 Cloud water Collection by Ice (Riming)

Riming process (the ice crystals settling through a population of supercooled cloud droplets, freezing them upon collision) is based on the geometric sweep-out integrated over all ice sizes (Lohmann 2004):

$$\left(\frac{\partial q_i}{\partial t}\right)_{\text{rim}} = -\left(\frac{\partial q_c}{\partial t}\right)_{\text{rim}} = \frac{\pi E_{\text{SW}} n_{0S} a q_c \Gamma(3+b)}{4\lambda_S^{(3+b)}}\left(\frac{\rho_0}{\rho}\right)^{0.5} \qquad (3.162)$$

where $n_{0S} = 3 \times 10^6$ m^{-4} is the intercept parameter, λ_S is the slope of the exponential Marshall-Palmer ice crystal size distribution, $a = 4.84, b = 0.25$, and $\rho_0 = 1.3$ kg m^{-3} is the reference density. Γ is the gamma fanction. The collection efficiency E_{sw} is highly dependent on the cloud droplet and snow crystal size (Pruppacher and Klett 1997). The size-dependent collection efficiency for aggregates is introduced as obtained from laboratory results by Lew et al. (1986) (simulation ESWagg).

$$E_{\mathrm{SW}}^{\mathrm{agg}} = 0.939 \mathrm{St}^{2.657} \tag{3.163}$$

The Stokes number (St) is given by

$$\mathrm{St} = \frac{2\,(V_t - v_t)\,v_t}{Dg} \tag{3.164}$$

V_t is the snow crystal terminal velocity, and D is the maximum dimension of the snow crystal. v_t is the cloud droplet terminal velocity. g is the acceleration due to gravity.

3.5.2.8 Ice Melt

Since this term is essentially a diffusion term, although of heat instead of moisture, its form is very similar to that of the deposition and evaporation of ice term. The rate of change of ice mass of a melting particle is given by:

$$\left(\frac{\partial q_r}{\partial t}\right)_{\mathrm{mlt}} = -\left(\frac{\partial q_i}{\partial t}\right)_{\mathrm{mlt}} = 4\pi C F \left\{k_{\mathrm{a}}/L_{\mathrm{m}}\left(T^{\mathrm{w}} - T_0\right)\right\} \tag{3.165}$$

,where L_{m} is the latent heat of melting of ice, T^{w} is the wet-bulb temperature of the air and $T_0 = 273.15$K is the freezing point of ice. Ice melt occurs when $T^{\mathrm{w}} - T_0 > 0$. The capacitance term, C, is considered to be that for spherical particles. Hence $C = D/2$. The ventilation factor, F is considered to be the same as in the deposition/sublimation process.

3.5.2.9 Warm Rain Cloud Microphysics

We assume N_c is the number of aerosols activated as droplets. The nucleation of cloud droplets is predicted in the aerosol module SPRINTARS (Takemura et al. 2000; 2002; 2005; 2009) based on the parameterization by Abdul-Razzak and Ghan (2000), which depends on the aerosol particle number concentrations, size distributions and chemical properties of of each aerosol species, and the updraft velocity.

The autoconversion term following Berry (1968) is a function of q_c and N_c.

$$\left(\frac{\partial q_r}{\partial t}\right)_{\mathrm{auto}} = -\left(\frac{\partial q_c}{\partial t}\right)_{\mathrm{auto}} = \frac{1}{\rho}\frac{b_1 \times m_c'^2}{b_2 + b_3\frac{N_c}{m_c'}} \tag{3.166}$$

The parameters are set as $b_1 = 0.035, b_2 = 0.12, b_3 = 1.0 \times 10^{-12}$. The effect of aerosol-cloud interaction on cloud lifetime is taken into account by the dependency on N_c.

The accretion term is given as

$$\left(\frac{\partial q_r}{\partial t}\right)_{\mathrm{auto}} = -\left(\frac{\partial q_c}{\partial t}\right)_{\mathrm{auto}} = \frac{1}{\rho}q_c q_r \tag{3.167}$$

Rain water q_r into the layer is from above the layer. q_r is treated as a diagnostic variables: q_r falls out to surface within the time step.

3.5.2.10 Total Precipitation

The total amount of precipitation at a certain pressure level, p, is obtained by integrating the relevant processes from the top of the model ($p = 0$) to the respective pressure level. The fluxes of rain and ice $\mathrm{kgm^{-2}\ s^{-1}}$ are then expressed as

$$P_{\mathrm{rain}}(p) = \frac{1}{g} \int_0^p \left(\left(\frac{\partial q_r}{\partial t} \right)_{\mathrm{auto}} + \left(\frac{\partial q_r}{\partial t} \right)_{\mathrm{accr}} + \left(\frac{\partial q_r}{\partial t} \right)_{\mathrm{mlt}} - \left(\frac{\partial q_r}{\partial t} \right)_{\mathrm{revap}} \right) dp \qquad (3.168)$$

$$P_{\mathrm{ice}}(p) = \frac{1}{g} \int_0^p \left(\left(\frac{\partial q_i}{\partial t} \right)_{\mathrm{fallin}} - \left(\frac{\partial q_i}{\partial t} \right)_{\mathrm{fallout}} + \left(\frac{\partial q_i}{\partial t} \right)_{\mathrm{rim}} - \left(\frac{\partial q_r}{\partial t} \right)_{\mathrm{mlt}} - \left(\frac{\partial q_r}{\partial t} \right)_{\mathrm{esnw}} \right) dp \qquad (3.169)$$

3.6 Radiation Scheme

3.6.1 Summary of the Radiation Flux Calculation

The radiation scheme in the MIROC was created based on the Discrete Ordinate Method and the k-distribution Method (Nakajima et al., 2000), and updated by Sekiguchi and Nakajima (2008). The scheme calculates the value of the radiation flux at each level by considering the absorption, emission, and scattering processes of terrestrial and solar radiation by gases and clouds/aerosols. The main input data are temperature T, specific humidity q, cloud water l, and cloud cover C. The output data are shortwave or longwave upward and downward radiation fluxes $F^{\mp}$, and derivative coefficient to surface temperature $dF^{\mp}/dT_g$, surface downward radiation flux F_{sf}^{+}, and 0.5 and 0.67 μm optical thickness τ^{vis}.

The calculation is separated for several wavelength bands. It is further divided into several sub-channels, based on the k-distribution method. As for gaseous absorption, the line absorption in H_2O, CO_2, O_2, O_3, N_2O, CH_4, the continuous absorption in H_2O, CO_2, O_2, O_3, and the CFC absorption are incorporated. As for scattering, Rayleigh scattering of gases and scattering by cloud and aerosol particles are considered.

Major subroutines used to calculate the radiation flux in `SUBROUTINE:[DTRN31]` of pradt.F are as follows.

1. Calculate the Planck function from atmospheric temperature `SUBROUTINE:[PLANKS, PLANKF]`
2. Calculate the optical thickness to the gas in each sub-channel `SUBROUTINE:[PTFIT2]`
3. Calculate the optical thickness to the CFC absorption `SUBROUTINE:[CNTCFC2]`
4. Calculate the optical thickness to aerosol, Rayleigh scattering, and cloud `SUBROUTINE:[SCATAE, SCATRY, SCATCL]`
5. Expand the Planck function by optical thickness for each sub-channel `SUBROUTINE:[PLKEXP]`
6. Calculate the transmission coefficient (T), reflection coefficient (R) and source function (S) `SUBROUTINE:[TWST]`
7. Make T, R, and S matrixes for maximal/random approximation `SUBROUTINE:[RTSMR]`
8. Calculate the radiation flux by adding method `SUBROUTINE:[ADDMR, ADDING]`

To account for the partial coverage of clouds, the transmission and reflection coefficients and source functions for each layer are calculated at weighted average of the cloud cover, separately for cloud cover and clear-sky conditions. The cloud cover of the cumulus is also considered. In addition, it also performs several adding and calculates the clear-sky radiation flux.

3.6.2 Wavelength and Sub-Channel

The basics of radiative flux calculations are represented by Beer-Lambert's Law.

$$F^{\lambda}(z) = F^{\lambda}(0)exp(-k^{\lambda}z) \qquad (3.170)$$

F^{λ} is the radiant flux density at the wavelength of λ and k^{λ} is the absorption coefficient. In order to calculate the radiative fluxes related to the heating rate, the integration operation with respect to the wavelength is required.

$$F(z) = \int F^{\lambda}(z)d\lambda = \int F^{\lambda}(0)exp(-k^{\lambda}z)d\lambda \qquad (3.171)$$

However, it is not easy to calculate this integration precisely because the absorption and emission of radiation by gas molecules have the complicated wavelength dependence of the

77
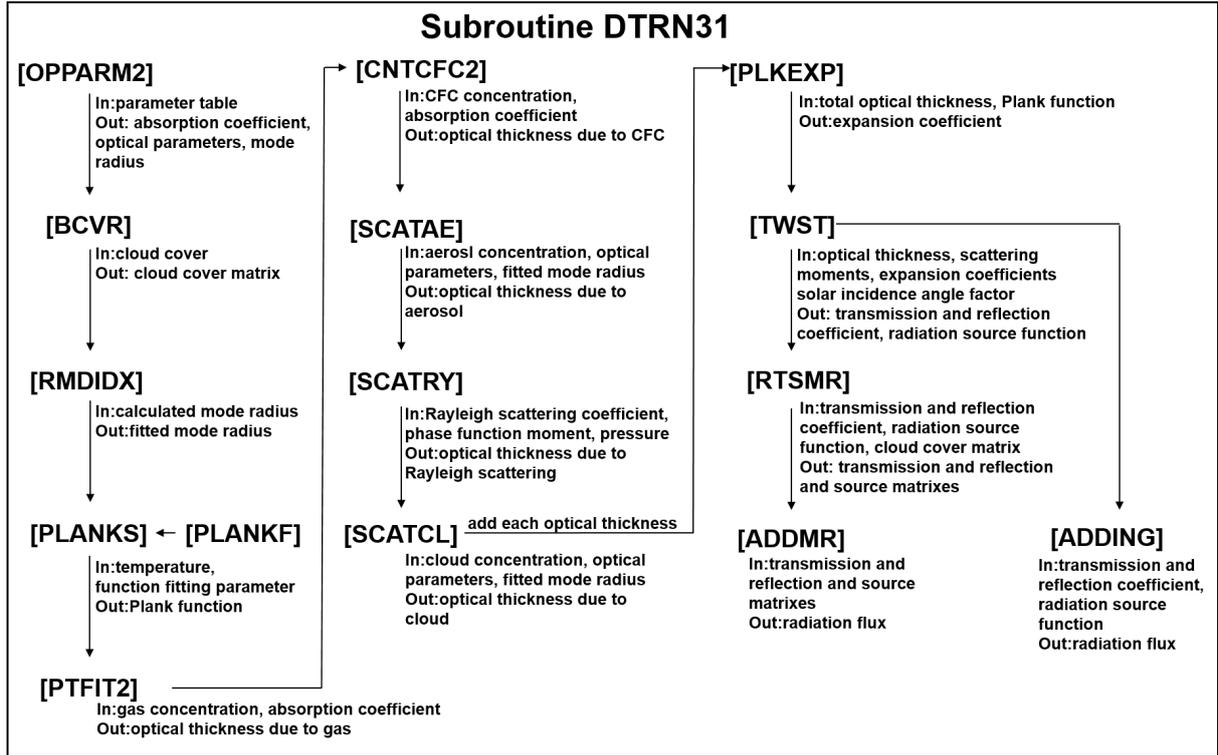
Figure 4: Flowchart of `SUBROUTINE:[DTRN31]`

absorption line attributed to the structure of the molecule. The k-distribution method is a method designed to make the relatively precise calculation easier. Within a certain wavelength range, considering the density function $F(k)$ for λ of the absorption coefficient of k, the above formula is approximated as follows,

$$\int F^\lambda(0)exp(-k^\lambda z)d\lambda \simeq \int \bar{F}^k(0)exp(-kz)F(k)dk \tag{3.172}$$

where $\bar{F}^k(0)$ is the flux averaged over a wavelength having the absorption coefficient in this wavelength k in $z = 0$.

If $\bar{F}^k(0)$ and $F(k)$ are a relatively smooth functions to the k,

$$\int F^\lambda(0)exp(-k^\lambda z)d\lambda \simeq \sum \bar{F}^i(0)exp(-k^i z)F^i \tag{3.173}$$

the formula, as such above, can be relatively precisely calculated by the addition of a finite number (sub-channels) of exponential terms. This method has furthermore the advantage easy to consider the absorption and scattering at the same time.

In the MIROC 6.0, by changing the radiation parameter data, the calculations can be performed at various wavelengths. In the standard version, the wavelength range is divided into 29 parts. In addition, each wavelength range is divided into 1 to 6 sub-channels (corresponding to the i in the above formula). There are 111 channels in total. The wavelength range is divided by the wavenumber (cm^{-1}), 1, 250, 400, 530, 610, 670, 750, 820, 980, 1175, 1225, 1325, 1400, 2000, 2500, 3300, 3800, 4700, 5200, 6000, 10000, 12750, 13250, 14750, 23000, 30000, 33500, 36000, 43500, 50000. Additionally, a chemical version is also with 37 bands and 126 channels

for chemical transport model and the boundary of the shortwave region is also changed to 54000 cm^{-1}.

3.6.3 Calculation of the Planck Function

In this section, SUBROUTINE:[PLANKS, PLANKF] in pradt.F is described.

The Planck function $\bar{B}^w(T)$, integrated in each wavelength range, is evaluated by the following formula.

$$\bar{B}^w(T) = \lambda^{-2} T exp \left\{ \sum_{n=1}^{5} B_n^w \left(\bar{\lambda}^w T \right)^{-n} \right\} \tag{3.174}$$

where $\bar{\lambda}^w$ is the averaged wavelength of the wavelength range, B_n^w is the parameter determined by function fitting. This is calculated to the atmospheric temperature of each layer T_l, and the boundary atmospheric temperature of each layer $T_{l+1/2}$, surface temperature T_g and temperature 1K higher than surface temperature T_{g+1K}. The calculations are performed for each wavelength and each layer. In the following description, the subscript of the wavelength range w is omitted.

3.6.4 Calculation of the Optical Thickness to Gas Absorption

In this section, SUBROUTINE:[PTFIT2] in pradt.F is described.

The optical thickness of the gas absorption (the line and continuum absorption are unified) τ^{KD} is expressed as follows by using the index m as the type of molecules.

$$\tau^{KD} = \sum_{m=1} k^{(m)} C^{(m)} \tag{3.175}$$

where $k^{(m)}$ is the absorption coefficient of the molecule m, which is different for each sub-channel and determined as a function of temperature T and atmospheric pressure p. $C^{(m)}$ represents the amount of gas in the layer represented by mol/cm^2/km, calculated by using the gas concentration $r^{(m)}$ in ppmv ($C^{(m)} = 10^{-1} r^{(m)} \rho dz$). In the MIROC 6.0, the number of the considered molecule types m is 6 (1:H_2O, 2:CO_2, 3:O_3, 4:N_2O, 5:CH_4, 6:O_2). Also, $k^{(m)}$ is represented as follows (the details are in Sekiguchi and Nakajima, 2008).

$$k^{(m)} = \exp \left(\log 10 k_2^{(m)} + (A + BT) \log \left(T/T_{\text{ref2}} \right) \right) \tag{3.176}$$

$$B = \left[\frac{\log 10 \left(k_3^{(m)} - k_2^{(m)} \right)}{\log \left(\frac{T_{ref3}}{T_{ref2}} \right)} - \frac{\log 10 \left(k_1^{(m)} - k_2^{(m)} \right)}{\log \left(\frac{T_{ref1}}{T_{ref2}} \right)} \right] / \left(T_{\text{ref3}} - T_{\text{ref1}} \right) \tag{3.177}$$

$$A = \frac{\log 10 \left(k_3^{(m)} - k_2^{(m)} \right)}{\log \left(T_{\text{ref3}} / T_{\text{ref2}} \right)} - BT_{\text{ref3}} \tag{3.178}$$

T_{ref1-3} are the reference temperatures prepared in advance (200, 260, 320 K), and $k_{1-3}^{(m)}$ are the absorption coefficients when the reference temperatures T_{ref1-3} is used (also fitted at 26 atmospheric pressure grids).

When considering the absorption of H_2O, we calculate the optical thickness of the self-broadening and add τ^{self}.

$$\tau^{KD(H_2O)} = \tau^{KD(H_2O)} + \tau^{self} \tag{3.179}$$

$$\tau^{self} = \frac{k^{(H_2O\_self)}C^{(H_2O)^2}}{C^{(H_2O)} + \rho dz 10^5} \tag{3.180}$$

$k^{(H_2O\_self)}$ is calculated in the same way as $k^{(m)}$. The self-broadening absorption coefficients in the reference temperatures T_{ref1-3} are prescribed and dependent on the pressure. In the above formula, 10^5 is multiplied to convert the unit from km to cm. This calculation is done for each sub-channel and each layer.

3.6.5 Calculation of the Optical Thickness to CFC Absorption

In this section, `SUBROUTINE:[CNTCFC2]` in pradt.F is described.

The optical thickness of the CFC absorption τ^{CFC} is considered for several types of CFCs m.

$$\tau^{CFC} = \sum_m 10^{k^{(m)}} r^{(m)} \rho \Delta z 10^{-1} \tag{3.181}$$

In MIROC 6.0, the number of the considered CFCs m is 28 (1:CFC-11, 2:CFC-12, 3:CFC-13, 4:CFC-14, 5:CFC-113, 6:CFC-114, 7:CFC-115, 8:HCFC-21, 9:HCFC-22, 10:HCFC-123, 11:HCFC-124, 12:HCFC-141b, 13:HCFC-142b, 14:HCFC-225ca, 15:HCFC-225cb, 16:HFC-32, 17:HFC-125, 18:HFC-134, 19:HFC-134a, 20:HFC-143a, 21:HFC-152a, 22:SF_6, 23:$ClONO_2$, 24:CCl_4, 25:N_2O_5, 26:C_2F_6, 27:HNO_4, 28:SF_5CF_3). In the above formula, 10^{-1} is multiplied to convert from km to cm, and from ppmv to ratio. This calculation is done for each sub-channel and each layer. This calculation is performed for each layer and the wavelength range from about 540 to 1800 cm^{-1}.

3.6.6 Optical Thickness to Scattering and Scattering Moment

Calculate the optical thickness of scattering and the scattering moment. These calculations are performed for each wavelength and each layer. The optical parameters for the particle matter $q_m^{(p)}$ are prepared, including the extinction coefficient ($m = 1$) including the scattering and absorption process and the absorption coefficient ($m = 2$) the moments of the volume scattering phase function ($m = 3\text{-}4$: first-second order).

3.6.6.1 Aerosol

In this section, `SUBROUTINE:[SCATAE]` in pradt.F is described.

The optical thickness τ^{ae}, the part of the optical thickness due to absorption τ_{ab}^{ae}, the scattering moment Q_m^{ae} for aerosol are

$$\tau^{ae} = \sum_p q_{1,n}^{(p)} r^{(p)} \times \rho \Delta z 10^{-1} \tag{3.182}$$

$$\tau_{ab}^{ae} = \sum_p q_{2,n}^{(p)} r^{(p)} \times \rho \Delta z 10^{-1} \tag{3.183}$$

$$Q_m^{ae} = \sum_p q_{m,n}^{(p)} r^{(p)} \times \rho \Delta z 10^{-1} (\text{ m} \geq 3) \tag{3.184}$$

p is the aerosol type, and $r^{(p)}$ is volume mixing ratio of the particle. The optical parameters for the particle $q_{m,n}^{(p)}$ depend on the mode radius index n prescribed for each particle (IRA). In the MIROC 6.0, the number of the considered aerosol types p 15 (1-6:soil dust (bin1-6), 7:carbonaceous (BC/OC=0.3), 8:carbonaceous (BC/OC=0.15), 9:carbonaceous (BC/OC=0), 10:black carbon (external mixture), 11:sulfate, 12-15:sea salt (bin 1-4)).

If the aerosol radius is used, the optical thickness τ^{ae}, the part of the optical thickness due to absorption τ_{ab}^{ae}, and the scattering moment Q_m^{ae} for the hygroscopic aerosols (e.g., carbonaceous, sulfate, sea salt) are

$$\tau^{ae} = \sum_p \left[(1 - FX_{ae}) q_{1,nfit}^{(p)} r^{(p)} + FX_{ae} q_{1,nfit+1}^{(p)} r^{(p)} \right] \times \rho \Delta z 10^{-1} \tag{3.185}$$

$$\tau_{ab}^{ae} = \sum_p \left[(1 - FX_{ae}) q_{2,nfit}^{(p)} r^{(p)} + FX_{ae} q_{2,nfit+1}^{(p)} r^{(p)} \right] \times \rho \Delta z 10^{-1} \tag{3.186}$$

$$Q_m^{ae} = \sum_p \left[(1 - FX_{ae}) q_{m,nfit}^{(p)} r^{(p)} + FX_{ae} q_{m,nfit+1}^{(p)} r^{(p)} \right] \times \rho \Delta z 10^{-1} (\text{ m} \geq 2) \tag{3.187}$$

$$FX_{ae} = \left(RH - RH_{nfit}^{(ref)} \right) \left(\frac{1}{RH_{nfit+1}^{(ref)} - RH_{nfit}^{(ref)}} \right) \tag{3.188}$$

where RH is the local relative humidity and $RH_{nfit}^{(ref)}$ is the relative humidity given in the parameter and $nfit$ is the number of the prescribed relative humidity closest to the RH. $nfit$ and FX_{ae} are calculated in the SUBROUTINE:[RMDIDX] in pradt.F and determined in advance. In the above formulas, 10^{-1} is multiplied to convert from km to cm, and from ppmv to ratio.

3.6.6.2 Rayleigh Scattering

In this section, SUBROUTINE:[SCATRY] in pradt.F is described.

The optical thickness τ^r of Rayleigh scattering and the part of the optical thickness due to absorption τ_{ab}^r are

$$\tau^r = \frac{e^r qmol_1 dp}{p_{STD}} \tag{3.189}$$

$$\tau_{ab}^r = \frac{e^r qmol_2 dp}{p_{STD}} \tag{3.190}$$

81

$$p_{STD} = 1013.25 \tag{3.191}$$

where e^r is the Rayleigh scattering coefficient, $qmol_m$ is the moments of the phase function. These calculations are performed up to $m = 2$. Also, this is added to the optical thickness for the aerosol.

$$\tau^{ae+r} = \tau^{ae} + \tau^r \tag{3.192}$$

$$\tau_{ab}^{ae+r} = \tau_{ab}^{ae} + \tau_{ab}^r \tag{3.193}$$

3.6.6.3 Cloud

In this section, SUBROUTINE:[SCATCL] in pradt.F is described.

The optical thickness τ^{cl}, the part of the optical thickness due to absorption τ_{ab}^{cl}, and the scattering moment Q_m^{cl} for cloud are

$$\tau^{cl} = \sum_{ct} q_{1,n}^{(ct)} r^{(ct)} \times \rho \Delta z 10^{-1} \tag{3.194}$$

$$\tau_{ab}^{cl} = \sum_{ct} q_{2,n}^{(ct)} r^{(ct)} \times \rho \Delta z 10^{-1} \tag{3.195}$$

$$Q_m^{cl} = \sum_{ct} q_{m,n}^{(ct)} \times r^{(ct)} \rho \Delta z 10^{-1} (\text{ m} \geq 3) \tag{3.196}$$

ct is the cloud particle type (1:liquid cloud, 2:ice cloud). The optical parameters for the particle $q_{m,n}^{(ct)}$ depend on the mode radius index n prescribed for each particle (IRC). If the cloud radius is used, the optical thickness τ^{cl}, the part of the optical thickness due to absorption τ_{ab}^{cl}, and the scattering moment Q_m^{cl} for cloud are

$$\tau^{cl} = \sum_{ct} \left[(1 - FX_{cl}) q_{1,nfit}^{(ct)} r^{(ct)} + FX_{cl} q_{1,nfit+1}^{(ct)} r^{(ct)} \right] \times \rho \Delta z 10^{-1} \tag{3.197}$$

$$\tau_{ab}^{cl} = \sum_{ct} \left[(1 - FX_{cl}) q_{2,nfit}^{(ct)} r^{(ct)} + FX_{cl} q_{2,nfit+1}^{(ct)} r^{(ct)} \right] \times \rho \Delta z 10^{-1} \tag{3.198}$$

$$Q_m^{cl} = \sum_{ct} \left[(1 - FX_{cl}) q_{m,nfit}^{(ct)} r^{(ct)} + FX_{cl} q_{m,nfit+1}^{(ct)} r^{(ct)} \right] \times \rho \Delta z 10^{-1} (\text{ m} \geq 3) \tag{3.199}$$

$$FX_{cl} = \left(R^{(ct)} - R_{nfit}^{(ref)} \right) \left(\frac{1}{R_{nfit+1}^{(ref)} - R_{nfit}^{(ref)}} \right) \tag{3.200}$$

where $R^{(ct)}$ is the calculated mode radius and $R^{(ref)}_{nfit}$ is the mode radius given in the parameter and $nfit$ is the number of the prescribed mode radius closest to the $R^{(ct)}$. $nfit$ and FX_{cl} are calculated in the subroutine `SUBROUTINE:[RMDIDX]` in pradt.F and determined in advance. In the above formulas, 10^{-1} is multiplied to convert from km to cm, and from ppmv to ratio.

Finally, the total optical thickness for particle scattering, Rayleigh scattering and absorption τ^p and the contribution of scattering τ^{scat} are obtained as follows.

$$\tau^P = \tau^{cl} + \tau^{ae+r} \tag{3.201}$$

$$\tau^{scat} = \tau^P - \left(T^{cl}_{ab} + T^{ae+r}_{ab} \right) \tag{3.202}$$

In addition, the moments of the normalized phase function G are calculated up to the three orders. The zeroth moment G_1 is trivial from the normalization condition of the phase function. The first and second moments G_2, G_3, are referred as the asymmetry factor g and the truncation factor f.

$$G_1 = 1.0 \tag{3.203}$$

$$G_{m-1} = \frac{Q^{cl}_m + Q^{ae}_m}{\tau^{scat}} (m \geq 3), \quad G_2 = g, \quad G_3 = f \tag{3.204}$$

This calculation is divided into the cloudy, clear sky and cumulus conditions. In the cloudy and cumulus conditions, τ^{cl} in the 0.5 and 0.67 μm regions is as recorded as τ^{vis} in subroutine DTRN31.

**R^{ct} is calculated in `SUBROUTINE:[RADFLX]` as follows.

$$R^{(ct)} = \left(\frac{3}{4\pi} \frac{\rho r^{(ct)}}{\rho^{(ct)}_w n^{(ct)}_c} \right)^{1/3} \tag{3.205}$$

$\rho^{(ct)}_w$ is the liquid or ice density. r^{ct} is the amount of the liquid or ice cloud and calculated as follows.

$$r^{(ct)} = \frac{C_{st} r^{(ct)}_{st} + C_{cu} r^{(ct)}_{cu}}{1 - (1 - C_{st})(1 - C_{cu})} \tag{3.206}$$

C is the area of the cloud, and the subscript st and cu mean the stratus and cumulus. When $r^{(ct)}_{st,cu}$ is the small amount in the stratosphere, it is reset to 0. $n^{(ct)}_c$ is the number density of cloud particles.

$$n^{(liq)}_c = \max \left(\frac{q^{liq}_{ae} p N_A}{R T_v (18 \times 10^{-3} R_v/R)}, f_{liq} n^{(liq)}_{\min} \right) \tag{3.207}$$

$$n^{(ice)}_c = \max \left(\frac{q^{ice}_{ae} p N_A}{R T_v (18 \times 10^{-3} R_v R_v/R)}, (1 - f_{liq}) n^{(ice)}_{\min} \right) \tag{3.208}$$

where q_{ae}^{liq} is the mixing ratio of the aerosol particles calculated by the SPRINTERS and converted to the number concentration, and $n_{min}^{(ct)}$ is the minimum number of the cloud particles. and f_{liq} is liquid fraction. Also, $n_c^{(ct)}$ is calculated as follows when using OPT_AECL_SIMPLE.

$$n_c^{(ct)} = \frac{\varepsilon n_a n_{max}^{(ct)}}{\varepsilon n_a + n_{max}^{(ct)}} \tag{3.209}$$

where n_a is the number density of aerosol particles give as an external condition, and ε and $n_{max}^{(ct)}$ are constants. f_{liq} is calculated by the following formula using the amount of cloud water w ($0 \leq f_{liq} \leq 1$).

$$f_{liq} = \frac{w_{st} f_{liq,st} + w_{cu} f_{liq,cu}}{w_{st} + w_{cu}} \tag{3.210}$$

3.6.7 Total Optical Thickness

All optical thickness including gaseous band absorption, and scattering is,

$$\tau = \tau^{KD} + \tau^{CON} + \tau^P \tag{3.211}$$

where because τ^{KD} is different for each subchannel, the calculation is done for each subchannel and each layer, and divided into the cloudy, clear sky, and cumulus conditions.

3.6.8 Expansion of the Plank Function

In this section, SUBROUTINE:[PLKEXP] in pradt.F is described.

In each layer, the Planck function B is expanded as follows and the expansion coefficients b_0, b_1, and b_2, are obtained.

$$B\left(\tau'\right) = b_0 + b_1 \tau' + b_2 \left(\tau'\right)^2 \tag{3.212}$$

Here, as $B\left(\tau'\right)$, B at the top of each layer (the boundary with the top layer) is used, and as $B(\tau)$, B at the bottom edge of each layer (the boundary with the layer below), and as $B(\tau/2)$, the B at the representative level of each layer.

$$b_0 = B(0) \tag{3.213}$$

$$b_1 = (4\ B(\tau/2) - B(\tau) - 3\ B(0))/\tau \tag{3.214}$$

$$b_2 = 2(\ B(\tau) - B(0) - 2\ B(\tau/2))/\tau^2 \tag{3.215}$$

This calculation is done for each sub-channel and each layer and divided into the cloudy, clear sky and cumulus conditions.
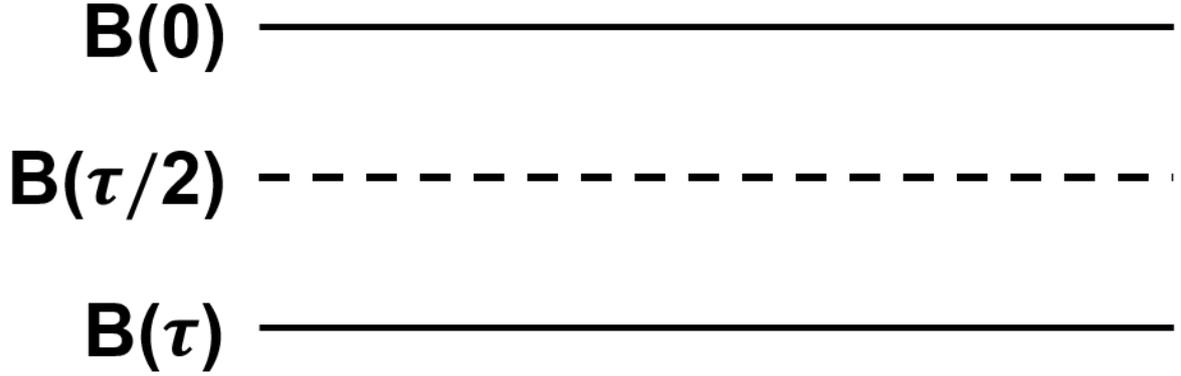
Figure 5: Second-order expansion using the optical thickness of the plank function

3.6.9 Transmission and Reflection Coefficients, and Source Function

In this section, `SUBROUTINE:[TWST]` in pradt.F is described.

Using the obtained optical thickness τ, optical thickness of scattering τ^{scat}, scattering moments g, f, expansion coefficients for Planck function b_n, and solar incidence angle factor μ_0, the transmission coefficient T, reflection coefficient R, downward radiation source function ϵ^+, and the upward radiation source function ϵ^- are founded, by assuming a uniform layer and using the two-stream approximation.

The single-scattering albedo ω is,

$$\omega = \tau^{\text{scat}}/\tau \tag{3.216}$$

The optical thickness τ^*, the single-scattering albedo ω^*, and asymmetric factor g^*, corrected by the contribution from the forward scattering factor f are,

$$\tau^* = \tau(1 - \omega f) \tag{3.217}$$

$$\omega^* = \frac{(1-f)\omega}{1-\omega f} \tag{3.218}$$

$$g^* = \frac{g-f}{1-f} \tag{3.219}$$

μ is a two-stream directional cosine.

$$\mu \equiv \left(\frac{1}{\sqrt{3}}, \frac{1}{1.66}\right) \text{ (shortwave, longwave)} \tag{3.220}$$

$$W^- \equiv \mu^{-1/2} \tag{3.221}$$

Furthermore,

$$\hat{P}^{\pm} = \omega^* W^{-2} \left(1 \pm 3g^* \mu^2\right) / 2 \tag{3.222}$$

$$\hat{S}_s^{\pm} = \omega^* W^- \left(1 \pm 3g^* \mu_0 \mu\right) \tag{3.223}$$

can be determined as above as a normalized scattering phase function.

$$\begin{aligned} X &= \mu^{-1} - \left(\hat{P}^+ - \hat{P}^+\right) \\ &= \mu^{-1} - 3\omega^* W^{-2} \mu^2 g^* \end{aligned} \tag{3.224}$$

$$\begin{aligned} Y &= \mu^{-1} - \left(\hat{P}^+ + \hat{P}^+\right) \\ &= \mu^{-1} - \omega^* W^{-2} \end{aligned} \tag{3.225}$$

$$\begin{aligned} \hat{\sigma}_S^+ &= \hat{S}_S^+ + \hat{S}_S^- \\ &= \omega^* W^- \end{aligned} \tag{3.226}$$

$$\begin{aligned} \hat{\sigma}_S^- &= \hat{S}_s^+ - \hat{S}_S^- \\ &= 3\omega^* \mu_0 W^- \mu g^* \end{aligned} \tag{3.227}$$

Using the above formula, the reflectance R and transmission T become

$$AA = \frac{X\left(1 + e^{-\lambda \tau^*}\right) - \lambda\left(1 - e^{-\lambda \tau^*}\right)}{X\left(1 + e^{-\lambda \tau^*}\right) + \lambda\left(1 - e^{-\lambda \tau^*}\right)} \tag{3.228}$$

$$BB = \frac{X\left(1 - e^{-\lambda \tau^*}\right) - \lambda\left(1 + e^{-\lambda \tau^*}\right)}{X\left(1 - e^{-\lambda \tau^*}\right) + \lambda\left(1 + e^{-\lambda \tau^*}\right)} \tag{3.229}$$

$$\lambda = \sqrt{XY} \tag{3.230}$$

$$R = \tfrac{1}{2}(AA + BB) \tag{3.231}$$

$$T = \tfrac{1}{2}(AA - BB) \tag{3.232}$$

Next, we find the source function derived from the Planck function.

$$\hat{b}_n = 2\pi \left(1 - \omega^*\right) W^- \left(\frac{1}{1 - \omega f}\right)^n b_n \tag{3.233}$$

The expansion coefficients of the radiation source function can be found from the above formulas.

$$D_2^\pm = \frac{\hat{b}_2}{Y} \tag{3.234}$$

$$D_1^\pm = \frac{\hat{b}_1}{Y} \mp \frac{2\hat{b}_2}{XY} \tag{3.235}$$

$$D_0^\pm = \frac{\hat{b}_0}{Y} + \frac{2\hat{b}_2}{XY^2} \mp \frac{\hat{b}_1}{XY} \tag{3.236}$$

$$D^\pm(\tau^*) = D_0^+ + D_1^+ \tau^* + D_2^+ \tau^{*2} \tag{3.237}$$

The radiation source function derived from the Planck function $\hat{\epsilon}_A^\pm$ is

$$\hat{\epsilon}_A^- = D_0^- - RD_0^- - TD^-(\tau^*) \tag{3.238}$$

$$\hat{\epsilon}_A^+ = D^+(\tau^*) - TD_0^+ - RD^-(\tau^*) \tag{3.239}$$

On the other hand, the radiation source function of the solar-induced radiation is

$$\hat{\epsilon}_S^+ = F_{\text{sol}} \left(V_s^+ e^{-\frac{\tau^*}{\mu_0}} - TV_s^+ - RV_s^- e^{-\frac{\tau^*}{\mu_0}} \right) \tag{3.240}$$

$$\hat{\epsilon}_S^+ = F_{\text{sol}} \left(V_s^+ e^{-\frac{\tau^*}{\mu_0}} - TV_s^+ - RV_s^- e^{-\frac{\tau^*}{\mu_0}} \right) \tag{3.241}$$

Here, $Q\gamma$ and $V_s^\pm$ are expressed by the following formulas, and F_{sol} is solar irradiance.

$$V_s^\pm = \frac{1}{2} \left[Q\gamma \pm \left(\frac{Q\gamma}{\mu_0} + \frac{\hat{\sigma}_S^-}{X} \right) \right] \tag{3.242}$$

$$Q\gamma = \frac{X\hat{\sigma}_S^+ \mu_0 + \mu_0^{-1}\hat{\sigma}_S^-}{XY\mu_0 + \mu_0^{-1}} \tag{3.243}$$

The direct solar transmission is also calculated in this subroutine.

$$Ex^{dir} = e^{-\tau^*/\mu_0} \tag{3.244}$$

This calculation is done for each sub-channel and each layer and divided into the cloudy, clear sky, and cumulus conditions.

3.6.10 T, R, S Matrixes for Maximal/Random Approximation

In this section, `SUBROUTINE:[RTSMR]` in pradt.F is described.

In this subroutine, T, R, S matrixes for maximal/random approximation is made. The radiation source function, which is the sum of both the plank function and the solar incident origins, is

$$\epsilon^{-(\text{cloud})} = \hat{\epsilon}_S^{-(\text{cloud})} Tr^{(\text{cloud})} + \hat{\epsilon}_A^{-(\text{cloud})} C \tag{3.245}$$

$$\epsilon^{-(\text{clear})} = \hat{\epsilon}_S^{-(\text{clear})} Tr^{(\text{clear})} + \hat{\epsilon}_A^{-(\text{clear})} (1 - C) \tag{3.246}$$

$$\epsilon^{+(\text{cloud})} = \hat{\epsilon}_S^{+(\text{cloud})} Tr^{(\text{cloud})} + \hat{\epsilon}_A^{-(\text{cloud})} C \tag{3.247}$$

$$\epsilon^{+(\text{clear})} = \hat{\epsilon}_S^{+(\text{clear})} Tr^{(\text{clear})} + \hat{\epsilon}_A^{-(\text{clear})} (1 - C) \tag{3.248}$$

Tr is the direct solar transmission for maximal/random approximation and calculated as follows in `SUBROUTINE:[DTRN31]`.

$$\text{Tr}_n^{(\text{cloud})} = Ex_n^{(\text{cloud})} B_n^{(3)} + Ex_n^{(\text{clear})} \left(1 - B_n^{(1)}\right) \tag{3.249}$$

$$Ex_{n+1}^{(\text{cloud})} = Tr_n^{(\text{cloud})} Ex_n^{\text{dir(cloud)}} \tag{3.250}$$

$$Tr_n^{(\text{clear})} = Ex_n^{(\text{cloud})} \left(1 - B_n^{(3)}\right) + Ex_n^{(\text{clear})} B_n^{(1)} \tag{3.251}$$

$$Ex_{n+1}^{(\text{clear})} = Tr_n^{(\text{clear})} Ex_n^{\text{dir(clear)}} \tag{3.252}$$

Ex is the cumulative direct solar transmission. $B_n^{(1-4)}$ is the cloud cover interaction index and calculated in `SUBROUTINE:[BCVR]` in pradt.F.

$$B_n^{(1)} = \frac{1 - \max(C_{n-1}, C_n)}{1 - C_{n-1}} \tag{3.253}$$

$$B_n^{(2)} = \frac{1 - \max(C_{n+1}, C_n)}{1 - C_{n+1}} \tag{3.254}$$

$$B_n^{(3)} = \frac{\min(C_{n-1}, C_n)}{C_{n-1}} \tag{3.255}$$

$$B_n^{(4)} = \frac{\min(C_{n+1}, C_n)}{C_{n+1}} \tag{3.256}$$

Next, T matrixes for maximal/random approximation are calculated.

$$T^{+(cloud,1)} = T^{(\text{cloud})} B^{(3)} \tag{3.257}$$

$$T^{+(\text{cloud},2)} = T^{(\text{cloud})} \left(1 - B^{(1)}\right) \tag{3.258}$$

$$T^{+(\text{clear},1)} = T^{(\text{clear})} \left(1 - B^{(3)}\right) \tag{3.259}$$

$$T^{+(\text{clear},2)} = T^{(\text{clear})} B^{(1)} \tag{3.260}$$

$$T^{-(\text{cloud},1)} = T^{(\text{cloud})} B^{(4)} \tag{3.261}$$

$$T^{-(\text{cloud},2)} = T^{(\text{cloud})} \left(1 - B^{(2)}\right) \tag{3.262}$$

$$T^{-(\text{clear},1)} = T^{(\text{clear})} \left(1 - B^{(4)}\right) \tag{3.263}$$

$$T^{-(\text{clear},2)} = T^{(\text{clear})} B^{(2)} \tag{3.264}$$

Also, R matrixes for maximal/random approximation are calculated.

$$R^{+(\text{cloud},1)} = R^{(\text{cloud})} B^{(3)} \tag{3.265}$$

$$R^{+(\text{cloud},2)} = R^{(\text{cloud})} \left(1 - B^{(1)}\right) \tag{3.266}$$

$$R^{+(\text{clear},1)} = R^{(\text{clear})} \left(1 - B^{(3)}\right) \tag{3.267}$$

$$R^{+(\text{clear},2)} = R^{(\text{clear})} B^{(1)} \tag{3.268}$$

$$R^{-(\text{cloud},1)} = R^{(\text{cloud})} B^{(4)} \tag{3.269}$$

$$R^{-(\text{cloud},2)} = R^{(\text{cloud})} \left(1 - B^{(2)}\right) \tag{3.270}$$

$$R^{-(\text{clear},1)} = R^{(\text{clear})} \left(1 - B^{(4)}\right) \tag{3.271}$$

$$R^{-(\text{clear},2)} = R^{(\text{clear})} B^{(2)} \tag{3.272}$$

This calculation is done for each sub-channel and each layer.
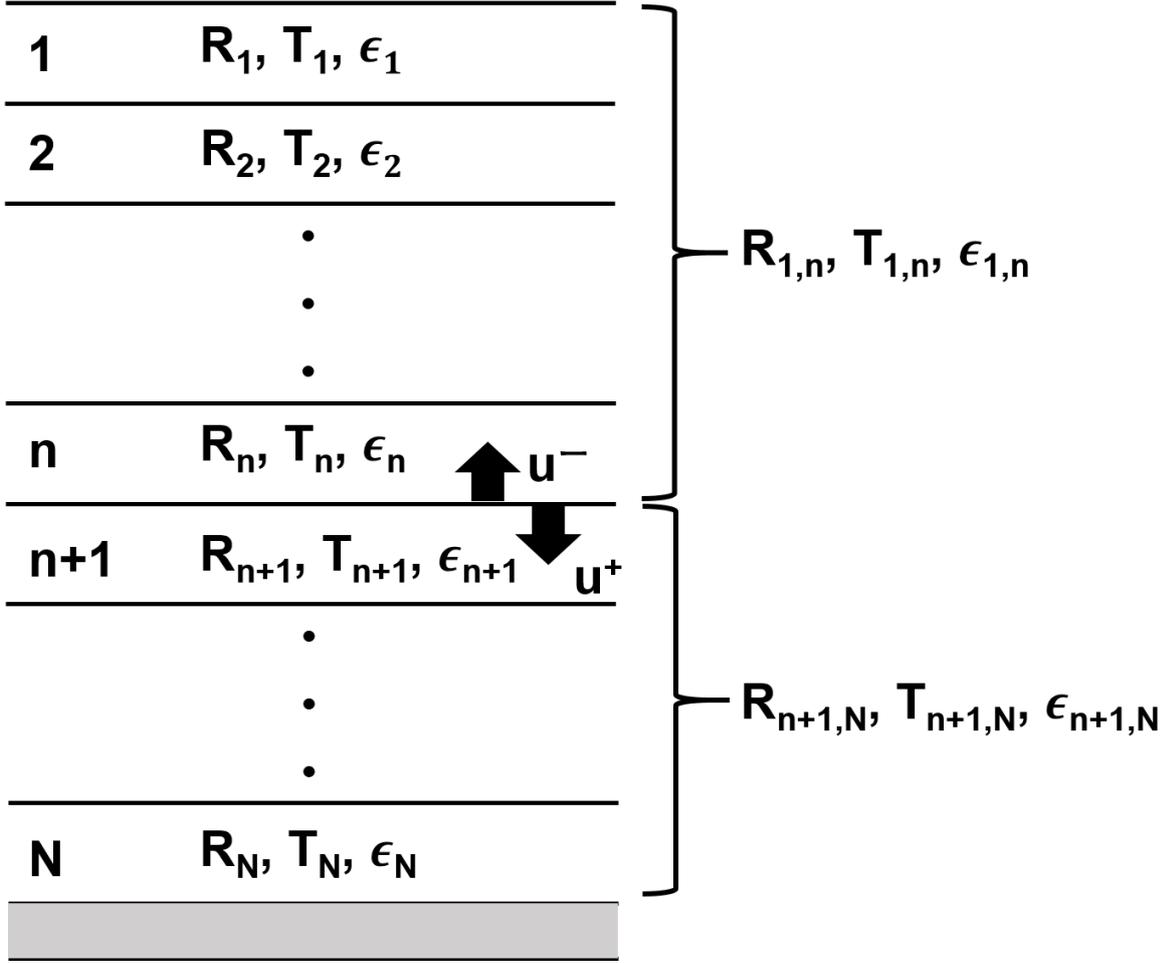
Figure 6: Schematic illustration of the adding method

3.6.11 Adding of Source Functions for Each Layer

In this section, `SUBROUTINE:[ADDMR]` and `SUBROTINE:[ADDING]` in pradt.F is described.

By using transmission coefficient T, reflection coefficient R, and radiation source function ε in all layers, the radiation fluxes u at each layer boundary can be obtained by using the adding method. This means that the when two layers of T, R, ε are known, the T, R, ε of the whole combined layer of the two layers can be easily calculated.

3.6.11.1 `SUBROUTINE:[ADDMR]`

In this subroutine, the maximal/random flux in cloudy conditions is calculated by the adding method and the T, R, and S matrixes are used for calculations.

First, the upward radiation source function the bottom layer is calculated.

In the shortwave region,

$$\epsilon_N^{-(\text{cloud})} = W^+ \alpha_s \mu_0 \left(\frac{1}{\mu}\right) F_0 e_N^{-\langle \tau^* \rangle / \mu_0 (\text{cloud})} \tag{3.273}$$

$$\epsilon_N^{-(\text{clear})} = W^+ \alpha_s \mu_0 \left(\frac{1}{\mu}\right) F_0 e_N^{-\langle \tau^* \rangle / \mu_0 (\text{clear})} \tag{3.274}$$

$\langle\tau^*\rangle$ indicates the total optical thickness τ^* of from the upper end of the atmosphere to the upper end of the layer currently being considered and $e^{-\langle\tau^*\rangle/\mu_0}$ is calculated in `SUBROUTINE:[ADDMR]` of pradt.F.

In the longwave region,

$$\epsilon_N^{-(\text{cloud})} = \epsilon_N^{-(\text{cloud})} + W^+ 2\pi \left(1 - \alpha_s\right) B_N C_N \tag{3.275}$$

$$\epsilon_N^{-(\text{clear})} = \epsilon_N^{-(\text{clear})} + W^+ 2\pi \left(1 - \alpha_s\right) B_N \left(1 - C_N\right) \tag{3.276}$$

Here,

$$W^+ \equiv \mu^{1/2} \tag{3.277}$$

The reflectance $R_{1,n}^-$ and source function $\epsilon_{1,n}^+$ regarded from the first to the n layers as a single layer are

$$\epsilon_{1,n}^+ = \epsilon_n^+ + T_n^+ \left(1 - R_n^+ R_{1,n-1}^-\right)^{-1} \left(R_{1,n-1}^- \epsilon_n^- + \epsilon_{1,n-1}^+\right) \tag{3.278}$$

$$R_{1,n}^- = R_n^- + T_n^+ \left(1 - R_n^+ R_{1,n-1}^-\right)^{-1} R_{1,n-1}^- T_n^- \tag{3.279}$$

The upward and downward fluxes at the bottom of the atmosphere are

$$u_{N+1/2}^+ = \left(1 - R_{1,N-1}^- R_N^+\right)^{-1} \left(\epsilon_{1,N-1}^+ + R_{1,N-1}^- \epsilon_N^-\right) \tag{3.280}$$

$$u_{N+1/2}^- = \left(1 - R_N^+ R_{1,N-1}^-\right)^{-1} \left(\epsilon_N^- + R_N^+ \epsilon_{1,N-1}^+\right) \tag{3.281}$$

Also, upward and downward fluxes at the boundary between layers n and $n+1$ are

$$u_{n+1/2}^+ = \left(1 - R_{1,n-1}^- R_n^+\right)^{-1} \left(R_{1,n-1}^- T_n^- u_{n+1/2}^- + R_{1,n-1}^- \epsilon_n^- + \epsilon_{1,n}^+\right) \tag{3.282}$$

$$u_{n+1/2}^- = \left(1 - R_n^+ R_{1,n-1}^-\right)^{-1} \left(T_n^- u_{n+1/2}^- + R_n^+ \epsilon_{1,n-1}^+ + \epsilon_n^-\right) \tag{3.283}$$

However, the upward and downward flux at the upper end of the atmosphere is as follows.

$$u_{1/2}^+ = 0 \tag{3.284}$$

$$u_{1/2}^- = T_1^- u_{1+1/2}^- + \epsilon_1^- \tag{3.285}$$

Finally, since this flux is scaled, we rescaled and added the direct solar incidence to the find the radiation flux. Furthermore, the flux in the cloudy area and the clear sky area is added.

$$F_{n+1/2}^+ = \frac{W^+}{W} \left(u_{n+1/2}^{+(\text{cloud})} + u_{n+1/2}^{+(\text{clear})} \right) + \mu_0 F_0 \left(e_{n+1/2}^{-\langle \tau^* \rangle / \mu_0 (\text{cloud})} \right) \tag{3.286}$$

$$F_{n+1/2}^- = \frac{W^+}{W} \left(u_{n+1/2}^{-(\text{cloud})} + u_{n+1/2}^{-(\text{clear})} \right) \tag{3.287}$$

Also, surface direct downward radiation flux F_{sf}^+ is

$$F_{sf}^+ = \mu_0 F_0 \left(e_N^{-\langle \tau^* \rangle / \mu_0 (\text{cloud})} + e_N^{-\langle \tau^* \rangle / \mu_0 (\text{clear})} \right) \tag{3.288}$$

This calculation is done for each sub-channel.

3.6.11.2 SUBROUTINE: [ADDING]

Since the maximal/random approximation cannot be used under the clear sky condition, this subroutine is used to calculate the flux.

First, the radiation source function, which is the sum of both the plank function origin and the solar incident origin, is

$$\epsilon^\pm = \hat{\epsilon}_S^\pm e^{-\langle \tau^* \rangle / \mu_0} + \hat{\epsilon}_A^\pm \tag{3.289}$$

There are layers $1, 2, \ldots, N$ from the top. The surface layer is considered to be a single layer and the N layer. Given the reflectance and source function of the layers from the n to the N layer as a single layer $R_{n,N}$, $\epsilon_{n,N}^-$,

$$R_{n,N} = R_{n,N} + T_n \left(1 - R_{n+1,N} R_n \right)^{-1} R_{n+1} T_n \tag{3.290}$$

$$\epsilon_{n,N}^- = \epsilon_n^- + T_n \left(1 - R_{n+1,N} R_n \right)^{-1} \left(R_{n+1,N} \epsilon_n^+ + \epsilon_{n,N}^- \right) \tag{3.291}$$

$$R_{n,N} = R_{n,N} + T_n \left(1 - R_{n+1,N} R_n \right)^{-1} R_{n+1} T_n \tag{3.292}$$

$$\epsilon_{n,N}^- = \epsilon_n^- + T_n \left(1 - R_{n+1,N} R_n \right)^{-1} \left(R_{n+1,N} \epsilon_n^+ + \epsilon_{n,N}^- \right) \tag{3.293}$$

This can be solved by $n = N - 1, \ldots, 1$ in sequence, starting from the values at the surface $R_{N,N}$, $\epsilon_{N,N}^-$.

$$R_{N,N} = R_N = \alpha_s \tag{3.294}$$

$$\epsilon_{N,N} = W^+ \left(\alpha_s \mu_0 \left(\frac{1}{\mu} \right) e^{-\langle \tau^* \rangle / \mu_0} F_0 + 2\pi \left(1 - \alpha_s \right) B_N \right) \tag{3.295}$$

The reflectance $R_{1,n}$ and source function $\epsilon_{1,n}^+$ regarded from the first to the n layers as a single layer are

$$R_{1,n} = R_n + T_n \left(1 - R_{1,n-1}R_n\right)^{-1} R_{1,n-1}T_n \tag{3.296}$$

$$\epsilon_{1,N}^+ = \epsilon_n^+ + T_n \left(1 - R_{1,n-1}R_n\right)^{-1} \left(R_{1,n-1}\epsilon_n^- + \epsilon_{1,n-1}^+\right) \tag{3.297}$$

It can be solved by $n = 2, \ldots, N$, starting from $R_{1,1} = R_1, \epsilon_{1,1}^+ = \epsilon_1^+$.

With these, downward flux at the boundary between layers n and $n + 1$, the downward and upward flux are came back to a problem between two layers of combined layer, the combinations of layers $1 - n$ and $n + 1 - N$.

$$u_{n+1/2}^+ = \left(1 - R_{1,n}R_{n+1,N}\right)^{-1} \left(\epsilon_{1,n}^+ + R_{1,n}\epsilon_{n+1,N}^-\right) \tag{3.298}$$

$$u_{n+1/2}^- = R_{n+1,N}u_{n,n+1}^+ + \epsilon_{n+1,N}^- \tag{3.299}$$

can be written as above. However, the flux at the top of the atmosphere is

$$u_{1/2}^+ = 0 \tag{3.300}$$

$$u_{1/2}^- = \epsilon_{1,N}^- \tag{3.301}$$

Finally, since this flux is scaled, we rescaled and added the direct solar incidence to the find the radiation flux.

$$F_{n+1/2}^+ = \frac{W^+}{W} u_{n+1/2}^+ + \mu_0 e^{-\langle \tau^* \rangle / \mu_0} F_0 \tag{3.302}$$

$$F_{n+1/2}^- = \frac{W^+}{W} u_{n+1/2}^- \tag{3.303}$$

Also, surface direct downward radiation flux F_{sf}^+ is

$$F_{sf}^+ = \mu_0 F_0 e^{-\langle \tau^* \rangle \, \mu_0} \tag{3.304}$$

3.6.12 Adding in the Flux

$$F^\pm = \sum_c w_c \left(1 - C_{cu}\right) \bar{F}^\pm + \sum_c w_c C_{cu} F^{c\pm} \tag{3.305}$$

$$F^{\circ\pm} = \sum_c w_c F^{\circ\pm} \tag{3.306}$$

93

If the radiation flux $F_C^\pm$ is found for each sub-channel in each layer, the wavelength-integrated flux is found by multiplying a weight w_c correspondingly to a wavelength representative of the sub-channel and adding. C_{cu} is the horizontal coverage of the cumulus cloud. It is divided into the short wavelength range and long wavelength range and added together. In addition, the downward flux of a part of the short wavelength region (shorter than the wavelength of 0.7-0.8 μm) at the surface is obtained as PAR (photosynthetically active radiation). Also, the radiation flux in the clear-sky condition is calculated ($F^{\circ\pm}$).

Also, in the shortwave region, we find the downward radiation at the lower end of the atmosphere and the difference between the surface direct downward radiation flux.

$$F_{sf}^+ = \sum_c w_c \left(1 - C_u\right) \bar{F}_{N+1/2}^+ + \sum_c w_c C_{cu} F_{N+1/2}^c \tag{3.307}$$

$$F_{sf,dif}^+ = \sum_c w_c \left(1 - C_{cu}\right) \left(\bar{F}_{N+1/2}^+ - \bar{F}_{sf}^+\right) + \sum_c w_c C_{cu} \left(F_{N+1/2}^c - F_{sf}^c\right) \tag{3.308}$$

This calculation is done in `SUBROUTINE:[DTRN31]`

3.6.13 Calculation of the Temperature Derivative of the Flux

To implicitly solve for surface temperature, calculate differential term of upward flux with respect to surface temperature $\mathrm{d}F^\mp/dT_g$. Therefore, we obtained the value for temperatures 1K higher than T_g $\bar{B}^w(T_g+1)$ and used it to redo the flux calculation using the addition method, and the difference from the original value is set to $\mathrm{d}F^\mp/dT_g$. This is a meaningful value only in the longwave region (earth radiation region). This calculation is done in `SUBROUTINE:[RADFLX]` of pradt.F.

3.6.14 Calculation of the Heating Rate

The heating rate of the nth layer H_n is calculated by using the radiation flux obtained so far. It is calculated separately for shortwave and longwave ranges, and finally add together (`SUBROUTINE:[RDTND]` in pradm.F).

$$H_n = -\frac{\left(F_n^- - F_n^-\right) - \left(F_n^+ - F_{n+1}^+\right)}{gC_p dp} \tag{3.309}$$

3.6.15 Flux of incidence and incident angle

In this section, `SUBROUTINE:[SHTINS]` in pradi.F is described.

The following parameters are determined using the orbital eccentricity e, with reference to Berger (1978).

$$\beta = \sqrt{1 - e^2} \tag{3.310}$$

$$a_1 = -2\left(\tfrac{1}{2}e + \tfrac{1}{8}e^3\right)(1 + \beta) \tag{3.311}$$

$$a_2 = -2\left(-\tfrac{1}{4}e^2\right)\left(\tfrac{1}{2} + \beta\right) \tag{3.312}$$

94

$$a_3 = -2\left(\tfrac{1}{8}e^3\right)\left(\tfrac{1}{2} + \beta\right) \tag{3.313}$$

$$b_1 = 2e - \tfrac{1}{4}e^3 \tag{3.314}$$

$$b_2 = \tfrac{5}{4}e^2 \tag{3.315}$$

$$b_3 = \tfrac{13}{12}e^3 \tag{3.316}$$

Additionally,

$$\epsilon = \tfrac{epsd}{180}\pi \tag{3.317}$$

$$\varpi = \tfrac{vpid+180}{180}\pi \tag{3.318}$$

where *epsd* and *vpid* are the angle of the obliquity, and the precession represented by the true longitude of the perihelion measured from the vernal equinox.

The mean longitude of the vernal equinox λ_0 is computed.

$$\lambda_0 = a_1 \sin(-\varpi) + a_2 \sin(-2\varpi) + a_3 \sin(-3\varpi) \tag{3.319}$$

The mean longitude of the Earth position λ_m at time t_m is represented by using the position of the vernal equinox λ_0.

$$\lambda_m = \tfrac{t_m - t_0}{2\pi \times t_{year}} + \lambda_0 \tag{3.320}$$

where t_{year} is the number of seconds in year, and the origin of the time t_0 is defined as the time of the vernal (March) equinox.

The true longitude of the Earth position V at time t_m is calculated as below.

$$\tag{3.321}$$

$$V = \lambda_m - \varpi + b_1 \sin\left(\lambda_m - \varpi\right) + b_2 \sin 2\left(\lambda_m - \varpi\right) + b_3 \sin 3\left(\lambda_m - \varpi\right) \tag{3.322}$$

The solar declination δ is

$$\delta = \arcsin(\sin\epsilon \sin(V + \varpi)) \tag{3.323}$$

The incident angle $\cos\zeta$ is founded by using the latitude φ, the solar declination δ, and the hour angle at a point of longitude h.

$$\mu_0 = \cos\zeta = \sin\varphi\sin\delta + \cos\varphi\cos\delta\cosh \tag{3.324}$$

Incident Flux F_0 is represented as follows,

$$F_0 = F_{00}r^{-2} \tag{3.325}$$

$$r = \frac{1-e^2}{1+e(\cos V + \varpi)} \tag{3.326}$$

where F_{00} is the solar constant and is the ratio to the time of the distance between the sun and the earth. The number of times when $\cos\zeta \geq 0$ (in the daytime) in time increments (set in NHSUB), is counted, and F_0 and $\cos\zeta$ are finally averaged.

It is also possible to give average annual insolation. In this case, the annual and day mean incidence and angle of incidence are approximated as follows.

$$\bar{F} = F_{00}/\pi \tag{3.327}$$

$$\bar{\mu}_0 \simeq 0.410 + 0.590\cos^2\varphi \tag{3.328}$$

3.6.16   Reading Each Parameter

In SUBROUTINE:[OPPARM2] of pradt.F, various parameters used for radiation calculation are read. The outline of the procedure is shown below.

1. Read the numbers of bands, the radiances representative of upward and downward radiation, the grids of the pressure log(p), grid of the temperatures, the optical flag, and CFCs.

2. Read the band boundaries and the information of the pressure grid and temperature grid.

3. First, the optical property flag, the number of channels, the weights for channels and the number of the molecules including in a waveband are read. The optical property flag is modified in order to distinguish the PAR, 0.67, 0.5, and 10.5 μm. Additionally, molecule ID and k-width are read for each molecule. Finally, the absorption coefficient for the self-broadening and CFC are also done only when the optical property flag in the band is positive. The k-width and the absorption coefficient for the self-broadening are arranged in the order of the grid of the temperatures, the grids of the pressures, and the channels. Step 3 is performed for each wavelength band.

4. First, the number of particles is read. Next, the numbers of the modes and the mode radius (or relative humidity) are read for each particle. Using the mode radius (or relative humidity), the following parameter required to interpolate the calculated values is calculated for each mode number.

$$\frac{1}{R_{n+1}^{(ref)} - R_n^{(ref)}} \tag{3.329}$$

5. Read the band boundaries again.

6. Read the Plank function coefficient, solar insolation, surface properties (not output), Rayleigh scattering coefficient, Rayleigh scattering phase function. The moment for particle scattering phase function is read in the order of the particle and the optical number and read up to the second moment. Step 6 is performed for each wavelength band.

3.6.17 Other Notes

The calculation of the radiation is usually not done at every step. Thus, the radiation flux is saved, and it is used if the time is not used for radiation calculation. As for the shortwave radiation, using the percentage of time (time is $\mu_0 > 0$) between the next calculation time f and the solar incidence angle factor averaged over the daylight hours $\bar{\mu}_0$, seek the Flux $\bar{F}$,

$$F = f \frac{\mu_0}{\bar{\mu}_0} \bar{F} \tag{3.330}$$

3.7 Turbulence Scheme

A turbulence scheme represents the effect of subgrid-scale turbulence on the grid-mean prognostic variables. It calculates the vertical diffusion of momentum, heat, water and other tracers. The Mellor-Yamada-Nakanishi-Niino scheme (MYNN scheme; Nakanishi 2001; Nakanishi and Niino 2004) has been used as a turbulence scheme in MIROC since its version 5, which is an improved version of the Mellor-Yamada scheme (Mellor 1973; Mellor and Yamada 1974; Mellor and Yamada 1982). Its closure level is 2.5. Level 3 is available, however it was not adopted as a standard option, since we could not gain large benefits despite its much greater computational costs.

In the MYNN scheme, liquid water potential temperature θ_l and total water q_w are used as key variables, which are defined as

$$\theta_l \equiv \left(T - \frac{L_v}{C_p} q_l - \frac{L_v + L_f}{C_p} q_i \right) \left(\frac{p_s}{p} \right)^{\frac{R_d}{C_p}}, \tag{3.331}$$

$$q_w \equiv q_v + q_l + q_i, \tag{3.332}$$

where T and p are temperature and pressure; q_v, q_l and q_i are specific humidity, liquid water content, and ice water content respectively; C_p and R_d are specific heat at constant pressure and gas constant of dry air respectively; L_v and L_f are latent heat of vaporization and fusion per unit mass respectively. p_s is $1000 hPa$. These variables conserve for the phase change of water.

In the level 2.5, the scheme predicts the time evolution of twice turbulent kinetic energy as a prognostic variable, which is defined by

$$q^2 \equiv \langle u^2 + v^2 + w^2 \rangle \tag{3.333}$$

where u, v, and w are velocities in zonal, meridional and vertical directions respectively. In this chapter, uppercase letters represent grid-mean variables and lowercase counterparts the deviation from the grid-mean. $\langle \ \rangle$ denotes an ensemble mean. In the Level 3, $\langle \theta_l^2 \rangle$, $\langle q_w^2 \rangle$, $\langle \theta_l q_w \rangle$ are also predicted, but we skip the details here.

The outline of the computational procedures is given as follows along with the names of the subroutines. All the subroutines listed here are written in a Fortran source code of pvdfm.F.

1. Calculation of friction velocity and the Obukhov length
2. Calculation of buoyancy coefficients [SUBROUTINE:`VDFCND`]
3. Calculation of stability functions of the Level 2 [SUBROUTINE:`VDFLEV2`]
4. Calculation of planetary boundary layer depth [SUBROUTINE:`PBLHGT`]
5. Calculation of master length scale [SUBROUTINE:`VDFMLS`]
6. Calculation of diffusion coefficients, vertical fluxes and their derivatives [SUBROUTINE:`VDFLEV3`]
7. Calculation of production and dissipation terms of twice turbulent kinetic energy [SUBROUTINE:`VDFLEV3`]
8. Calculation of tendencies of prognostic variables with implicit scheme

3.7.1 Surface Layer

The friction velocity u_* and the Obukhov length L_M are given as

$$u_* = \left(\langle uw \rangle_g{}^2 + \langle vw \rangle_g{}^2 \right)^{\frac{1}{4}}, \tag{3.334}$$

$$L_M = -\frac{\Theta_{v,g} u_*{}^3}{kg \langle w\theta_v \rangle_g}, \tag{3.335}$$

where the subscript g indicates the values near the surface Θ_v and θ_v denote virtual potential temperature, k the von Kármán constant, and g the acceleration of gravity. The values of the lowest model layer is used for $\Theta_{v,g}$.

3.7.2 Calculation of the Buoyancy Coefficients

The buoyancy-production term in the prognostic equation of the twice turbulent kinetic energy contains $\langle w\theta_v \rangle$. Following Mellor and Yamada (1982), we assume the probability distribution of θ_l and q_w in a given grid and rewrite this term as

$$\langle w\theta_v \rangle = \beta_\theta \langle w\theta_l \rangle + \beta_q \langle wq_w \rangle. \tag{3.336}$$

However, note that unlike Mellor and Yamada (1982) and Nakanishi and Niino (2004), the probability distribution assumed here is not Gaussian. It is triangular documented in the PDF-based prognostic large-scale condensation scheme (Watanabe et al. 2009). In this case, the buoyancy coefficients, β_θ and β_q are written as

$$\beta_\theta = 1 + \epsilon Q_w - (1+\epsilon)Q_l - Q_i - \tilde{R}abc, \tag{3.337}$$

$$\beta_q = \epsilon\Theta + \tilde{R}ac, \tag{3.338}$$

where $\epsilon = R_v/R_d - 1$. R_v is the gas constant for water vapor, and

$$a = \left(1 + \frac{L_v}{C_p} \left. \frac{\partial Q_s}{\partial T} \right|_{T=T_l} \right)^{-1}, \tag{3.339}$$

$$b = \frac{T}{\Theta} \left. \frac{\partial Q_s}{\partial T} \right|_{T=T_l}, \tag{3.340}$$

$$c = \frac{\Theta}{T} \frac{L_v}{C_p} \left[1 + \epsilon Q_w - (1+\epsilon)Q_l - Q_i \right] - (1+\epsilon)\Theta, \tag{3.341}$$

$$\tilde{R} = R \left\{ 1 - a \left[Q_w - Q_s(T_l) \right] \frac{Q_l}{2\sigma_s} \right\} - \frac{Q_l{}^2}{4\sigma_s{}^2}, \tag{3.342}$$

$$\sigma_s{}^2 = \langle q_w{}^2 \rangle - 2b\langle \theta_l q_w \rangle + b^2 \langle \theta_l{}^2 \rangle, \tag{3.343}$$

where R and Q_l are cloud amount and liquid water computed from the probability distribution in the grids, respectively, and Q_s is saturation water vapor.

3.7.3 Stability Functions for the Level 2

It is known that the Mellor-Yamada Level 2.5 scheme fails to capture the behavior of growing turbulence realistically (Helfand and Labraga 1988). Thus, the MYNN scheme first calculates the twice turbulent kinetic energy of the Level2 $q_2{}^2$, and then make a correction to the diffusion when $q < q_2$, i.e., the turbulence is in a growing phase. The stability functions of the level 2, S_{H2} and S_{M2}, required for the calculation of q_2, are represented by

$$S_{H2} = S_{HC}\frac{Rf_c - Rf}{1 - Rf}, \tag{3.344}$$

$$S_{M2} = S_{MC}\frac{R_{f1} - Rf}{R_{f2} - Rf}S_{H2}, \tag{3.345}$$

where Rf is the flux Richardson number and calculated as

$$Rf = R_{i1}\left[Ri + R_{i2} - (Ri^2 - R_{i3}Ri + R_{i2}{}^2)^{1/2}\right]. \tag{3.346}$$

Here, Ri is the gradient Richardson number represented by

$$Ri = \frac{g}{\Theta}\left(\beta_\theta\frac{\partial\Theta_l}{\partial z} + \beta_q\frac{\partial Q_w}{\partial z}\right)\bigg/\left[\left(\frac{\partial U}{\partial z}\right)^2 + \left(\frac{\partial V}{\partial z}\right)^2\right]. \tag{3.347}$$

The other symbols indicate quantities independent of the environmental field, which are given as follows.

$$S_{HC} = 3A_2(\gamma_1 + \gamma_2), \tag{3.348}$$

$$S_{MC} = \frac{A_1}{A_2}\frac{F_1}{F_2}, \tag{3.349}$$

$$Rf_c = \frac{\gamma_1}{\gamma_1 + \gamma_2}, \tag{3.350}$$

$$R_{f1} = B_1\frac{\gamma_1 - C_1}{F_1}, \tag{3.351}$$

$$R_{f2} = B_1\frac{\gamma_1}{F_2}, \tag{3.352}$$

$$R_{i1} = \frac{1}{2S_{Mc}}, \tag{3.353}$$

$$R_{i2} = R_{f1}S_{MC}, \tag{3.354}$$

$$R_{i3} = 4R_{f2}S_{MC} - 2R_{i2}, \tag{3.355}$$

where

$$A_1 = B_1 \frac{1 - 3\gamma_1}{6}, \tag{3.356}$$

$$A_2 = A_1 \frac{\gamma_1 - C_1}{\gamma_1 Pr}, \tag{3.357}$$

$$C_1 = \gamma_1 - \frac{1}{3A_1 B_1^{\frac{1}{3}}}, \tag{3.358}$$

$$F_1 = B_1(\gamma_1 - C_1) + 2A_1(3 - 2C_2) + 3A_2(1 - C_2)(1 - C_5), \tag{3.359}$$

$$F_2 = B_1(\gamma_1 + \gamma_2) - 3A_1(1 - C_2), \tag{3.360}$$

$$\gamma_2 = \frac{B_2}{B_1}(1 - C_3) + \frac{2A_1}{B_1}(3 - 2C_2), \tag{3.361}$$

and

$$(Pr, \gamma_1, B_1, B_2, C_2, C_3, C_4, C_5) = (0.74, 0.235, 24.0, 15.0, 0.7, 0.323, 0.0, 0.2). \tag{3.362}$$

3.7.4 Master Length Scale

3.7.4.1 Original Formulation by Nakanishi (2001)

Nakanishi (2001) proposed the following formulation for the master length scale L.

$$\frac{1}{L} = \frac{1}{L_S} + \frac{1}{L_T} + \frac{1}{L_B}, \tag{3.363}$$

where L_S, L_T, L_B represent length scales in the surface layer, convective boundary layer, and stably stratified layer respectively. These length scales are formulated as

$$L_S = \begin{cases} kz/3.7 & \zeta \geq 1 \\ kz/(2.7 + \zeta) & 0 \leq \zeta < 1 \\ kz(1 - \alpha_4\zeta)^{0.2} & \zeta < 0, \end{cases} \tag{3.364}$$

$$L_T = \alpha_1 \frac{\displaystyle\int_0^\infty qz \, dz}{\displaystyle\int_0^\infty q \, dz}, \tag{3.365}$$

101

$$
L_B = \begin{cases} \alpha_2 q/N & \partial\Theta_v/\partial z > 0 \quad \text{and} \quad \zeta \geq 0 \\ \left[\alpha_2 + \alpha_3(q_c/L_T N)^{1/2}\right] q/N & \partial\Theta_v/\partial z > 0 \quad \text{and} \quad \zeta < 0 \\ \infty & \partial\Theta_v/\partial z \leq 0, \end{cases}
\tag{3.366}
$$

where $\zeta \equiv z/L_M$ is a height normalized by the Monin-Obukhov length L_M, $N \equiv [(g/\Theta)(\partial\Theta_v/\partial z)]^{1/2}$ is the Brunt-Väisälä frequency and $q_c \equiv [(g/\Theta)\langle w\theta_v\rangle_g L_T]^{1/3}$ is a velocity scale in the convective boundary layer.

3.7.4.2 Modifications in MIROC

The above formulation works well when the domain of the model is limited to the planetary boundary layer (PBL) and its surrounding area. However, if the the upper troposphere is included, the formulation gives inappropriate behaviors depending on the conditions: e.g. L_T, the length scale of the convective boundary layer, is used in the free atmosphere, and the turbulent kinetic energy in the free atmosphere is taken into account in the calculation of L_T.

In order to avoid such misbehaviors, the top height of the convective boundary layer H_{PBL} is estimated in MIROC and we consider that the region below $h = \left[(F_H H_{PBL})^2 + H_0^2\right]^{1/2}$ is the one where the PBL-derived turbulence is dominant. Here, we adopted $F_H = 1.5$ and $H_0 = 500$m.

Below the altitude h, equation (3.363) is used as the master length scale, but the vertical range of the integration in L_T is modified as

$$
L_T = \alpha_1 \frac{\displaystyle\int_0^h qz \, dz}{\displaystyle\int_0^h q \, dz},
\tag{3.367}
$$

and then the master length scale above h is represented as

$$
\frac{1}{L} = \frac{1}{L_S} + \frac{1}{L_A} + \frac{1}{L_{max}}
\tag{3.368}
$$

where $L_A = \alpha_5 \, q/N$ is a length scale of air parcel vertically transported by turbulence in a stably stratified layer. α_5 represents the effect of dissipation set to 0.53. $L_{max} = 500$m gives the upper limit of L.

3.7.4.3 Estimation of the Top Height of the Convective Boundary Layer

Based on Holtslag and Boville (1993), H_{PBL} is estimated using the bulk Richardson number Ri_B given as

$$
Ri_B = \frac{[g/\Theta_v(z_1)][\Theta_v(z_k) - \Theta_{v,g}](z_k - z_g)}{[U(z_k) - U(z_1)]^2 + [V(z_k) - V(z_1)]^2 + F_u u_*^2},
\tag{3.369}
$$

where z_k is the altitude of a k-th model layer from the bottom at full level, z_1 the altitude of the lowest layer at full level, z_g the altitude of the surface. F_u is a dimensionless tuning parameter, and

$$
\Theta_{v,g} = \Theta_v(z_1) + F_b \frac{\langle w\theta_v\rangle_g}{w_m},
\tag{3.370}
$$

$$w_m = u_*/\phi_m, \tag{3.371}$$

$$\phi_m = \left(1 - 15\frac{z_s}{L_M}\right)^{-\frac{1}{3}}, \tag{3.372}$$

where z_s is the altitude of the surface layer assumed to be $0.1H_{PBL}$. F_b is a dimensionless tuning parameter.

Ri_B is successively calculated from $k = 2$ upward, and then if Ri_B exceeds 0.5 for the first time, it is linearly interpolated between this level and the level immediately below it. The height satiffying $Ri_B = 0.5$ is used as H_{PBL}. Since H_{PBL} is necessary for the calculation of z_s, we first calculate z_s using a temporary value of $H_{PBL} = z_1 - z_g$, from which we calculate the first guess of H_{PBL}. Then we use this value for the recalculation of z_s, and then it is used for the final estimate of H_{PBL}.

3.7.5 Calculation of Diffusion Coefficients

3.7.5.1 Twice Turbulent Kinetic Energy of Level 2

The twice turbulent kinetic energy of the level 2, $q_2{}^2$, is calculated from the following equation, which neglects the time derivative, advection and diffusion terms in the prognostic equation of the twice turbulent kinetic energy.

$$P_s + P_b - \varepsilon = 0, \tag{3.373}$$

where P_s and P_b denote the production terms by shear and buoyancy respectively. ε is the dissipation term. P_s and P_b are written as

$$P_s = -\langle wu \rangle \frac{\partial U}{\partial z} - \langle wv \rangle \frac{\partial V}{\partial z}, \tag{3.374}$$

$$P_b = \frac{g}{\Theta} \langle w\theta_v \rangle, \tag{3.375}$$

respectively. In the level 2 of the MYNN scheme, these are represented as

$$P_s = LqS_{M2} \left[\left(\frac{\partial U}{\partial z}\right)^2 + \left(\frac{\partial V}{\partial z}\right)^2\right], \tag{3.376}$$

$$P_b = LqS_{H2} \frac{g}{\Theta} \left[\beta_\theta \frac{\partial \Theta_l}{\partial z} + \beta_q \frac{\partial Q_w}{\partial z}\right], \tag{3.377}$$

$$\varepsilon = \frac{q^3}{B_1 L}. \tag{3.378}$$

From (3.373), (3.376), (3.377), and (3.378), q_2^2 is calculated by

$$q_2{}^2 = B_1 L^2 \left\{ S_{M2} \left[\left(\frac{\partial U}{\partial z}\right)^2 + \left(\frac{\partial V}{\partial z}\right)^2\right] + S_{H2} \frac{g}{\Theta} \left(\beta_\theta \frac{\partial \Theta_l}{\partial z} + \beta_q \frac{\partial Q_w}{\partial z}\right) \right\}. \tag{3.379}$$

3.7.5.2 Stability Functions of the Level 2.5

When $q < q_2$, i.e., the turbulence is in a growing phase, the stability functions of the Level 2.5 for momentum and heat, S_M and S_H respectively, are calculated using $\alpha = q/q_2$ introduced by Helfand and Labraga (1998) as

$$S_M = \alpha S_{M2}, \tag{3.380}$$

$$S_H = \alpha S_{H2}. \tag{3.381}$$

When $q \geq q_2$, S_M and S_H are calculated as

$$S_M = A_1 \frac{E_3 - 3C_1 E_4}{E_2 E_4 + E_5 E_3}, \tag{3.382}$$

$$S_H = A_2 \frac{E_2 + 3C_1 E_5}{E_2 E_4 + E_5 E_3}, \tag{3.383}$$

where

$$E_1 = 1 - 3A_2 B_2 (1 - C_3) G_H, \tag{3.384}$$

$$E_2 = 1 - 9A_1 A_2 (1 - C_2) G_H, \tag{3.385}$$

$$E_3 = E_1 + 9A_2{}^2 (1 - C_2)(1 - C_5) G_H, \tag{3.386}$$

$$E_4 = E_1 - 12A_1 A_2 (1 - C_2) G_H, \tag{3.387}$$

$$E_5 = 6A_1{}^2 G_M, \tag{3.388}$$

$$G_M = \frac{L^2}{q^2} \left[\left(\frac{\partial U}{\partial z} \right)^2 + \left(\frac{\partial V}{\partial z} \right)^2 \right], \tag{3.389}$$

$$G_H = -\frac{L^2}{q^2} \frac{g}{\Theta} \left(\beta_\theta \frac{\partial \Theta_l}{\partial z} + \beta_q \frac{\partial Q_w}{\partial z} \right). \tag{3.390}$$

The above formulas appear to be different from those in Nakanishi (2001), but are equivalent and can be computed with a smaller computational cost.

3.7.5.3   Calculation of Diffusion Coefficients

The diffusion coefficients for momentum, twice turbulent kinetic energy, heat and water are represented by

$$K_M = Lq S_M, \tag{3.391}$$

$$K_q = 3Lq S_M, \tag{3.392}$$

$$K_H = Lq S_H, \tag{3.393}$$

$$K_w = Lq S_H, \tag{3.394}$$

respectively.

3.7.5.4   Calculation of Fluxes

The vertical fluxes for U, V, q^2, C_pT and Q_w at half levels are calculated as

$$F_{u,k-1/2} = -\rho_{k-1/2} K_{M,k-1/2} \frac{U_k - U_{k-1}}{\Delta z_{k-1/2}}, \tag{3.395}$$

$$F_{v,k-1/2} = -\rho_{k-1/2} K_{M,k-1/2} \frac{V_k - V_{k-1}}{\Delta z_{k-1/2}}, \tag{3.396}$$

$$F_{q,k-1/2} = -\rho_{k-1/2} K_{q,k-1/2} \frac{q^2{}_k - q^2{}_{k-1}}{\Delta z_{k-1/2}}, \tag{3.397}$$

$$F_{T,k-1/2} = -\rho_{k-1/2} K_{H,k-1/2} C_p \Pi_{k-1/2} \frac{\Theta_{l,k} - \Theta_{l,k-1}}{\Delta z_{k-1/2}}, \tag{3.398}$$

$$F_{w,k-1/2} = -\rho_{k-1/2} K_{w,k-1/2} \frac{Q_{w,k} - Q_{w,k-1}}{\Delta z_{k-1/2}}, \tag{3.399}$$

respectively, where ρ denotes density and Π the Exner function. In order to perform time integration with an implicit scheme, the derivative of each of the vertical fluxes is also calculated as

$$\frac{\partial F_{u,k-1/2}}{\partial U_{k-1}} = \frac{\partial F_{v,k-1/2}}{\partial V_{k-1}} = -\frac{\partial F_{u,k-1/2}}{\partial U_k} = -\frac{\partial F_{v,k-1/2}}{\partial V_k} = \rho_{k-1/2} K_{M,k-1/2} \frac{1}{\Delta z_{k-1/2}}, \tag{3.400}$$

$$\frac{\partial F_{q,k-1/2}}{\partial q^2{}_{k-1}} = -\frac{\partial F_{q,k-1/2}}{\partial q^2{}_{k}} = \rho_{k-1/2} K_{q,k-1/2} \frac{1}{\Delta z_{k-1/2}}, \tag{3.401}$$

$$\frac{\partial F_{T,k-1/2}}{\partial T_{k-1}} = \rho_{k-1/2} K_{H,k-1/2} C_p \frac{\Pi_{k-1/2}}{\Pi_{k-1}} \frac{1}{\Delta z_{k-1/2}}, \tag{3.402}$$

$$\frac{\partial F_{T,k-1/2}}{\partial T_k} = -\rho_{k-1/2} K_{H,k-1/2} C_p \frac{\Pi_{k-1/2}}{\Pi_k} \frac{1}{\Delta z_{k-1/2}}, \tag{3.403}$$

$$\frac{\partial F_{w,k-1/2}}{\partial Q_{w,k-1}} = -\frac{\partial F_{w,k-1/2}}{\partial Q_{w,k}} = \rho_{k-1/2} K_{w,k-1/2} \frac{1}{\Delta z_{k-1/2}}, \tag{3.404}$$

where $\Delta z_{k-1/2} = z_k - z_{k-1}$. The fluxes for other tracers are also calculated in the same way using K_w.

3.7.6   Calculation of Turbulent Variables

3.7.6.1   Calculation of Twice Turbulent Kinetic Energy

The prognostic equation for q^2 is expressed as

$$\frac{dq^2}{dt} = -\frac{1}{\rho}\frac{\partial F_q}{\partial z} + 2\left(P_s + P_b - \varepsilon\right). \tag{3.405}$$

In the Level 2.5, P_s, P_b, ε are written as

$$P_s = LqS_M \left[\left(\frac{\partial U}{\partial z}\right)^2 + \left(\frac{\partial V}{\partial z}\right)^2 \right], \tag{3.406}$$

$$P_b = LqS_H \frac{g}{\Theta} \left(\beta_\theta \frac{\partial \Theta_l}{\partial z} + \beta_q \frac{\partial Q_w}{\partial z} \right), \tag{3.407}$$

$$\varepsilon = \frac{q^3}{B_1 L}. \tag{3.408}$$

Advection terms are calculated using the tracer transport routines in the dynamical core. The turbulence scheme calculates the time evolution by the diffusion, production and dissipation terms with an implicit scheme.

3.7.6.2 Diagnosis of Variance and Covariance

The prognostic equations for $\langle \theta_l^2 \rangle, \langle q_w^2 \rangle, \langle \theta_l q_w \rangle$ are expressed as

$$\frac{d \langle \theta_l^2 \rangle}{dt} = -\frac{\partial}{\partial z} \langle w\theta_l^2 \rangle - 2 \langle w\theta_l \rangle \frac{\partial \Theta_l}{\partial z} - 2\varepsilon_{\theta l}, \tag{3.409}$$

$$\frac{d \langle q_w^2 \rangle}{dt} = -\frac{\partial}{\partial z} \langle wq_w^2 \rangle - 2 \langle wq_w \rangle \frac{\partial Q_w}{\partial z} - 2\varepsilon_{qw}, \tag{3.410}$$

$$\frac{d \langle \theta_l q_w \rangle}{dt} = -\frac{\partial}{\partial z} \langle w\theta_l q_w \rangle - \langle wq_w \rangle \frac{\partial \Theta_l}{\partial z} - \langle w\theta_l \rangle \frac{\partial Q_w}{\partial z} - 2\varepsilon_{\theta q}. \tag{3.411}$$

In the Level 2.5, the time derivative, advection, and diffusion terms in these equations are neglected assuming the following local balances.

$$-\langle w\theta_l \rangle \frac{\partial \Theta_l}{\partial z} - \varepsilon_{\theta l} = 0, \tag{3.412}$$

$$-\langle wq_w \rangle \frac{\partial Q_w}{\partial z} - \varepsilon_{qw} = 0, \tag{3.413}$$

$$-\langle wq_w \rangle \frac{\partial \Theta_l}{\partial z} - \langle w\theta_l \rangle \frac{\partial Q_w}{\partial z} - 2\varepsilon_{\theta q} = 0. \tag{3.414}$$

In the Level 2.5 of the MYNN scheme, $-\langle w\theta_l \rangle, -\langle wq_w \rangle, \varepsilon_{\theta l}, \varepsilon_{qw}, \varepsilon_{\theta q}$ are represented as

$$-\langle w\theta_l \rangle = LqS_H \frac{\partial \Theta_l}{\partial z}, \tag{3.415}$$

$$-\langle wq_w \rangle = LqS_H \frac{\partial Q_w}{\partial z}, \tag{3.416}$$

$$\varepsilon_{\theta l} = \frac{q}{B_2 L} \langle \theta_l^2 \rangle, \tag{3.417}$$

$$\varepsilon_{qw} = \frac{q}{B_2 L} \langle q_w^2 \rangle, \tag{3.418}$$

$$\varepsilon_{\theta q} = \frac{q}{B_2 L} \langle \theta_l q_w \rangle. \tag{3.419}$$

from (3.412)-(3.419), $\langle \theta_l^2 \rangle, \langle q_w^2 \rangle, \langle \theta_l q_w \rangle$ can be diagnosed as

$$\langle \theta_l^2 \rangle = B_2 L^2 S_H \left(\frac{\partial \Theta_l}{\partial z} \right)^2, \tag{3.420}$$

$$\langle q_w^2 \rangle = B_2 L^2 S_H \left(\frac{\partial Q_w}{\partial z} \right)^2, \tag{3.421}$$

$$\langle \theta_l q_w \rangle = B_2 L^2 S_H \frac{\partial \Theta_l}{\partial z} \frac{\partial Q_w}{\partial z}. \tag{3.422}$$

3.7.6.3 Treatment in the Bottom Layer

Since the lowest model layer corresponds to the surface layer where values of physical variables rapidly change in the vertical direction, the following Monin-Obukhov similarity theory is used to accurately evaluate the vertical gradient of the variables.

$$\frac{\partial M}{\partial z} = \frac{u_*}{kz}\phi_m, \tag{3.423}$$

$$\frac{\partial \Theta}{\partial z} = \frac{\theta_*}{kz}\phi_h, \tag{3.424}$$

$$\frac{\partial Q_v}{\partial z} = \frac{q_{v*}}{kz}\phi_h, \tag{3.425}$$

where M is the horizontal wind velocity for the horizontal axis aligned to the direction of the horizontal wind in the surface layer. ϕ_m and ϕ_h are the dimensionless gradient functions for momentum and heat respectively. θ_* and q_{v*} are the scales of potential temperature and water vapor in the surface layer respectively, and satisfy the following relationships.

$$\langle wm \rangle_g = -u_*^2, \tag{3.426}$$

$$\langle w\theta \rangle_g = -u_*\theta_*, \tag{3.427}$$

$$\langle wq_v \rangle_g = -u_*q_{v*}, \tag{3.428}$$

where m is the deviation of M from the grid mean. Using M and m, the production term of the turbulence kinetic energy is written as

$$P_s + P_b = \langle wm \rangle \frac{\partial M}{\partial z} + \frac{g}{\Theta}\langle w\theta_v \rangle. \tag{3.429}$$

Using (3.423), (3.426) and the definition of the Obukhov length, it is rewritten as

$$P_s + P_b = \frac{u_*^3}{kz_1}\left[\phi_m\left(\zeta_1\right) - \zeta_1\right], \tag{3.430}$$

where ζ_1 is ζ at the full level of the lowest model layer.

Assuming that the effect of cloud particles are negligible in the surface layer, $\langle \theta_l^2 \rangle$, $\langle q_w^2 \rangle$, $\langle \theta_l q_w \rangle$ is calculated diagnostically from (3.412)-(3.414), (3.417)-(3.419), (3.424), (3.425), (3.427), and (3.428) as

$$\langle \theta_l^2 \rangle = \frac{\phi_h\left(\zeta_1\right)}{u_*kz_1}\langle w\theta \rangle_g^2 \left/ \frac{q}{B_2 L}\right., \tag{3.431}$$

$$\langle q_w{}^2 \rangle = \frac{\phi_h\left(\zeta_1\right)}{u_* k z_1} \langle w q_v \rangle_g{}^2 \Bigg/ \frac{q}{B_2 L}, \tag{3.432}$$

$$\langle \theta_l q_w \rangle = \frac{\phi_h\left(\zeta_1\right)}{u_* k z_1} \langle w \theta \rangle_g \langle w q_v \rangle_g \Bigg/ \frac{q}{B_2 L}. \tag{3.433}$$

ϕ_m and ϕ_h are formulated following Businger et al. (1971) as

$$\phi_m(\zeta) = \begin{cases} 1 + \beta_1 \zeta, & \zeta \geq 0 \\ \left(1 - \gamma_1 \zeta\right)^{-1/4}, & \zeta < 0 \end{cases} \tag{3.434}$$

$$\phi_h(\zeta) = \begin{cases} \beta_2 + \beta_1 \zeta, & \zeta \geq 0 \\ \beta_2 \left(1 - \gamma_2 \zeta\right)^{-1/2}, & \zeta < 0 \end{cases} \tag{3.435}$$

$$(\beta_1, \beta_2, \gamma_1, \gamma_2) = (4.7, 0.74, 15.0, 9.0). \tag{3.436}$$

3.7.7 Time Integration with Implicit Scheme

3.7.7.1 Tendency of q^2

The prognostic equation for q^2 is discretized as

$$\left(\frac{q_{k,n+1}^2 - q_{k,n}^2}{\Delta t}\right)_{\text{turb}} = -\frac{1}{\rho_k \Delta z_k}\left(F_{q,k+1/2,n+1} - F_{q,k-1/2,n+1}\right) + 2\left(P_{s,k,n} + P_{b,k,n} - \frac{q_{k,n}}{B_1 L} q_{k,n+1}^2\right) \tag{3.437}$$

where n and $n+1$ indicate the current and next time steps respectively, and $\Delta z_k \equiv z_{k+1/2} - z_{k-1/2}$. The subscript *turb* indicates the calculation by the turbulence scheme and the advection term is omitted. F_q at $n+1$ is computed by

$$F_{q,k-1/2,n+1} = F_{q,k-1/2,n} + \frac{\partial F_{q,k-1/2}}{\partial q_k^2}(q_{k,n+1}^2 - q_{k,n}^2) + \frac{\partial F_{q,k-1/2}}{\partial q_{k-1}^2}(q_{k-1,n+1}^2 - q_{k-1,n}^2). \tag{3.438}$$

With a definition of

$$\mu_k = \left(\frac{q_{k,n+1}^2 - q_{k,n}^2}{\Delta t}\right)_{\text{turb}}, \tag{3.439}$$

(3.437) and (3.438) lead to

$$X_{1,k}\, \mu_{k+1} + X_{2,k}\, \mu_k + X_{3,k}\, \mu_{k-1} = Y_k, \tag{3.440}$$

where

$$X_{1,k} = \frac{\partial F_{q,k+1/2}}{\partial q_{k+1}^2} \Delta t, \tag{3.441}$$

$$X_{2,k} = \rho_k \Delta z_k \left(1 + 2 \frac{q_{k,n}}{B_1 L} \Delta t \right) + \left(\frac{\partial F_{q,k+1/2}}{\partial q_k^2} - \frac{\partial F_{q,k-1/2}}{\partial q_k^2} \right) \Delta t, \tag{3.442}$$

$$X_{3,k} = -\frac{\partial F_{q,k-1/2}}{\partial q_{k-1}^2} \Delta t, \tag{3.443}$$

$$Y_k = F_{q,k-1/2,n} - F_{q,k+1/2,n} + 2\rho_k \Delta z_k \left(P_{s,k,n} + P_{b,k,n} - \frac{q_{k,n}^3}{B_1 L} \right). \tag{3.444}$$

(3.440) makes the following matrix equation,

$$\begin{pmatrix} X_{2,K} & X_{3,K} & 0 & 0 & 0 & \cdots & 0 \\ X_{1,K-1} & X_{2,K-1} & X_{3,K-1} & 0 & 0 & \cdots & 0 \\ 0 & X_{1,K-2} & X_{2,K-2} & X_{3,K-2} & 0 & \cdots & 0 \\ \vdots & & & \ddots & & & \vdots \\ 0 & \cdots & 0 & X_{1,3} & X_{2,3} & X_{3,3} & 0 \\ 0 & \cdots & 0 & 0 & X_{1,2} & X_{2,2} & X_{3,2} \\ 0 & \cdots & 0 & 0 & 0 & X_{1,1} & X_{2,1} \end{pmatrix} \begin{pmatrix} \mu_K \\ \mu_{K-1} \\ \mu_{K-2} \\ \vdots \\ \mu_3 \\ \mu_2 \\ \mu_1 \end{pmatrix} = \begin{pmatrix} Y_K \\ Y_{K-1} \\ Y_{K-2} \\ \vdots \\ Y_3 \\ Y_2 \\ Y_1 \end{pmatrix} \tag{3.445}$$

where the subscript K denote the index for the top model layer. (3.445) is solved for μ_k using the LU decomposition.

3.7.7.2 Tendencies of the Other Prognostic Variables

Letting ψ be a substitute for u, v, T, q_w, the tendency of ψ is calculated by

$$\left(\frac{\psi_{k,n+1} - \psi_{k,n}}{\Delta t} \right)_{\mathrm{turb}} = -\frac{1}{\rho_k \Delta z_k} \left(F_{\psi,k+1/2,n+1} - F_{\psi,k-1/2,n+1} \right), \tag{3.446}$$

where

$$F_{\psi,k-1/2,n+1} = F_{\psi,k-1/2,n} + \frac{\partial F_{\psi,k-1/2}}{\partial \psi_k} (\psi_{k,n+1} - \psi_{k,n}) + \frac{\partial F_{\psi,k-1/2}}{\partial \psi_{k-1}} (\psi_{k-1,n+1} - \psi_{k-1,n}) \tag{3.447}$$

These equations lead to (3.445) again and computed with the LU decomposition, but μ_k, $X_{1,k}$, $X_{2,k}$, $X_{3,k}$ and Y_k are redefined as

$$\mu_k = \left(\frac{\psi_{k,n+1} - \psi_{k,n}}{\Delta t} \right)_{\mathrm{turb}}, \tag{3.448}$$

$$X_{1,k} = \frac{\partial F_{\psi,k+1/2}}{\partial \psi_{k+1}} \Delta t, \tag{3.449}$$

$$X_{2,k} = \rho_k \Delta z_k + \left(\frac{\partial F_{\psi,k+1/2}}{\partial \psi_k} - \frac{\partial F_{\psi,k-1/2}}{\partial \psi_k} \right) \Delta t, \tag{3.450}$$

$$X_{3,k} = -\frac{\partial F_{\psi,k-1/2}}{\partial \psi_{k-1}} \Delta t, \tag{3.451}$$

$$Y_k = F_{\psi,k-1/2,n} - F_{\psi,k+1/2,n}. \tag{3.452}$$

3.8 Surface Flux Scheme (Sea Surface)

Until CCSR/NIES AGCM (1997), both land surface and sea surface were treated as one of the atmospheric physical processes, but after MIROC3 (Hasumi and Emori, 2004), land surface processes became independent as MATSIRO. However, since MIROC3 (Hasumi and Emori, 2004), land surface processes have been separated into MATSIRO (Takata et al., 2003; Nitta et al., 2014). In `SUBROUTINE:[SURFCE]` in pgsfc.F, `ENTRY:[OCNFLX]` (in `SUBROUTINE:[OCEAN]` of pgocn.F) is called for the sea surface, and `ENTRY:[LNDFLX]` (in `SUBROUTINE:[MATSIRO]` of matdrv.F) is called for the land surface, respectively. This chapter describes sea surface processes, which are still treated within the framework of atmospheric physical processes in MIROC6 (Tatebe et al., 2019)). For the land surface processes, please refer to Description of ILS (https://github.com/integrated-land-simulator/model_description).

Sea surface processes provide the boundary conditions at the lower end of the atmosphere through the exchange of momentum, heat, and water fluxes between the atmosphere and the surface. In `ENTRY:[OCNFLX]`, the following procedure is used to deal with sea surface processes.

1. Prepare variables for sea ice extent and no ice extent, respectively, using sea ice concentration.
2. Determine the surface boundary conditions.
3. Calculate the flux balance.
4. Calculate the radiation budget at the sea surface.
5. Calculate the deposition by CHASER.
6. Solve the heat balance at the sea surface and update the skin temperature and each flux value.

No prognostic variables are used in this scheme.
Practically, precipitation flux from 2 schemes are treated together.

$$Pr = Pr_c + Pr_l \tag{3.453}$$

where Pr is total precipitation flux, Pr_c is precipitation flux from the cumulus convection scheme, and Pr_l is precipitation flux from the large scale condensation scheme, respectively.

Sea ice covered/free areas are represented by $L = 1, 2$. Each area is calculated then weighted by sea ice concentration (R_{ice}).

In the sea ice area ($L = 1$), the skin temperature (T_s) is the sea ice skin temperature (T_{ice}). However, if T_{ice} is higher than the melting point ($T_{melt} = 273.15[\text{K}]$), then T_{melt} is used.

$$T_s = min(T_{ice}, T_{melt}) \tag{3.454}$$

The sea ice bottom temperature (T_b) is assumed to be the sea skin temperature ($T_{o(1)}$).

$$T_b = T_{o(1)} \tag{3.455}$$

The amount of sea ice (W_{ice}) and the amount of snow on it (W_{snow}) are converted per unit area by considering sea ice concentration (R_{ice}) and used in the calculation. However, a limiter (ϵ) is provided to prevent the values from becoming too small.

$$R_{ice} = \max(R_{ice,orginal}, \epsilon) \tag{3.456}$$

In the ice-free area ($L = 2$), the skin temperature (T_s) and sea ice bottom temperature (T_b) are assumed to be the sea temperature temperature ($T_{o(1)}$).

$$T_s = T_b = T_{o(1)} \tag{3.457}$$

The evaporation efficiency is set to 1 for both $L = 1, 2$.

If sea ice concentration (R_{ice}) is not given (as a boundary condition or from an OGCM), it is simply diagnosed with the sea ice volume (W_{ice}) in ENTRY:[OCNICR] (in SUBROUTINE:[OCNICR] of pgocn.F).

$$R_{ice} = \min\left(\sqrt{\frac{\max(W_{ice}, 0)}{W_{ice,c}}}, 1.0\right) \tag{3.458}$$

The standard gives the amount of sea ice per area as $W_{ice,c} = 300[\text{kg/m}^2]$.

3.8.1 Boundary Conditions

In ENTRY[OCNBCS] (in SUBROUTINE:[OCNSUB] of pgocn.F), surface albedo and roughness are calculated. They are calculated supposing ice-free conditions, then modified to take into account the effects of ice and snow cover.

First, let us consider the sea surface level albedo ($\alpha_{(d,b)}$), $b = 1, 2, 3$ represent the visible, near-infrared, and infrared wavelength bands, respectively. Also, $d = 1, 2$ represents direct and scattered light, respectively. The albedo for the visible bands are calculated in SUBROUTINE [SEAALB] (of pgocn.F), supposing ice-free conditions. The albedo for near-infrared is set to same as the visible one. The albedo for infrared is uniformly set to a constant value.

The grid-averaged albedo, taking into account sea ice concentration (R_{ice}), is

$$\alpha = \alpha - R_{ice}\alpha_{ice} \tag{3.459}$$

α_{ice} is given as $\alpha_{ice,1} = 0.5, \alpha_{ice,2} = 0.5, \alpha_{ice,3} = 0.05$, respectively.

In addition, we want to consider the effect of snow cover. Here, we consider the albedo modification by temperature. Standard threshold values for snow temperature are $T_{al,2} = 258.15[\text{K}]$ and $T_{al,1} = 273.15[\text{K}]$. The snow albedo changes linearly with temperature change from $\alpha_{snow,1} = 0.75$ to $\alpha_{snow,2}$. Let the coefficient τ_{snow}, which is $0 \le \tau \le 1$.

$$\tau_{snow} = \frac{T_s - T_{al,1}}{T_{al,2} - T_{al,1}} \tag{3.460}$$

Update the snow albedo (α_{snow}) as

$$\alpha_{snow} = \alpha_{snow,0} + \tau_{snow}(\alpha_{snow,2} - \alpha_{snow,1}) \tag{3.461}$$

Second, let us consider sea surface roughnesses. Roughnesses of for momentum, heat and vapor are calculated in SUBROUTINE:[SEAZOF] (of pgocn.F), supposing the ice-free conditions, then modified to take into account the effects of ice and snow cover.

When the sea ice exists ($L = 1$), roughnesses of momentum, heat and vapor ($r_{0,M}, r_{0,H}, r_{0,E}$) is modified to take into account sea ice concentration (R_{ice}),

$$z_{0,M} = z_{0,M} + (z_{0,ice,M} - z_{0,M})R_{ice} \tag{3.462}$$

$$z_{0,H} = z_{0,H} + (z_{0,ice,H} - z_{0,H})R_{ice} \tag{3.463}$$

$$z_{0,E} = z_{0,E} + (z_{0,ice,E} - z_{0,E})R_{ice} \tag{3.464}$$

where, $r_{0,ice,M}, r_{0,ice,H}, r_{0,ice,E}$ is the roughness of sea ice for momentum, heat and vapor, respectively.

$$z_{0,M} = z_{0,M} + (z_{0,snow,M} - z_{0,M})R_{snow} \tag{3.465}$$

$$z_{0,H} = z_{0,H} + (z_{0,snow,H} - z_{0,H})R_{snow} \tag{3.466}$$

$$z_{0,E} = z_{0,E} + (z_{0,snow,E} - z_{0,E})R_{snow} \tag{3.467}$$

where, $r_{0,snow,M}, r_{0,snow,H}, r_{0,snow,E}$ is the roughness of snow ice for momentum, heat and vapor, respectively.

Third, let us consider conductivity of ice. When sea ice exists ($L = 1$), thermal conductivity of sea ice ($k_{ice}^{\star}$) is obtained by

$$k_{ice}^{\star} = \frac{D_{f,ice}}{\max(R_{ice}/\sigma_{ice}, \epsilon)} \tag{3.468}$$

where $D_{f,ice}$ is thermal diffusivity of sea ice, and σ_{ice} is sea ice density, respectively.

The calculated thermal conductivity is modified to k_{ice} to take into account that it varies with snow cover.

$$h_{snow} = \min(\max(R_{snow}/\sigma_{snow}), \epsilon), h_{snow,max}) \tag{3.469}$$

$$k_{ice} = k_{ice}^{\star}(1 - R_{ice}) + \frac{D_{ice}}{1 + \|D_{ice}/D_{snow} \cdot h_{snow}\|}R_{ice} \tag{3.470}$$

where h_{snow} is snow depth, R_{snow} is snow area fraction, σ_{snow} is snow density, $h_{snow,max}$ is maximum snow depth, and D_{snow} is thermal diffusivity of snow, respectively.

Therefore, heat conduction flux and its derivative are

$$G = k_{ice}(T_b - T_s) \tag{3.471}$$

$$\frac{\partial G}{\partial T} = k_{ice} \tag{3.472}$$

Note that in the ice-free area ($L = 2$)

$$G = k_{ocn} \tag{3.473}$$

where k_{ocn} is heat flux in the sea temperature layer, and k_{ocn} is heat flux in the sea temperature layer, respectively.

3.8.1.1 Albedo for Visible

In SUBROUTINE [SEAALB] (of pgocn.F), albedo for the visible bands are calculated supposing ice-free conditions, then modified to take into account the effects of ice and snow cover.

For sea surface level albedo $(\alpha_{L(d)})$, $d = 1, 2$ represents direct and scattered light, respectively. Using the solar zenith angle at latitude ζ, albedo for direct light is presented by

$$\alpha_{L(1)} = e^{(C_3 A^* + C_2) A^* + C_1} \tag{3.474}$$

where

$$A^* = \min(\max(\cos(\theta), 0.03459), 0.961) \tag{3.475}$$

and C_1, C_2, C_3 are constant parameters, respectively.

On the other hand, albedo for scattered light $(\alpha_{L(2)})$ is uniformly set to a constant parameter.

$$\alpha_{L(2)} = 0.06 \tag{3.476}$$

3.8.1.2 Roughnesses

In SUBROUTINE:[SEAZOF] (of pgocn.F), the roughnesses of for momentum, heat and vapor are calculated supposing the ice-free conditions. calculated, according to Miller et al. (1992), then modified to take into account the effects of ice and snow cover.

The roughness variation of the sea surface is determined by the friction velocity $(u^\star)$.

$$u^\star = \sqrt{C_{M_0}(u_a{}^2 + v_a{}^2)} \tag{3.477}$$

where C_{M_0} is a bulk coefficient for momentum, and u_a, v_a are zonal and vertical winds of the 1st layer of the atmosphere. We perform successive approximation calculation of C_{M_0}, because F_u, F_v, F_θ, F_q are required.

Then, roughnesses of sea surface for momentum, heat and vapor are

$$z_{0,M} = z_{0,M_0} + z_{0,M_R} + \frac{z_{0,M_R} u^{\star 2}}{g} + \frac{z_{0,M_S} \nu}{u^\star} \tag{3.478}$$

$$z_{0,H} = z_{0,H_0} + z_{0,H_R} + \frac{z_{0,H_R} u^{\star 2}}{g} + \frac{z_{0,H_S} \nu}{u^\star} \tag{3.479}$$

$$z_{0,E} = z_{0,E_0} + z_{0,E_R} + \frac{z_{0,E_R} u^{\star 2}}{g} + \frac{z_{0,E_S} \nu}{u^\star} \tag{3.480}$$

where, $\nu = 1.5 \times 10^{-5} [\mathrm{m^2/s}]$ is the kinetic viscosity of the atmosphere, $z_{0,M}, z_{0,H}$ and $z_{0,E}$ are surface roughness for momentum, heat, and vapor, z_{0,M_0}, z_{0,H_0} and z_{0,E_0} are base, and rough factor $(z_{0,M_R}, z_{0,M_R}$ and $z_{0,E_R})$, and smooth factor $(z_{0,M_S}, z_{0,M_S}$ and $z_{0,E_S})$, respectively.

3.8.2 Calculation of Momentum, Heat and Water Vapor Fluxes

Treatment of sea surface flux is basically the same with CCSR/NIES AGCM (1997). The surface flux scheme evaluates the physical quantity fluxes between the atmospheric surfaces due to turbulent transport in the boundary layer. The main input are horizontal wind speed (u_a, v_a), temperature (T_a), and specific humidity (q_a) from the 1st layer of the atmosphere. The output are the vertical fluxes and the differential values (for obtaining implicit solutions) of momentum, heat, and water vapor.

Surface fluxes $(F_u, F_v, F_\theta, F_q)$ are expressed using bulk coefficients for momentum, head and vapor (C_M, C_H, C_E) as follows

$$F_u = -\rho C_M |\mathbf{V_a}| u_a \tag{3.481}$$

$$F_v = -\rho C_M |\mathbf{V_a}| v_a \tag{3.482}$$

$$F_\theta = \rho c_p C_H |\mathbf{V_a}| (\theta_s - \theta_a) \tag{3.483}$$

$$F_q^P = \rho C_E |\mathbf{V_a}| (q_s - q_a) \tag{3.484}$$

where F_q^P is the possible evaporation flux, where $\mathbf{V_a}$ is horizontal wind vector, and θ_s, θ_a are potential temperature of surface and 1st layer of the atmosphere, respectively. Although there is no description, surface fluxes are calculated using wind speed relative to ocean current speed. For example, F_u=-¥rho C_M | V_a - V_o | (u_a - u_o). Here, V_o = (u_o, v_o) represents ocean current vector at the uppermost layer. Note that in a stand-alone AGCM, V_o = (0,0) is assumed.

Turbulent fluxes at the sea surface are solved by bulk formulae as follows. Then, by solving the surface energy balance, the ground skin temperature (T_s) is updated, and the surface flux values with respect to those values are also updated. The solutions obtained here are temporary values. In order to solve the energy balance by linearizing with respect to T_s, the differential with respect to T_s of each flux is calculated beforehand.

- Momentum flux

$$\tau_x = -\rho C_M |\mathbf{V_a}| u_a \tag{3.485}$$

$$\tau_y = -\rho C_M |\mathbf{V_a}| v_a \tag{3.486}$$

where τ_x and τ_y are the momentum fluxes (surface stress) of the zonal and meridional directions, respectively.

- Sensible heat flux

$$H_s = c_p \rho C_{Hs} |\mathbf{V_a}| (T_s - (P_s/P_a)^\kappa T_a) \tag{3.487}$$

where H_s is the sensible heat flux from the sea surface; $\kappa = R_{air}/c_p$ and R_{air} are the gas constants of air, and c_p is the specific heat of air.

- Bare sea surface evaporation flux

$$F_q^P = \rho C_E |\mathbf{V_a}| (q^*(T_s) - q_a) \tag{3.488}$$

3.8.2.1 Bulk factors

In SUBROUTINE:[BLKCOF] (of psfcl.F), the bulk factors are calculated. The bulk Richardson number (R_{iB}), which is used as a benchmark for the stability between the atmospheric surfaces, is

$$R_{iB} = \frac{\frac{g}{\theta_s}(\theta_a - \theta(z_0))/z_a}{(u_a/z_1)^2} = \frac{g}{\theta_s} \frac{T_a(p_s/p_a)^\kappa - T_0}{u_a^2/z_1} f_T \tag{3.489}$$

Here, g is the gravitational accerelation, θ_s is surface potential temperature, T_a is the atmospheric temperature of the 1st layer, T_s is the surface skin temperature, p_s is the surface pressure, p_a is the pressure of the 1st layer, κ is the Karman constant, and

$$f_T = (\theta_a - \theta(z_0))/(\theta_a - \theta_s) \tag{3.490}$$

The bulk coefficients of C_M, C_H, C_E are calculated according to Louis (1979) and Louis et al. (1982) However, corrections are made to take into account the difference between momentum and heat roughness. If the roughnesses for momentum, heat, and water vapor are set to $z_{0,M}, z_{0,H}, z_{0,E}$, respectively, the results are generally $z_{0,M} > z_{0,H}, z_{0,E}$, but the bulk coefficients for heat and water vapor for the fluxes from the height of $z_{0,M}$ are also set to $\widetilde{C_H}, \widetilde{C_E}$, then corrected.

$$C_M = \begin{cases} C_{0,M}[1 + (b_M/e_M)R_{iB}]^{-e_M} & , R_{iB} \geq 0 \\ C_{0,M}\left[1 - b_M R_{iB}\left(1 + d_M b_M C_{0,M}\sqrt{\frac{z_1}{z_{0,M}}|R_{iB}|}\right)^{-1}\right] & , R_{iB} < 0 \end{cases} \tag{3.491}$$

$$\widetilde{C_H} = \begin{cases} \widetilde{C_{0,H}}[1 + (b_H/e_H)R_{iB}]^{-e_H} & , R_{iB} \geq 0 \\ \widetilde{C_{0,H}}\left[1 - b_H R_{iB}\left(1 + d_H b_H \widetilde{C_{0,H}}\sqrt{\frac{z_1}{z_{0,M}}|R_{iB}|}\right)^{-1}\right] & , R_{iB} < 0 \end{cases} \tag{3.492}$$

$$C_H = \widetilde{C_H} f_T \tag{3.493}$$

$$\widetilde{C_E} = \begin{cases} \widetilde{C_{0,E}}[1 + (b_E/e_E)R_{iB}]^{-e_E} & , R_{iB} \geq 0 \\ \widetilde{C_{0,E}}\left[1 - b_E R_{iB}\left(1 + d_E b_E \widetilde{C_{0,E}}\sqrt{\frac{z_1}{z_{0,M}}|R_{iB}|}\right)^{-1}\right] & , R_{iB} < 0 \end{cases} \tag{3.494}$$

$$C_E = \widetilde{C_E} f_q \tag{3.495}$$

$C_{0M}, \widetilde{C_{0H}}, \widetilde{C_{0E}}$ is the bulk coefficient (for fluxes from z_{0M}) at neutral,

$$C_{0M} = \widetilde{C_{0H}} = \widetilde{C_{0E}} = \frac{k^2}{\left[\ln\left(\frac{z_1}{z_{0M}}\right)\right]^2} \tag{3.496}$$

Correction Factor f_q is ,

$$f_q = (q_a - q(z_0))/(q_a - q^*(\theta_0)) \tag{3.497}$$

but the method of calculation is omitted. The coefficients of Louis factors are $(b_M, d_M, e_M) = (9.4, 7.4, 2.0)$, $(b_H, d_H, e_H) = (b_E, d_E, e_E) = (9.4, 5.3, 2.0)$.

is a correction factor, which is approximated from the uncorrected bulk Richardson number, but we abbreviate the calculation here.

3.8.3 Radiation Flux Calculation

In SUBROUTINE:[RADSFC] (of pgsfc.F), the radiation flux at sea surface is calculated. For the ground surface albedo ($\alpha_{(d,b)}$), $b = 1, 2$ represent the visible and near-infrared wavelength bands, respectively. Also, $d = 1, 2$ are direct and scattered, respectively. For the downward shortwave radiation ($SW^\downarrow$) and upward shortwave radiation ($SW^\uparrow$) incident on the earth's surface, the direct and scattered light together are

$$\begin{aligned} SW^\downarrow &= SW^\downarrow_{(1,1)} + SW^\downarrow_{(1,2)} + SW^\downarrow_{(2,1)} + SW^\downarrow_{(2,2)} \\ SW^\uparrow &= SW^\downarrow_{(1,1)} \cdot \alpha_{(1,1)} + SW^\downarrow_{(1,2)} \cdot \alpha_{(1,2)} + SW^\downarrow_{(2,1)} \cdot \alpha_{(2,1)} + SW^\downarrow_{(2,2)} \cdot \alpha_{(2,2)} \end{aligned} \tag{3.498}$$

3.8.4 Solving Heat Balance

In SUBROUTINE:[OCNSLV] (of pgocn.F), heat balance at the sea surface is solved. Downward radiative fluxes are not directly dependent on the condition of the sea surface, and their observed values are simply specified to drive the model (Hasumi, 2015). Shortwave emission from the sea surface is negligible, so the upward part of the shortwave radiative flux is accounted for solely by reflection of the incoming downward flux. Let α_S be the sea surface albedo for shortwave radiation. The upward shortwave radiative flux is represented by

$$SW^\uparrow = -\alpha_S SW^\downarrow \tag{3.499}$$

On the other hand, the upward longwave radiative flux ($LW^\uparrow$) has both reflection of the incoming flux and emission from the sea surface. Let α be the sea surface albedo for longwave radiation and ϵ be emissivity of the sea surface relative to the black body radiation, respectively. The upward shortwave radiative flux is represented by

$$LW^\uparrow = -\alpha LW^\downarrow + \epsilon \sigma T_s^4 \tag{3.500}$$

where σ is the Stefan-Boltzmann constant and T_s is skin temperature, respectively . If sea ice exists $(L = 1)$, snow or sea ice temperature is considered by fractions. When radiative equilibrium is assumed, emissivity becomes identical to co-albedo:

$$\epsilon = 1 - \alpha \tag{3.501}$$

The net surface flux (F^*) is presented by

$$F^* = H + \left((1 - \alpha_{Lk})\sigma T_s^4 + \alpha_{Lk}LW^\downarrow\right) - LW^\downarrow + SW^\uparrow - SW^\downarrow \tag{3.502}$$

where H is sensible heat flux.

With the surface heat flux calculated in SUBROUTINE:[SFCFLX] (of psfcm.F) (G), heat flux into the sea surface (G^*) is presented as

$$G^* = G - F^* \tag{3.503}$$

Note that G^* is downward positive.

The temperature derivative term of G^* is

$$\frac{\partial G^*}{\partial T_s} = \frac{\partial G}{\partial T_s} + \frac{\partial H}{\partial T_s} + \frac{\partial R}{\partial T_s} \tag{3.504}$$

When the sea ice exists $(L = 1)$, the surface flux G_{ice} is considered with the sublimation flux $(l_s E)$.

$$G_{ice} = G^* - l_s E \tag{3.505}$$

The temperature derivative term of G_{ice} is

$$\frac{\partial G_{ice}}{\partial T_s} = \frac{\partial G^*}{\partial T_s} + l_s \frac{\partial E}{\partial T_s} \tag{3.506}$$

We can update the skin temperature with sea ice concentration and $\Delta T_s = G_{ice}(\frac{\partial G_{ice}}{\partial T_s})^{-1}$

$$T_s = T_s + R_{ice}\Delta T_s \tag{3.507}$$

Then, the sensible and latent heat flux on the sea ice (E_{ice}, H_{ice}) is updated.

$$E_{ice} = E + \frac{\partial E}{\partial T_s}\Delta T_s \tag{3.508}$$

$$H_{ice} = H + \frac{\partial H}{\partial T_s}\Delta T_s \tag{3.509}$$

When the sea ice does not existed $(L = 2)$, otherwise, the surface heat flux (G_{free}) is calculated by addition of evaporation flux $l_c E$ and the net flux F^*.

$$G_{free} = F^* + l_c E \tag{3.510}$$

Finally each flux is updated. For sensible heat flux (H), the temperature change on the sea ice is considered.

$$H = H + R_{ice} H_{ice} \tag{3.511}$$

Then, the heat used for the temperature change (F) is saved.

$$F = R_{ice} H_{ice} \tag{3.512}$$

For upward longwave radiative flux ($LW^\uparrow$), temperature change on the sea ice (ΔT_s) is considered.

$$LW^\uparrow = LW^\uparrow + 4\frac{\sigma}{T_s} R_{ice} \Delta T_s \tag{3.513}$$

For the surface heat flux (G), sea ice existence is considered.

$$G = (1 - R_{ice})G_{free} + R_{ice}G_{ice} \tag{3.514}$$

For latent heat flux E, sea ice existence is considered.

$$E = (1 - R_{ice})E + R_{ice}E_{ice} \tag{3.515}$$

Then, each term above are saved as freshwater fluxes (W_{free}, W_{ice}) of ice covered and free areas.

$$W_{free} = (1 - R_{ice})E \tag{3.516}$$

$$W_{ice} = R_{ice}E_{ice} \tag{3.517}$$

3.9 Gravity Waves

Effects of sub-grid scale gravity waves on the grid scale flows are represented by two kinds of gravity wave parameterizations. The orographic gravity wave drag scheme represents decelerations of the grid scale flow due to momentum deposition of orographic gravity waves, which is described below. In contrast, the non-orographic gravity wave scheme may either accelerate or decelerate the grid scale flow. At present this document does not contain a detailed description of the non-orographic gravity wave scheme, and readers may find if in Watanabe (2008) and Tatebe et al. (2019).

3.9.1 Overview of a Gravity Wave Drag Parameterization

The orographic gravity wave drag scheme represents the upward momentum flux of the gravity waves induced by sub-grid scale topography and calculates the horizontal wind deceleration associated with its convergence (McFarlane, 1987). The main input data are eastward wind (u), northward wind (v), and temperature (T), and the output data are the tendency of eastward wind and northward wind, $\partial u/\partial t, \partial v/\partial t$.

The outline of the calculation procedure is as follows.

1. The momentum flux at the ground surface is calculated from the variance of sub-grid scale orography, the horizontal wind speed at the lowest level, and the static stability.

2. The upward propagation of gravity waves is considered. If the momentum flux exceeds its critical value, which is determined by the critical Froude number, then wave breaking occurs and the momentum is limited by the critical value.

3. The tendency of horizontal wind is obtained by calculating the vertical convergence of momentum flux in each layer.

3.9.2 Relationship between Local FroudeNnumber and Momentum Flux

Considering the vertical flux of horizontal momentum due to orographic gravity waves, the difference between the flux (τ) and the local Froude number ($F_L = NH/U$) at a certain altitude is

$$F_L = \left(\frac{\tau N}{E_f \rho U^3} \right)^{1/2} , \qquad (3.518)$$

This relationship holds for the following cases where $N = g/\theta \partial \theta/\partial z$ is the Brant-Väisälä frequency, ρ is the density of the atmosphere, U is the wind speed, and E_f is the proportional constant corresponding to the horizontal scale of the rippling of the surface. From now on,

$$\tau = \frac{E_f F_L^2 \rho U^3}{N} \qquad (3.519)$$

The local Froude number (F_L) cannot exceed the critical Froude number (F_c). If the local Froude number calculated from (3.518) exceeds the critical Froude number F_c, the gravity wave becomes supersaturated and the flux decreases to the momentum flux corresponding to the critical Froude number.

3.9.3 Momentum Fluxes at the Surface

The magnitude of the vertical flux of horizontal momentum due to gravity waves excited at the earth's surface, $\tau_{1/2}$, is calculated by substituting the local Froude number $(F_L)_{1/2} = N_1 h / U_1$ into (3.519),

$$\tau_{1/2} = E_f h^2 \rho_1 N_1 U_1 , \tag{3.520}$$

where $U_1 = |\mathbf{v}_1| = (u_1^2 + v_1^2)^{1/2}$ is the surface wind speed, N_1, ρ_1 are estimated to be the stability and density of the atmosphere near the earth's surface, respectively. h is an indicator of the change in the sub-grid orography and is assumed to be equal to the standard deviation of the surface height (Z_{SD}).

Here, when the local Froude number $((F_L)_{1/2} = N_1 Z_{SD}/U_1)$ exceeds the critical Froude number (F_c), the momentum flux is suppressed to the value obtained by substituting (3.519) for F_c. In other words,

$$\tau_{1/2} = \min \left(E_f Z_{SD}^2 \rho_1 N_1 U_1, \ \frac{E_f F_c^2 \rho_1 U_1^3}{N_1} \right) \tag{3.521}$$

3.9.4 Momentum Fluxes in the Upper Levels

Suppose that the momentum flux $\tau_{k-1/2}$ is computed at level $k - 1/2$. When no saturation occurs, $\tau_{k+1/2}$ is equal to $\tau_{k-1/2}$. If the momentum flux ($\tau_{k-1/2}$) exceeds the momentum flux calculated from the critical Froude number at the $k + 1/2$ level, wave breaking occurs in the k layer and the momentum flux decreases to the critical flux.

$$\tau_{k+1/2} = \min \left(\tau_{k-1/2}, \ \frac{E_f F_c^2 \rho_{k+1/2} U_{k+1/2}^3}{N_{k+1/2}} \right) , \tag{3.522}$$

Note that $U_{k+1/2}$ is the magnitude of the horizontal wind speed projected on to the direction of the lowest level of the horizontal wind,

$$U_{k+1/2} = \frac{\mathbf{v}_{k+1/2} \cdot \mathbf{v}_1}{|\mathbf{v}_1|} \tag{3.523}$$

3.9.5 The Magnitude of the Time Variation of Horizontal Wind due to Momentum Convergence

The tendency of the projected component of the horizontal wind, U_k, is ,

$$\frac{\partial U}{\partial t} = -\frac{1}{\rho} \frac{\partial \tau}{\partial z} = g \frac{\partial \tau}{\partial p}. \tag{3.524}$$

That is

$$\frac{\partial U_k}{\partial t} = g \frac{\tau_{k+1/2} - \tau k - 1/2}{\Delta p}. \tag{3.525}$$

Using this, tendency for the eastward and northward winds are calculated as follows

$$\frac{\partial u_k}{\partial t} = \frac{\partial U_k}{\partial t} \frac{u_1}{U_1} \tag{3.526}$$

$$\frac{\partial v_k}{\partial t} = \frac{\partial U_k}{\partial t} \frac{v_1}{U_1} \tag{3.527}$$

3.9.6 Other Notes

1. It is assumed that no gravity waves are excited at the ground surface when the wind speed is small ($U_1 \leq v_{min}$) or when the undulations at the surface are small ($Z_{SD} \leq (Z_{SD})_{min}$).

4 Miscellaneous

4.1 Coupler

4.1.1 Fluxes to Atmospheric Models

4.1.1.1 Fluxes between Atmosphere and Ocean

Fluxes from the sea surface to the atmosphere ($FLXO$) are calculated on the sea surface grid of the atmospheric model.

Boundary conditions such as sea surface temperature, sea ice concentration, sea ice thickness, snow depth over sea ice, sea ice internal temperature, and ocean surface current velocity are obtained from the ocean model through an exchanger (sea ice surface temperature is determined from the sea ice internal temperature, sea ice thickness, and atmospheric conditions over the sea ice. The sea ice velocity is not currently used for flux calculations in MIROC). The atmospheric boundary conditions such as wind speed, temperature, and specific humidity at sea are converted from the atmospheric grid to the sea surface grid using linear or cubic spline completion. The fluxes from the sea surface are calculated separately for seawater and sea ice, averaged by area weight, and passed to the atmosphere. When using a sea ice model categorized by sea ice thickness, it may be necessary to calculate fluxes for each sea ice thickness category, but the current model specification calculates fluxes for the average sea ice thickness. The conversion of fluxes and boundary conditions between the atmosphere and ocean by the exchanger will be described in detail later.

4.1.1.2 Fluxes between Atmospheric land Surface

Fluxes from the land surface to the atmosphere ($FLXL$) are calculated on a land surface grid. A land surface grid consists of multiple soil covers and lakes. Freezing and thawing of lakes and snow cover are considered by a vertical 1D ice model (0-layer model). If the area of the land surface grid is SL, the area occupied by the lake and each soil cover is respectively

$$SL^{lake} = SL \times LKFRC \times FLND \tag{4.1}$$

$$SL_k^{grd} = SL \times GRFRC_k \times (1 - LKFRC) \times FLND \tag{4.2}$$

where $LKFRC$ is the percentage of lakes on land, k is the type of soil cover, and $GRFRC_k$ is the percentage of soil cover k on land excluding lakes. Fluxes from the land surface are calculated separately over each of these soil covers and lakes, averaged by area weight, and passed to the atmosphere.

$$FLXL = LKFRC \times FLXL^{lake} + (1 - LKFRC) \times \sum_{k=1}^{km}(GRFRC_k \times FLXL_k^{grd}) \tag{4.3}$$

where $FLXL^{lake}$ is the flux at the lake surface, $FLXL_k^{grd}$ is the flux at soil cover k, and km is the number of soil cover types.

4.1.1.3 Total Flux to the Atmosphere

Since the river is treated without area property in the model, the flux to the atmosphere ($FLXA$) can be obtained as a weighted average of the sea-land distribution of the fluxes on the land grid ($FLXL$) and at the sea grid ($FLXO$) as follows

$$
\begin{aligned}
FLXA = \frac{1}{SA} \times [&\sum_{j=1}^{jldiv} \sum_{i=1}^{ildiv} (SL_{ij} \times FLND_{ij}^{land} \times FLXL_{ij}) \\
&+ \sum_{j=1}^{jodiv} \sum_{i=1}^{iodiv} (SO_{ij} \times (1 - FLND_{ij}^{oc}) \times FLXO_{ij})]
\end{aligned} \tag{4.4}
$$

.

where, (ildiv,jldiv) is the number of east-west and north-south divisions of the land surface grid. Fluxes computed in the atmospheric model, such as precipitation, are also included in $FLXL$ and $FLXO$. In the case of such fluxes, all the fluxes in the partitioned land and sea surface grids have the same value as the corresponding grid.

4.1.2 Fluxes between Land Surface Model and River Model

4.1.2.1 Fluxes between Land Surfaces and the River

In the current specification of the model, the fluxes of water between river and land surfaces deal only with the inflow of water from the river to the lake ($RUNIN$), the outflow from the lake to the river ($RUNOFF$), the inflow of water to the land surface at the inland vanishing point ($RUNIN$), and the outflow of water overflowing the soil to the river ($RUNOFF$). Here, the inland vanishing point indicates the point where the endpoint of the river disappears, such as in deserts. The water balance in the river model is divided into ice and water. The ice in the river model corresponds to a pseudo-glacier. Here, the phase change in the river model is not considered to guarantee the conservation of melting heat. In addition, the flow rate of a river is defined as the amount of water present in the river grid divided by its area. Water and ice are transported downstream in the river model according to the river channel network data. In the river model in MIROC6, the river discharge at the inland vanishing point of the river is scattered over the global ocean to obtain the water balance.

4.1.2.2 Water Runoff from Land Surface

When each soil cover in the land surface grid can no longer hold water or snow and ice, water or ice is passed from each soil model to the river model through the coupler.

$$
RUNOFF_{all}^{grd} = (1 - LKFRC) \times \sum_{k=1}^{km} (GFLRC_k \times RUNOFF_k^{grd}) \tag{4.5}
$$

The details of the runoff from each soil cover can be found in the documentation of the land surface model MATSIRO. In the lake model, when the lake level or snow/ice thickness (H) exceeds a constant value (H_c), the water flows out to the river at a time constant τ_h

$$
RUNOFF^{lake} = LKFRC \times \frac{(H - H_c)}{\tau_h}, \qquad (H > H_c) \tag{4.6}
$$

$$RUNOFF^{lake} = 0, \qquad (H < H_c) \tag{4.7}$$

The average runoff from the land surface is as follows.

$$RUNOFF^{land}_{all} = RUNOFF^{lake} + RUNOFF^{grd}_{all} \tag{4.8}$$

When considering the average runoff volume of the land surface grid, it is necessary to multiply the above equation by the percentage of land surface $FLND$. In the river model, $RUNOFF^{land}_{all}$ is converted to the river grid with the weight of sea-land distribution, and the runoff amount $RUNOFF^{riv}$ is used for calculation.

4.1.2.3 Runin of Water from a River to a Lake

When a lake exists in the middle of a river channel, water flows into the lake according to the river flow rate. In order to calculate the amount of water flowing into the lake, the river flow $GDRIV$ in the river grid is converted to the river flow $GDRIVL$ in the land surface grid through the coupler. Here, $GDRIVL$ is the amount normalized by the area of the land surface grid. In the land surface grid, the river inflow to the lake, $RUNINN$, is defined by the river flow ($GDRIVL$) and the time constant τ as follows

$$RUNINN^{lake} = GDRIVL/\tau \tag{4.9}$$

.

Since the current specification only considers inflow from rivers to lakes, except at the inland vanishing point, the average inflow at the land surface is

$$RUNINN^{land} = RUNINN^{lake} \times LKFRC \tag{4.10}$$

.

When there are multiple river grids corresponding to a land surface grid, if the river water inflow to the land surface averaged over the land surface grid is returned to the river grid using only the area weights as in $RUNOFF$, it is possible that more water will flow out of the river than exists in the river grid. Therefore, we convert the ratio of discharge to river flow from the land surface grid to the river grid, and estimate the river discharge (inflow to the land surface) in each river grid. The runoff ratio of the river flow to the land surface grid is

$$RINN^{land} = RUNINN^{land}/GDRIVL \tag{4.11}$$

.

If the discharge rate converted to the river grid is $RINN^{riv}$, the discharge (inflow to the land surface) in the river grid is

$$RUNINN^{riv} = RINN^{riv} \times GDRIV \tag{4.12}$$

.

4.1.3 Fluxes to the Ocean Model

4.1.3.1 Boundary Conditions for the Ocean on a Sea Level Grid

As mentioned above, the fluxes between the atmosphere and the ocean are calculated on the sea level grid. In this section, we describe the conversion from the ocean model grid to the sea surface grid. The standard variables to be converted from the ocean model to the atmospheric sea surface grid are sea surface temperature (SST), sea ice concentration (AI), sea ice thickness (HI), snow depth over sea ice (HSN), sea ice internal temperature (TI), and ocean surface current velocity (UO, VO). In order to clarify which grid we are dealing with in the future, variables in the ocean model grid will be denoted by superscript $OGCM$ and variables in the sea surface grid by superscript oc. In addition, the position in the ocean grid is denoted by LO and the position in the sea surface grid by LC. The boundary condition of the ocean in the sea level grid is defined as follows.

$$SST^{oc}(LC) = \sum_{N=1}^{IJO(LC)} [SST^{OGCM}(IJO2C(LC,N)) \times SOCN(LC,N)]/SOCNG(LC) \quad (4.13)$$

$$AI^{oc}(LC) = \sum_{N=1}^{IJO(LC)} [AI^{OGCM}(IJO2C(LC,N)) \times SOCN(LC,N)]/SOCNG(LC) \quad (4.14)$$

$$HI^{oc}(LC) = \frac{1}{SOCNG(LC) \times AI^{oc}(LC)} \sum_{N=1}^{IJO(LC)} [HI^{OGCM}(IJO2C(LC,N))$$
$$\times AI^{OGCM}(IJO2C(LC,N)) \times SOCN(LC,N)] \quad (4.15)$$

$$HSN^{oc}(LC) = \frac{1}{SOCNG(LC) \times AI^{oc}(LC)} \sum_{N=1}^{IJO(LC)} [HSN^{OGCM}(IJO2C(LC,N))$$
$$\times AI^{OGCM}(IJO2C(LC,N)) \times SOCN(LC,N)] \quad (4.16)$$

$$TI^{oc}(LC) = \frac{1}{SOCNG(LC) \times HI^{oc}(LC) \times AI^{oc}(LC)} \sum_{N=1}^{IJO(LC)} [TI^{OGCM}(IJO2C(LC,N))$$
$$\times HI^{OGCM}(IJO2C(LC,N)) \times AI^{OGCM}(IJO2C(LC,N)) \times SOCN(LC,N)](4.17)$$

$$UO^{oc}(LC) = RUO(LC) \times \frac{\sum_{N=1}^{IJO(LC)}[UO^{OGCM}(IJO2C(LC,N)) \times SOCN(LC,N)]}{SOCNG(LC)}$$
$$+ RVO(LC) \times \frac{\sum_{N=1}^{IJO(LC)}[VO^{OGCM}(IJO2C(LC,N)) \times SOCN(LC,N)]}{SOCNG(LC)} \quad (4.18)$$

$$VO^{oc}(LC) = -RVO(LC) \times \frac{\sum_{N=1}^{IJO(LC)}[UO^{OGCM}(IJO2C(LC,N)) \times SOCN(LC,N)]}{SOCNG(LC)}$$
$$+ RUO(LC) \times \frac{\sum_{N=1}^{IJO(LC)}[VO^{OGCM}(IJO2C(LC,N)) \times SOCN(LC,N)]}{SOCNG(LC)} \quad (4.19)$$

$$SOCNG(LC) = \sum_{N=1}^{IJO(LC)} SOCN(LC, N) \tag{4.20}$$

where, $IJO(LC)$: Number of ocean grids corresponding to the sea level grid (LC) in the atmospheric node.

$IJO2C(LC, N)$: Location of the ocean grid corresponding to the sea surface grid in the atmospheric node.

$SOCN(LC, N)$: Area of the ocean grid corresponding to the sea surface grid in the atmospheric node.

$RUO(LC)$: Cosine of the rotation angle of the vector.

$RVO(LC)$: Sine of the rotation angle of the vector

$SOCNG(LC)$: Area of ocean occupied by sea surface grid.

The ratio of land surface to the sea level grid is also defined as follow.

$FLND^{oc} = (1 - SOCNG)/SO$

where, SO is the area of sea surface grid.

The variables related to sea ice that are converted to the sea surface grid are calculated as the average of variables categorized by sea ice layer thickness (AIM, HIM, HSM, TIM) as follows.

$$AI^{OGCM} = \sum_{L=1}^{NIC} AIM^{OGCM}(L) \tag{4.21}$$

$$HI^{OGCM} = \sum_{L=1}^{NIC} HIM^{OGCM}(L) \times AIM^{OGCM}(L)/AI^{OGCM} \tag{4.22}$$

$$HSN^{OGCM} = \sum_{L=1}^{NIC} HSM^{OGCM}(L) \times AIM^{OGCM}(L)/AI^{OGCM} \tag{4.23}$$

$$TI^{OGCM} = \sum_{L=1}^{NIC} TIM^{OGCM}(L) \times AIM^{OGCM}(L)/(AI^{OGCM} \times HI^{OGCM}) \tag{4.24}$$

where, NIC is the number of category of sea ice.

4.1.3.2 Conversion of Air-Sea Fluxes Calculated on the Sea Surface Grid to the Ocean Grid

Fluxes calculated on the sea surface grid are calculated at sea surface and sea ice surface, respectively, and fluxes to the atmosphere are calculated as

$$FLXO = (1 - AI) \times FLUXO + AI \times FLUXI \tag{4.25}$$

These fluxes are time-integrated by the flux coupler in the atmospheric model with weights for sea surface and sea ice extent, and then converted to the ocean grid by the coupled atmosphere-ocean time step and passed to the ocean model.

$$FLUXOA^{OGCM}(LO) = ROCN(LO)$$

$$\times \sum_{N=1}^{IJA(LO)} \frac{FLUXOA^{oc}(IJC2O(LO,N)) \times SATM(LO,N)}{SATMG(LO)} \quad (4.26)$$

$$FLUXIA^{OGCM}(LO) = ROCN(LO)$$

$$\times \sum_{N=1}^{IJA(LO)} \frac{FLUXIA^{oc}(IJC2O(LO,N)) \times SATM(LO,N)}{SATMG(LO)} \quad (4.27)$$

$$SATMG(LO) = ROCN(LO) \times \sum_{N=1}^{IJA(LO)} SATM(LO,N) \quad (4.28)$$

$$ROCN(LO) = SATMG(LO)/S^{OGCM}(LO) \quad (4.29)$$

$$FLUXOA^{oc} = (1 - AI^{oc}) \times FLUXO^{oc} \quad (4.30)$$

$$FLUXIA^{oc} = AI^{oc} \times FLUXI^{oc} \quad (4.31)$$

where, $IJA(LO)$: Number of sea level grids in the atmospheric model corresponding to the ocean grid (LO)

$IJC2O(LO,N)$: Location of the sea surface grid of the atmospheric model corresponding to the ocean grid

$SATM(LO,N)$: Area of the sea surface grid of the atmospheric model corresponding to the ocean grid

$SATM(LO,N) = SOCN(LC,L), LC = IJC2O(LO,N), LO = IJO2C(LC,L)$

$S^{OGCM}(LO)$: Area of the ocean grid

The area of the ocean grid and the sum of the areas of the corresponding ocean grids should match, although the coordinate systems of the atmospheric model and the ocean model are different (the surface areas of the earth in the atmospheric model and the ocean model do not match exactly).

When creating the conversion file, the grid of the atmospheric model is divided into small areas, and the area of the corresponding ocean grid is estimated from the sum of these areas, so they do not match exactly. For this reason, the flux balance between the atmosphere and the ocean is adjusted by multiplying by the ratio ($ROCN$). The wind stresses to the ocean are also calculated as wind stresses over sea level (TXO, TYO) and over sea ice (TXI, TYI), but without multiplying the weights of sea level and sea ice area.

$$TXO^{OGCM}(LO) =$$

$$+RU(LO) \times ROCN(LO) \times \sum_{N=1}^{IJA(LO)} \frac{[TXO^{oc}(IJC2O(LO,N)) \times SATM(LO,N)]}{SATMG(LO)}$$

$$+RV(LO) \times ROCN(LO) \times \sum_{N=1}^{IJA(LO)} \frac{[TYO^{oc}(IJC2O(LO,N)) \times SATM(LO,N)]}{SATMG(LO)} \quad (4.32)$$

$$TYO^{OGCM}(LO) =$$

$$-RV(LO) \times ROCN(LO) \times \sum_{N=1}^{IJA(LO)} \frac{[TXO^{oc}(IJC2O(LO,N)) \times SATM(LO,N)]}{SATMG(LO)}$$

$$+RU(LO) \times ROCN(LO) \times \sum_{N=1}^{IJA(LO)} \frac{[TYO^{oc}(IJC2O(LO,N)) \times SATM(LO,N)]}{SATMG(LO)} \quad (4.33)$$

where,
$RU(LO)$: cosine of the rotation angle of the vector
$RV(LO)$: sine of the rotation angle of the vector

4.1.3.3 Redistribution of Fluxes in the Ocean Model

The fluxes converted to the ocean grid are updated at each time step of the coupling. Since the coupling time step is longer than the ocean model time step, the sea level/sea ice area ratio in the ocean model is updated to a different value than the one used to calculate the flux. Therefore, in order to obtain an accurate heat and water balance, the fluxes need to be distributed according to the updated sea surface and sea ice area ratios. The fluxes $FLUXOA$ and $FLUXIA$ at sea surface and sea ice surface are ocean grid-averaged values. Fluxes to each sea ice category are currently distributed evenly independent of sea ice thickness.

$$FLUXIAM(L) = FLUXIA \times AIM(L) \quad (4.34)$$

$$FLUXOA = FLUXOA + FLUXIA \times [1.0 - \sum_{L=1}^{LMAX} AIM(L)] \quad (4.35)$$

where, AIM denotes the percentage of area covered by sea ice in the grid (sea ice concentration), L denotes the type of sea ice thickness category, and $LMAX$ denotes the number of thickness categories. If there is no sea ice surface, all fluxes will be at sea surface. If sea ice disappears in the middle of the coupling time step, the flux due to sublimation is divided into the heat flux assuming a sea ice surface and the freshwater flux (sea ice loss). The heat flux is directly reflected in the temperature change of the first layer of ocean. On the other hand, the freshwater flux due to sublimation is converted into heat flux and freshwater flux and given to the first layer of the ocean, assuming that sea ice is generated by the sublimation. As for the wind stress, it is not weighted by sea level and sea ice area before the grid transformation, so it is driven by the respective area weights in each sea ice thickness category in the ocean model. For this reason, momentum is not conserved.

4.1.3.4 Water Runoff from Rivers to the Ocean

At the end of the river model, we calculate the water flowing from the estuary of river to the ocean. Water arriving at the estuary of the river grid is first converted to the atmospheric sea surface grid and time integrated in a flux coupler. After that, it is converted to the ocean grid via an exchanger and passed to the ocean model in the same way as the atmospheric precipitation data. At this point, the temperature of the river water is treated as the same as the sea surface temperature, as is the case with precipitation. Therefore, strictly speaking, heat is not conserved. Ice runoff is handled in the same way as snowfall.

4.1.3.5 Number of Divisions in the Sea Surface Grid and Resolution of the Ocean Model

The sea surface grid is created by dividing the latitude and longitude of the atmospheric grid, but if the number of divisions is not sufficient and the ocean model grid has a higher resolution than the atmospheric sea surface grid, the structure of the atmospheric grid size may remain when the flux is converted to the ocean grid through the exchanger. . In addition, data such as precipitation from the atmosphere is not interpolated when converting from the atmospheric grid to the ocean grid, so the atmospheric grid structure remains in the ocean grid for these fluxes. When linear interpolation is used instead of cubic spline interpolation when converting to the sea surface grid, the atmospheric grid structure may remain for differential quantities such as wind stress curl.

4.2 Definition of Land-Sea Distribution

The land-sea distribution in MIROC is prioritized by the land-sea distribution defined by the ocean model. While one grid in the ocean model is defined by land or sea only, the land and ocean grids in the atmospheric model are determined in proportion to the land and sea to be consistent with the ocean model's land-sea distribution.

SA : area of the atmospheric grid, SL_{ij} : area of the land grid, SO_{ij} : area of the sea surface grid, $FLND^{atm}$, $FLND_{ij}^{land}$, $FLND_{ij}^{oc}$: percentage of land surface is occupied by each grid. Then, following equation is satisfied.

$$SA * FLND^{atm} = \sum_{j=1}^{jldiv} \sum_{i=1}^{ildiv} (SL_{ij} * FLND_{ij}^{land}) = \sum_{j=1}^{jodiv} \sum_{i=1}^{iodiv} (SO_{ij} * FLND_{ij}^{oc}) \qquad (4.36)$$

where, (ildiv,jldiv) is the number of east-west and north-south divisions of the land surface grid, and (iodiv,jodiv) is the number of east-west and north-south divisions of the sea surface grid. In the land surface grid, if even a small amount of land is defined to exist, boundary values such as land cover are required.

5   References

1. Abdul-Razzak, H., and Ghan, S. J. (2000). A parameterization of aerosol activation: 2. Multiple aerosol types. Journal of Geophysical Research: Atmospheres. `https://doi.org/10.1029/1999jd901161`

2. Arakawa, A., , and W. H. Schubert, (1974). Interaction of a cumulus cloud ensemble with the large-scale environment, Part I. Journal of Atmospheric Science, 31 , 674–701.

3. Arakawa, A., , and K.-M. Xu, (1990). The macroscopic behavior of simulated cumulus convection and semiprognostic tests of the Arakawa–Schubert cumulus parameterization. Proc. Indo-U.S. Seminar on Parameterization of Subgrid-Scale Processes in Dynamical Models of Medium-Range Prediction and Global Climate, Pune, India, Indian Institute of Tropical Meteorology, 3–18.

4. Arakawa, A., and K.-M. Xu, (1992). The macroscopic behavior of simulated cumulus convection and semiprognostic tests of the Arakawa-Schubert cumulus parameterization. Physical Process in Atmospheric Models., 3–18.

5. Arakawa, A., and Konor, C. S. (1996). Vertical Differencing of the Primitive Equations Based on the Charney–Phillips Grid in Hybrid andsigma–p Vertical Coordinates. Monthly Weather Review, 124(3), 511–528.

6. Asselin, R. (1972). Frequency Filter for Time Integrations. Monthly Weather Review, 100(6), 487–490.

7. Berry, E. X. (1968). Modification of the warm rain process. In Proc. First Conf. on Weather Modification, AMS, 1968, 81-85.

8. Berger, A. (1978). Long-term variations of caloric insolation resulting from the Earth's orbital elements. Quaternary research, 9(2), 139-167.

9. Bourke, W. (1988). Spectral Methods in Global Climate and Weather Prediction Models. In M. E. Schlesinger (Ed.), Physically-Based Modelling and Simulation of Climate and Climatic Change: Part 1 (pp. 169–220). Dordrecht: Springer Netherlands.

10. Bretherton, C. S., McCaa, J. R., and Grenier, H. (2004). A new parameterization for shallow cumulus convection and its application to marine subtropical cloud-topped boundary layers. Part I: Description and 1D results. Monthly Weather Review, 132(4), 864–882.

11. Bushell, A. C., Wilson, D. R., and Gregory, D. (2003). A description of cloud production by non-uniformly distributed processes. Quarterly Journal of the Royal Meteorological Society, 129(590), 1435–1455.

12. Businger, J. A., Wyngaard, J. C., Izumi, Y., and Bradley, E. F. (1971). Flux-Profile Relationships in the Atmospheric Surface Layer. Journal of the Atmospheric Sciences, 28(2), 181–189.

13. Cesana, G., Waliser, D. E., Jiang, X., and Li, J.‐L F. (2015). Multimodel evaluation of cloud phase transition using satellite and reanalysis data. Journal of Geophysical Research, 120(15), 7871–7892.

14. Chikira, M., and Sugiyama, M. (2010). A Cumulus Parameterization with State-Dependent Entrainment Rate. Part I: Description and Sensitivity to Temperature and Humidity Profiles. Journal of the Atmospheric Sciences, 67(7), 2171–2193.

15. Colella, P., and Woodward, P. R. (1984). The Piecewise Parabolic Method (PPM) for gas-dynamical simulations. Journal of Computational Physics.

`https://doi.org/10.1016/0021-9991(84)90143-8`

16. Diehl, K., Simmel, M., and Wurzler, S. (2006). Numerical sensitivity studies on the impact of aerosol properties and drop freezing modes on the glaciation, microphysics, and dynamics of clouds. Journal of Geophysical Research, 111(D7).
`https://doi.org/10.1029/2005jd005884`

17. Gregory, D. (2001). Estimation of entrainment rate in simple models of convective clouds. Quarterly Journal of the Royal Meteorological Society, 127(571), 53–72.

18. Gregory, D., Kershaw, R., and Inness, P. M. (1997). Parametrization of momentum transport by convection. II: Tests in single-column and general circulation models. Quarterly Journal of the Royal Meteorological Society, 123(541), 1153–1183.

19. Haltiner, G. J., and Williams, R. T. (1980). Numerical prediction and dynamic meteorology (No. 551.5 HAL). sidalc.net. Retrieved from
`http://www.sidalc.net/cgi-bin/wxis.exe/?IsisScript=FCL.xisandmethod=`
`postandformato=2andcantidad=1andexpresion=mfn=004222`

20. Hasumi, H. (2015). CCSR ocean component model (COCO) (Version 4.0) (p. 68). Atmosphere and Ocean Research Institute, The University of Tokyo. Retrieved from
`https://ccsr.aori.u-tokyo.ac.jp/ hasumi/COCO/coco4.pdf`

21. Helfand, H. M., and Labraga, J. C. (1988). Design of a Nonsingular Level 2.5 Second-Order Closure Model for the Prediction of Atmospheric Turbulence. Journal of the Atmospheric Sciences, 45(2), 113–132.

22. Hines, C. O. (1997) Doppler-spread parameterization of gravity wave momentum deposition in the middle atmosphere, Part 2: Broad and quasi monochromatic spectra, and implementation, Journal of Atmosphere Sol.-Terr. Physics, 59, 387–400.

23. Holtslag, A. A. M., and Boville, B. A. (1993). Local Versus Nonlocal Boundary-Layer Diffusion in a Global Climate Model. Journal of Climate, 6(10), 1825–1842.

24. K-1 model developers (2004). K-1 coupled GCM (MIROC) description, K-1 Tech. Rep., 1, edited by: Hasumi, H. and Emori, S., Center for Climate System Research, the Univ. of Tokyo, Tokyo, 34 pp.

25. Kain, J. S., and Michael Fritsch, J. (1990). A One-Dimensional Entraining/Detraining Plume Model and Its Application in Convective Parameterization. Journal of the Atmospheric Sciences, 47(23), 2784–2802.

26. Lew, J. K., , D. C. Montague, , and H. R. Pruppacher, (1986) A wind tunnel investigation on the riming of snowflakes. Part I: Porous disks and large stellars. Journal of Atmospheric Science, 43, 2392–2409.

27. Lin, S.-J., and Rood, R. B. (1996). Multidimensional Flux-Form Semi-Lagrangian Transport Schemes. Monthly Weather Review, 124(9), 2046–2070.

28. Lohmann, U. (2004). Can anthropogenic aerosols decrease the snowfall rate?. Journal of the atmospheric sciences, 61(20), 2457-2468.

29. Lohmann, U., and Diehl, K. (2006). Sensitivity studies of the importance of dust ice nuclei for the indirect aerosol effect on stratiform mixed-phase clouds. Journal of the Atmospheric Sciences, 63(3), 968–982.

30. Louis, J., Tiedtke, M., and Geleyn, J. (1982). A short history of the PBL parameterization at ECMWF, paper presented at Workshop on Planetary Boundary Layer Parameterization, Eur. Cent. for Medium Range Weather Forecasts. Reading, UK.

31. Louis, J.-F. (1979). A parametric model of vertical eddy fluxes in the atmosphere. Boundary-Layer Meteorology, 17(2), 187–202.

32. McFarlane, N. (1987). The Effect of Orographically Excited Gravity Wave Drag on the General Circulation of the Lower Stratosphere and Troposphere. Journal of the Atmospheric Sciences, 44(14), 1775-1800.

33. Mellor, G. L. (1973). Analytic Prediction of the Properties of Stratified Planetary Surface Layers. Journal of the Atmospheric Sciences, 30(6), 1061–1069.

34. Mellor, G. L., and Yamada, T. (1974). A Hierarchy of Turbulence Closure Models for Planetary Boundary Layers. Journal of the Atmospheric Sciences, 31(7), 1791–1806.

35. Mellor, G. L., and Yamada, T. (1982). Development of a turbulence closure model for geophysical fluid problems. Reviews of Geophysics, 20(4), 851-875.

36. Mesinger, F., and Arakawa, A. (1976). Numerical methods used in atmospheric models (GARP Publications Series) (p. 64). CAU. Retrieved from
http://eprints.uni-kiel.de/40278/

37. Miller, M.J., A.C.M. Beljaars and T.N. Palmer, (1992). The sensitivity of the ECMWF model to the parameterization of evaporation from the tropical oceans. Journal of Climate, 5, 418-434.

38. Miura, H. (2002). Vertical differencing of the primitive equations in a $\sigma - p$ hybrid coordinate (For Spectral AGCM)) (Version DRAFT). Center for Climate System Research,University of Tokyo.

39. Nakajima, T., Tsukamoto, M., Tsushima, Y., Numaguti, A., and Kimura, T. (2000). Modeling of the radiative process in an atmospheric general circulation model. Applied Optics, 39(27), 4869–4878.

40. Nakanishi, M. (2001). IMPROVEMENT OF THE MELLOR–YAMADA TURBULENCE CLOSURE MODEL BASED ON LARGE-EDDY SIMULATION DATA. Boundary-Layer Meteorology, 99, 349–378.

41. Nakanishi, M., , and H. Niino, (2004). An improved Mellor–Yamada level-3 model with condensation physics: Its design and verification. Boundary-Layer Meteor, 112 , 1–31.

42. Nitta, T., Yoshimura, K., Takata, K., O'ishi, R., Sueyoshi, T., Kanae, S., et al. (2014). Representing Variability in Subgrid Snow Cover and Snow Depth in a Global Land Model: Offline Validation. Journal of Climate, 27(9), 3318–3330.

43. Ogura, T. (2015). Implementation of shallow cumulus Parameterization. National Institute of Environmental Studies.

44. Ogura, T., Shiogama, H., Watanabe, M., Yoshimori, M., Yokohata, T., Annan, J. D., Hargreaves, J. C., Ushigami, N., Hirota, K., Someya, Y., Kamae, Y., Tatebe, H., and Kimoto, M. (2017). Effectiveness and limitations of parameter tuning in reducing biases of top-of-atmosphere radiation and clouds in MIROC version 5, Geoscience Model Development, 10, 4647–4664

45. Pan, D.-M. (1995, January 1). Development and Application of a Prognostic Cumulus Parametrization. ui.adsabs.harvard.edu. Retrieved from
https://ui.adsabs.harvard.edu/abs/1995PhDT........74P

46. Pan, D-M., , and D. A. Randall, 1998: A cumulus parameterization with a prognostic closure. Quarterly Journal of the Royal Meteorological Society, 124 , 949–981.

47. Park, S., and Bretherton, C. S. (2009). The University of Washington Shallow Convection and Moist Turbulence Schemes and Their Impact on Climate Simulations with the Community Atmosphere Model. Journal of Climate, 22(12), 3449–3469.

48. Pruppacher, H. R., , and J. D. Klett, (1997). Microphysics of Clouds and Precipitation. Kluwer Academic, 954 pp.

49. Randall, D. A. (1980). Conditional Instability of the First Kind Upside-Down. Journal of the Atmospheric Sciences, 37(1), 125–130.

50. Randall, D. A., and Pan, D.-M. (1993). Implementation of the Arakawa-Schubert Cumulus Parameterization with a Prognostic Closure. In K. A. Emanuel and D. J. Raymond (Eds.), The Representation of Cumulus Convection in Numerical Models (pp. 137–144). Boston, MA: American Meteorological Society.

51. Randall, D. A., , D-M. Pan, , P. Ding, , and D. G. Cripe, (1997). Quasi-equilibrium. The Physics and Parameterization of Moist Atmospheric Convection, R. K. Smith, Ed., Kluwer Academic, 359–386.

52. Sekiguchi, M., and Nakajima, T. (2008). A k-distribution-based radiation code and its computational optimization for an atmospheric general circulation model. Journal of Quantitative Spectroscopy and Radiative Transfer, 109(17), 2779–2793. vSmith, R. K. (2013). The Physics and Parameterization of Moist Atmospheric Convection. Springer Science and Business Media.

53. Sommeria, G., and Deardorff, J. W. (1977). Subgrid-Scale Condensation in Models of Nonprecipitating Clouds. Journal of the Atmospheric Sciences, 34(2), 344–355.

54. Stevens, B. (2005). ATMOSPHERIC MOIST CONVECTION. Annual Review of Earth and Planetary Sciences, 33(1), 605–643.

55. Suzuki, T., Saito, F., Nishimura, T., and Ogochi, K. (2009). Coupling procedures of heat and freshwater fluxes in the MIROC (Model for Interdisciplinary Research on Climate) version 4. JAMSTEC report of research and development

56. Takata, K., Emori, S., and Watanabe, T. (2003). Development of the minimal advanced treatments of surface interaction and runoff. Global and Planetary Change, 38(1), 209–222.

57. Takemura, T. (2005). Simulation of climate response to aerosol direct and indirect effects with aerosol transport-radiation model. Journal of Geophysical Research, 110(D2). `https://doi.org/10.1029/2004jd005029`

58. Takemura, T., Okamoto, H., Maruyama, Y., Numaguti, A., Higurashi, A., and Nakajima, T. (2000). Global three-dimensional simulation of aerosol optical thickness distribution of various origins. Journal of Geophysical Research, 105(D14), 17853–17873.

59. Takemura, T., Nakajima, T., Dubovik, O., Holben, B. N., and Kinne, S. (2002). Single-scattering albedo and radiative forcing of various aerosol species with a global three-dimensional model. Journal of Climate, 15(4), 333–352.

60. Takemura, T., Egashira, M., Matsuzawa, K., Ichijo, H., O ' ishi, R., and Abe-Ouchi, A. (2009). A simulation of the global distribution and radiative forcing of soil dust aerosols at the Last Glacial Maximum. Atmospheric Chemistry and Physics, 9(9), 3061–3073.

61. Tatebe, H., Ogura, T., Nitta, T., Komuro, Y., Ogochi, K., Takemura, T., et al. (2019). Description and basic evaluation of simulated mean state, internal variability, and climate sensitivity in MIROC6. Geoscientific Model Development, 12(7), 2727–2765.

62. Tompkins, A. M. (2002). A prognostic parameterization for the subgrid-scale variability of

water vapor and clouds in large-scale models and its use to diagnose cloud cover. Journal of the Atmospheric Sciences, 59(12), 1917–1942.

63. Watanabe, M., Emori, S., Satoh, M., and Miura, H. (2009). A PDF-based hybrid prognostic cloud scheme for general circulation models. Climate Dynamics, 33(6), 795–816.

64. Watanabe, S. (2008). Constraints on a Non-orographic Gravity Wave Drag Parameterization Using a Gravity Wave Resolving General Circulation Model, SOLA, 4, 61-64. Watanabe, S., Hajima, T., Sudo, K., Nagashima, T., Takemura, T., Okajima, H., Nozawa, T., Kawase, H., Abe, M., Yokohata, T., Ise, T., Sato, H., Kato, E., Takata, K., Emori, S., and Kawamiya, M. (2011) MIROC-ESM 2010: model description and basic results of CMIP5-20c3m experiments, Geoscience Model Development, 4, 845-872.

65. Williams, P. D. (2009). A Proposed Modification to the Robert–Asselin Time Filter. Monthly Weather Review, 137(8), 2538–2546.

66. Wilson, D. R., and Ballard, S. P. (1999). A microphysically based precipitation scheme for the UK meteorological office unified model. Quarterly Journal of the Royal Meteorological Society, 125(557), 1607-1636.

67. Wood, R., and Bretherton, C. S. (2006). On the relationship between stratiform low cloud cover and lower-tropospheric stability. Journal of Climate, 19(24), 6425-6432.

68. Xu, K.-M. (1991). The coupling of cumulus convection with large-scale processes (Ph.D.). University of California. Retrieved from
https://elibrary.ru/item.asp?id=5851863

69. Xu, K.-M., (1993). Cumulus ensemble simulation. The Representation of Cumulus Convection in Numerical Models, Meteor. Monogr., American Meteorological Society,46, 221-235.